

PCT

WELTORGANISATION FÜR GEISTIGES EIGENTUM
Internationales Büro

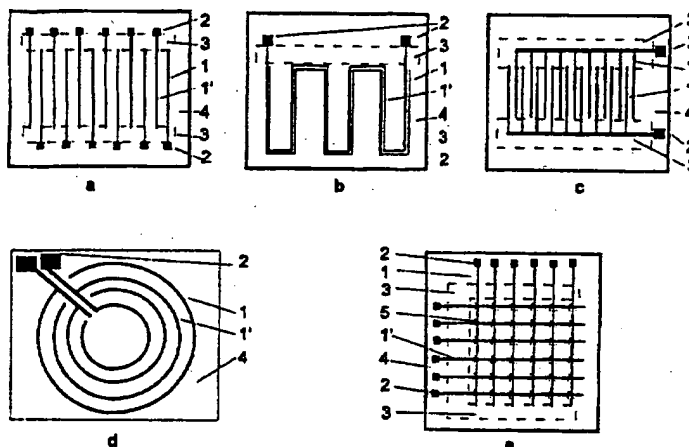


INTERNATIONALE ANMELDUNG VERÖFFENTLICHT NACH DEM VERTRAG ÜBER DIE
INTERNATIONALE ZUSAMMENARBEIT AUF DEM GEBIET DES PATENTWESENS (PCT)

(51) Internationale Patentklassifikation ⁶ : G01N 27/12, 33/543		A1	(11) Internationale Veröffentlichungsnummer: WO 97/34140
		(43) Internationales Veröffentlichungsdatum:	18. September 1997 (18.09.97)
(21) Internationales Aktenzeichen: PCT/DE97/00494		(81) Bestimmungsstaaten: JP, US, europäisches Patent (AT, BE, CH, DE, DK, ES, FI, FR, GB, GR, IE, IT, LU, MC, NL, PT, SE).	
(22) Internationales Anmeldedatum: 12. März 1997 (12.03.97)			
(30) Prioritätsdaten: 196 10 115.8 14. März 1996 (14.03.96) DE		Veröffentlicht <i>Mit internationalem Recherchenbericht. Vor Ablauf der für Änderungen der Ansprüche zugelassenen Frist. Veröffentlichung wird wiederholt falls Änderungen eintreffen.</i>	
(71) Anmelder (für alle Bestimmungsstaaten ausser US): FRAUNHOFER GESELLSCHAFT ZUR FÖRDERUNG DER ANGEWANDTEN FORSCHUNG E.V. [DE/DE]; Leonrodstrasse 54, D-80636 München (DE).			
(72) Erfinder; und (75) Erfinder/Anmelder (nur für US): HINTSCHE, Rainer [DE/DE]; Schwedter Strasse 14, D-10119 Berlin (DE). PAESCHKE, Manfred [DE/DE]; An der Wildbahn 59, D-16352 Basdorf (DE).			
(74) Anwalt: OLGEMÖLLER, Luitgard; Leonhard Olgemöller Fricke, Josephspitalstrasse 7, D-80331 München (DE).			

(54) Title: DETECTION OF MOLECULES AND MOLECULE COMPLEXES

(54) Bezeichnung: DETEKTION VON MOLEKÜLEN UND MOLEKÜLKOMPLEXEN



(57) Abstract

The invention concerns a process for detecting molecules or molecule complexes. A measurement probe is brought into contact with an ultra-microelectrode arrangement comprising at least two electrode structures configured in such a way that the distances between the different structures lie in the ultra-micro range; an alternating electrical field is created by application of an electrical potential; and the current or potential fluctuations caused by species present or created in the measurement probe are measured.

BEST AVAILABLE COPY

(57) Zusammenfassung

Die Erfindung betrifft ein Verfahren zum Detektieren von Molekülen oder Molekülkomplexen, wobei eine Meßprobe mit einer Ultra-Mikroelektrodenanordnung (1, 1', 2, 3, 4, 5) in Kontakt gebracht wird, welche mindestens zwei Elektrodenstrukturen (1, 1') aufweist, die derartig zueinander angeordnet sind, daß die Abstände zwischen den verschiedenen Strukturen im Ultra-Mikrobereich liegen, durch Anlegen eines elektrischen Potentials ein elektrisches Wechselfeld erzeugt wird und die Strom- oder Potentialveränderungen gemessen werden, die durch in der Meßprobe vorhandene oder entstehende Spezies verursacht werden.

LEDIGLICH ZUR INFORMATION

Codes zur Identifizierung von PCT-Vertragsstaaten auf den Kopfbögen der Schriften, die internationale Anmeldungen gemäss dem PCT veröffentlichen.

AM	Armenien	GB	Vereinigtes Königreich	MX	Mexiko
AT	Österreich	GE	Georgien	NE	Niger
AU	Australien	GN	Guinea	NL	Niederlande
BB	Barbados	GR	Griechenland	NO	Norwegen
BE	Belgien	HU	Ungarn	NZ	Neuseeland
BF	Burkina Faso	IE	Irland	PL	Polen
BG	Bulgarien	IT	Italien	PT	Portugal
BJ	Benin	JP	Japan	RO	Rumänien
BR	Brasilien	KE	Kenya	RU	Russische Föderation
BY	Belarus	KG	Kirgisistan	SD	Sudan
CA	Kanada	KP	Demokratische Volksrepublik Korea	SE	Schweden
CF	Zentrale Afrikanische Republik	KR	Republik Korea	SG	Singapur
CG	Kongo	KZ	Kasachstan	SI	Slowenien
CH	Schweiz	LI	Liechtenstein	SK	Slowakei
CI	Côte d'Ivoire	LK	Sri Lanka	SN	Senegal
CM	Kamerun	LR	Liberia	SZ	Swasiland
CN	China	LX	Litauen	TD	Tschad
CS	Tschechoslowakei	LU	Luxemburg	TG	Togo
CZ	Tschechische Republik	LV	Lettland	TJ	Tadschikistan
DE	Deutschland	MC	Monaco	TT	Trinidad und Tobago
DK	Dänemark	MD	Republik Moldau	UA	Ukraine
EE	Estland	MG	Madagaskar	UG	Uganda
ES	Spanien	ML	Mali	US	Vereinigte Staaten von Amerika
FI	Finnland	MN	Mongolei	UZ	Usbekistan
FR	Frankreich	MR	Mauretanien	VN	Vietnam
GA	Gabon	MW	Malawi		

Detektion von Molekülen und Molekülkomplexen

Die Erfindung betrifft ein Verfahren zum Detektieren von molekularen Spezies sowie einen elektrischen Sensor hierfür.

5 Solche elektrischen Sensoren, auch Ultra-Mikroelektrodenarrays genannt, sind für die chemische Analytik und Prozeßkontrolle auf verschiedenen Gebieten wie Gesundheitswesen, Biotechnologie, Umweltschutz und chemischer Industrie einsetzbar. Sie stellen ein vergleichsweise einfaches Meßsystem dar, das die Bindung
10 oder Anlagerung von Molekülen im elektrodennahen Raum meßbar erfaßt.

Bisher bekannt sind optische Sensoren, die unter anderem nach dem Prinzip der **Evanescence-Wave** [vgl. Feldman, et al., Biosens. & Bioelectron., 10 (1995) 423] oder der **Lichtreflexion** [vgl.
15 Domenici et al., Biosens. & Bioelectron., 10 (1995) 371 oder Brecht, Gauglitz, Biosens. & Bioelectron., 10 (1995), 923] oder der **Surface Plasmon Resonanz** [vgl. Häuselung et al., Langmuir, 7 (1991) 1837 oder U.Jönsson et al., BioTechniques 11 (1991), 620]
20 Bindungseffekte oder die Anlagerung von Molekülen in dünnen Schichten nachzuweisen gestatten.

Für die direkte elektrische Auslesung solcher Bindungsereignisse wurden bereits ein potentiometrisches Meßverfahren [vgl.
25 Bergfeld, Biosens. & Bioelectron., 6 (1991), 55], ein kapazitives Meßverfahren [vgl. Swietlow, Electroanalysis, 4 (1992), 921] und ein impedimetrisches Meßverfahren [vgl. Knicke et al. Sens.&Act. B 28, (1995), 85] beschrieben. Auch Elektrodenanordnungen nach dem EIS-Prinzip (EIS: Elektrolyt-
30 Insulator-Semiconductor) wurden vorgeschlagen [vgl. Schyberg et al. Sens.&Act. B 26-27 (1995) 457 oder Souteyrand et al. Sens.&Act. B 20, (1994) 63], wobei der Isolator als Kopplungs- und Übertragungselement wirkt.

35 Bei diesen elektrochemischen Meßanordnungen dienen räumlich weit voneinander entfernte Elektroden zur Erfassung von Molekülen in der elektrodennahen dünnen Grenzschicht, die aber durch eine vergleichsweise große Menge an Elektrolyten und anderen

Substanzen zwischen den Elektroden in vielfacher Weise negativ beeinflusst werden.

Es wurden auch Anwendungen bekannt, bei denen dünne
5 Molekülschichten als Gate zwischen Drain und Source von Transistoren abgeschieden wurden und Informationen über die organische Schicht liefern [vgl. Kruse et al. Sens.&Act. B 6 (1992), 101 oder Uhe et al. Electroanalysis, 6(7) (1994), 543].

10 Allen diesen beschriebenen elektrischen Verfahren mit Elektroden ist gemeinsam, daß sie keine Anordnungen aufweisen, die molekularen Dimensionen nahekomen; in allen diesen Anwendungen sind die sensortypischen Abmessungen, z.B. zwischen Meß-, Referenz- und Arbeitselektroden, um Größenordnungen von den
15 molekularen Dimensionen entfernt.

Der Erfindung liegt die Aufgabe zugrunde, ein Verfahren mit Hilfe eines elektrischen Sensors vorzuschlagen, das die Detektion von Molekülen und Molekülkomplexen mit höherer
20 Nachweisempfindlichkeit bei vergleichsweise geringerem Systemaufwand ermöglicht.

Die erfindungsgemäße Lösung dieser Aufgabe ist in Anspruch 1 umschrieben. Die weiteren Ansprüche zeigen bevorzugte
25 Ausgestaltungen auf.

Erfindungsgemäß wird das Verfahren zur Detektion von Molekülen und Molekülkomplexen mit einer Anordnung durchgeführt, die Ultramikroelektrodenarrays aufweist, deren Elektrodenstrukturen
30 so eng beieinander angeordnet werden, daß sie der Größe großer Molekülkomplexe, z. B. von Immunoproteinen oder DNS-Molekülen, nahekomen. Benutzt wird insbesondere der Effekt, daß sich zwischen nahe benachbarten Elektroden elektrische Wechselfelder erzeugen lassen und der resultierende Strom hauptsächlich von
35 den detektierten Molekülen und Molekülkomplexen im elektrodennahen Raum beeinflusst wird. Die Form und Feinstruktur der Elektroden ist dabei relativ frei wählbar, während die minimale Entfernung der Elektroden selbst typischerweise 3 µm,

bevorzugt 1 μm unterschreiten sollte.

Die Beeinflussung kann durch Diffusion, durch Anlagerung oder Bindung der zu messenden Spezies erfolgen. Durch diese Art der Felderzeugung und Messung mit Hilfe insbesondere der
5 Impedanzspektroskopie erreicht man erfindungsgemäß, daß Elektrolyt-Moleküle sowie andere Substanzen in einer Meßprobe das zwischen den Elektroden anliegende elektrische Feld nur geringfügig beeinflussen und somit die Messung nicht stören.

10

Eine mehrfache Anordnung dieser Art feinstrukturierter Ultra-Mikroelektrodenarrays führt in vorteilhafter Weise zur Verstärkung des eben beschriebenen Effekts, in dem mit geeigneter Meßtechnik, (z. B. Impedanzmeßbrücken) sequentiell
15 oder parallel gleichartige Messungen realisiert werden. Die Ultramikroelektrodenarrays können aus dünnen Schichten von Edelmetallen wie Gold, Platin oder Iridium oder auch Kohlenstoffmaterialien bestehen oder diese Materialien enthalten (Anspruch 16). Sie werden besonders vorteilhaft auf planare
20 isolierende Trägermaterialien wie Siliziumverbindungen, Glas, Keramik oder organische Polymere aufgebracht, können aber auch zur Planarisierung und mechanischen Stützung in diese Materialien eingegraben oder eingelegt sein (Anspruch 17). Die optimale Annäherung zweier voneinander isolierter
25 Ultramikroelektroden läßt sich, wie in Fig. 1 dargestellt, z.B. durch Bänder oder parallele Streifen oder mäanderförmige und runde oder schneckenartige Strukturen wie auch durch fingerartige Interdigitalanordnungen in Abständen von bevorzugt
30 <1 μm erreichen. In Fig. 1 sind dazu Anordnungsbeispiele a bis d ausgeführt (siehe unten). Die Elektroden sind vorzugsweise zum Meßraum hin nicht abgedeckt.

Als eine besondere Ausgestaltung der Anordnung der Ultramikroelektrodenarrays kann vorgesehen sein, daß man ein
35 Elektrodenarray mit einem zweiten oder mehreren überlagert und die Kreuzungspunkte durch Isolationsschichten voneinander isoliert (Anspruch 19). Auf diese Weise können Elektroden in Abständen von nur noch wenigen nm voneinander angeordnet werden,

wobei die Isolationsschicht die minimale Entfernung definiert (Fig. 1e). Allen Anordnungen der Ultra-Mikroelektrodenarrays gemeinsam ist, daß sie gut voneinander isoliert sein müssen, damit zwei, drei oder noch mehr Ultramikroelektrodenarrays durch isolierte Zuleitung auf dem Chip elektrisch unabhängig einzeln oder in Gruppen mit Gleich- und/oder Wechselstrom beaufschlagt werden können (Anspruch 20). Die für die Isolierung eingesetzten Werkstoffe (z.B. Kunststoffe oder anorganische Verbindungen wie Siliciumoxide, -nitride und keramische Materialien) müssen über den Nutzungszeitraum inert gegenüber den in der Probe verwendeten Verdünnungs- oder Lösungsmitteln (häufig Wasser) sein. Unter "Lösungsmittel" sind Reaktionsflüssigkeiten zu verstehen, in denen eine Molekülbindung, eine -anlagerung oder eine -diffusion möglich ist. Die Meßprobe muß jedoch nicht zwingend flüssig sein, auch andere Zustände sind möglich. So können die zu messenden Vorgänge auch in einem Gel ablaufen..

Zwischen den Ultramikroelektroden kann das zur Detektion benutzte elektrische Feld durch Wechselstrom mit Frequenzen zwischen 1 MHz und 10 MHz und Amplituden zwischen ca. 10 mV und 50 mV erzeugt werden. Dabei werden Potentiale zwischen 0 V und +/-5 V gewählt.

Das vorliegende Verfahren ermöglicht die Erfassung auch komplexer Reaktionsabläufe und bietet daher erweiterte Einsatzmöglichkeiten. Das Eindringen von Molekülen in den elektrodennahen Bereich mit dem aufgebauten Feld (z.B. durch Diffusion) oder die Anordnung von Molekülen in diesem Bereich, die z.B. durch sog. "self assembling" oder auch durch Komplexbildung geschehen kann, verändern sowohl die realen als auch die imaginären Größen der komplexen Impedanz und können zeitunabhängig - z.B. nach Abschluß der Ereignisse -, bei Bedarf ebenso wie der Phasenwinkel aber auch zeitabhängig, d. h. vom Fortgang des Bindungsereignisses oder der Diffusion abhängig, gemessen werden (Ansprüche 3 und 4). Für ein komplettes Impedanzspektrum wird der gesamte Frequenzbereich vermessen und ausgewertet. Besonders vorteilhaft ist die erfindungsgemäße Nutzung nur einzelner ausgewählter Frequenzen oder

Frequenzbereiche, die maximal beeinflußt werden. Dadurch gelingt es, miniaturisierte Nachweissysteme zu konstruieren.

Bei der Nutzung der Ultramikroelektrodenarrays in Flüssigkeiten
5 oder dergleichen ist es auch möglich, zusätzlich zum Meßvorgang
- oder aber in Meßpausen - Gleichstromanteile zu überlagern oder
zu applizieren (Anspruch 6). Diese können z.B. elektrochemische
Reaktionen wie Oxidationen oder Reduktionen von elektrisch
aktiven Molekülen induzieren, wobei solche Vorgänge simultan
10 oder sequentiell mit den Impedanzmessungen gemessen werden
(Anspruch 7). Erfindungsgemäß ist dadurch eine Kombination
elektrischer und elektrochemischer Messungen mit derselben
Sensor-Anordnung (Ultramikroelektrodenarray) möglich.

15 Erfindungsgemäß kann das Verfahren zur Detektion von Molekülen
und Molekülkomplexen ausgeführt werden, indem man die Moleküle,
die man messen will, auf den Mikroelektrodenflächen selbst
bindet. Diese Bindung kann eine physikalische (Adsorption) oder
eine chemische sein. Für letztere eignen sich besonders gut die
20 bekannten Verfahren der Selbstanordnung (englisch "self
assembling" genannt), die es gestatten, z. B. monomolekulare
Thiolverbindungen auf Goldelektroden zu binden und zu messen.
Dieses Verfahren ist universell für eine große Zahl von
Molekülen anwendbar, nicht nur für solche, die eine Thiolgruppe
25 besitzen oder damit versehen werden können.

Ein zweites selektives Verfahren zur Anheftung von Molekülen
oder Molekülkomplexen an die leitenden Mikroelektroden-
Oberflächen ist die bekannte Methode der Elektropolymerisation
30 (Anspruch 9). Dabei kann jede Elektrode individuell, in Gruppen
oder parallel auf ihrer Oberfläche mit Elektropolymeren, z. B.
aus den monomeren Molekülen Streptavidin, Pyrrol, Anilin,
Vinylferrocen oder anderen elektrisch polymerisierbaren
Substanzen, modifiziert werden. Die Bindung solcher Verbindungen
35 in monomolekularen oder multimolekularen Schichten auf den
Elektroden verändert das Impedanzspektrum oder einzelne
Frequenzen in sehr charakteristischer Weise und läßt sich damit
zeitabhängig oder nach Abschluß der Reaktion messen.

Weiterhin läßt sich das Impedanzspektrum auch dadurch meßbar verändern, daß man die Moleküle anstatt auf den Elektroden in den Elektrodenzwischenräumen positioniert (Anspruch 10). Diese
5 Positionierung kann zum Beispiel durch chemische Bindungen (so z.B. an Siliciumdioxid) oder durch Adhäsion oder durch Reaktionen wie Kondensationsreaktionen, z.B. Silanisierungen, erfolgen. Zur Beschichtung der Gesamtflächen des Elektrodenarrays, also der Elektroden selbst wie auch der
10 Elektrodenzwischenräume, kann man das bekannte Langmuir-Blodgett-Verfahren heranziehen (Tachibana Matsumoto, Advanced Materials Ab. 11 (1993), 5/796-803), mit dem z. B. Lipide oder Phthalocyanine durch Aufziehen von monomolekularen Filmen in Schichten angeordnet werden können.

15
Einer weiteren Variante des erfindungsgemäßen Verfahrens zur Detektion von Molekülen und Komplexen gemäß kann die Konzentration von Molekülen in der elektrodennahen Schicht durch Diffusion verändert und die Änderung gemessen werden. Dies läßt
20 sich sowohl mit Hilfe chemisch/physikalisch bedingter Konzentrationsänderungen als auch durch das Anlegen eines elektrischen Potentials, das einen Diffusionsgradienten erzeugt, erreichen. Weiterhin ist es möglich, die Produktion spezifischer Moleküle, beispielsweise durch Enzyme, in Elektrodennähe zu
25 bewirken und zu messen.

Erfindungsgemäß umfaßt das Verfahren zur Detektion von Molekülen und Molekülkomplexen in einer bevorzugten Ausgestaltung die Maßnahme, daß die zuvor auf den Elektrodenarrays erzeugten
30 Molekül-Schichten mit chemischen Haftgruppen versehen sind oder werden, die durch eine chemische Reaktion oder eine Komplexbildung weitere Moleküle binden können (Anspruch 11). Es gelingt dabei, mit hoher Empfindlichkeit derartige Bindungsereignisse zu verfolgen. Wenn beispielsweise ein
35 niedermolekularer Komplexbildner wie Biotin über eine Thiolfunktion an die Elektrode gebunden wird, kann dieser anschließend mit einem höhermolekularen Komplexbildungspartner, z.B. Streptavidin, an welches beliebige weitere Moleküle

gebunden sein können, komplexiert werden.

Eine besonders wichtige und sehr breit einsetzbare Anwendung des vorliegenden Verfahrens ist die Immunodetektion (Anspruch 12).

5 Dabei wird der Aufbau von Molekülschichten auf dem Ultramikroelektrodenarray nach dem Sandwich-Prinzip einer Antikörper/Antigen-Immunoreaktion vorgenommen. Zum Nachweis von Antikörpern in der Meßprobe kann man dafür beispielsweise Haptene (niedermolekulare Antigene) oder andere Antigene (häufig

10 Proteine) an die Mikroelektrodenarrays binden. Durch die spezifische Komplexbildung zwischen den fest verankerten Antigenen und den in der Meßprobe befindlichen Antikörpern gelingt auf diese Weise ein spezifischer Antikörpernachweis. In Umkehrung dieses Prinzips kann man auch die Antikörper auf den

15 Elektroden binden und Haptene oder dergleichen aus der Meßprobe detektieren. Das Antigen kann auch ein höhermolekulares Virus-Protein sein, das am Mikroelektrodenarray fest gebunden ist und Antikörper aus der Meßprobe zu messen gestattet. Varianten dieses Verfahrens sind der Einsatz von multivalenten

20 Antikörpern, mit denen drei- oder mehrfache Molekülkomplexe konstruiert und gemessen werden können.

Eine weitere Ausgestaltung des erfindungsgemäßen Verfahrens ist dadurch gegeben, daß man das Ultramikroelektrodenarray zur

25 elektrischen Auslesung von Hybridisierungsvorgängen in der Nucleinsäurechemie einsetzt (Anspruch 13). Applikationen in der Gentechnologie lassen sich dann dadurch realisieren, daß man Nucleotide über Thiolbindungen oder dgl. an die Elektrodenstrukturen koppelt und die Bindung komplementärer

30 Nucleinsäure-Bausteine durch das erfindungsgemäße Verfahren erfaßt. Diese Detektion läßt sich dadurch variieren, daß man zusätzliche Anlagerungen von Nucleinsäuren, z. B. zur Triple-DNS oder die zusätzliche Einlagerung komplexierender Moleküle in Doppel- oder Triple-Helices als Bindungsereignis einer Messung

35 zugänglich macht (Anspruch 14). Für diese Komplexierung oder Einlagerung können vorteilhafterweise auch Metallkomplexe genutzt werden, die das elektrodennahe Feld elektrisch besonders intensiv verändern.

Das Meßprinzip und die Veränderung des elektrischen Feldes gestattet es prinzipiell, die Molekülstruktur und -art mittels einer quantitativen Analyse des Impedanzspektrums zu unterscheiden. Eine Differenzierung nach der Art und Größe der Moleküle ist durch die quantitative Auswertung und insbesondere durch die Eichung der Impedanzspektren mit bekannten Molekülspezies möglich.

Die Erfindung wird nachfolgend anhand mehrerer Figuren und einem Beispiel erläutert.

- Figur 1 zeigt mögliche Anordnungen der
5 Ultramikroelektrodenarrays;
Figur 2 zeigt die Adsorption von SH-Biotin;
Figur 3 zeigt Nyquist-Plots einer mit SH-Biotin modifizierten
und einer zusätzlich mit Streptavidin komplexierten
Elektrode;
10 Figur 4 zeigt den amperometrischen Nachweis von p-Aminophenol.

Figur 1 zeigt verschiedene mögliche Anordnungen von
Ultramikroelektrodenarrays. Dabei ist

- 1a eine streifenförmige parallele Anordnung;
15 1b eine mäanderförmige parallele Anordnung;
1c eine fingerartige interdigitale Anordnung;
1d eine kreisförmige parallele Anordnung;
1e eine kreuzförmig gestapelte und voneinander isolierte
Anordnung;

20

Der Anordnung der Figur 1d sehr ähnlich ist die Anordnung der
Elektroden als parallel verlaufende Schnecke.

- Die voneinander isolierten Ultramikroelektroden 1 und 1' mit
25 ihren Kontakten zur elektrischen Verbindung 2 sowie den
Isolationsschichten (z.B. Siliciumnitrid) 3 auf dem Chip sind
auf einem planaren Träger (z.B. ein Siliciumchip) 4 angeordnet.
Bei der mehrlagigen Anordnung der Figur 1e wird durch eine
Zwischenisolierung 5 die Elektrodenebene 1 von der
30 Elektrodenebene 1' isoliert.

Ausführungsbeispiel

- Ein interdigitales Goldelektrodenarray, strukturiert nach
35 Figur 1c, besitzt eine Elektrodenbreite von 1 μm und einen
Elektrodenabstand von 0.7 μm . Die Elektroden werden mit einer 1
ml, 10 mmol/l SH-Biotin-Lösung mittels Self Assembling
modifiziert.

In Figur 2 ist die Adsorption von 10 mmol/l SH-Biotin in einer 0.1 mol/l Natriumpufferlösung als Kapazitäts-Zeit-Verhalten bei einem angelegten Potential von 50 mV und einer zusätzlich aufgeprägten Amplitude von 10 mV an einem Paar interdigitaler Goldelektroden dargestellt. Die Kapazität der Elektrode erniedrigt sich nach einer Zugabe von SH-Biotin in die Lösung. Nach ca. 2000 Sekunden ist die Goldoberfläche vollständig mit -S-Biotin bedeckt. Nach 10 min. Waschen der Elektrode in 0.1 mol/l Natriumpufferlösung wird in einem nachfolgenden Schritt die adsorbierte monomolekulare Molekülschicht mit Streptavidin durch Eintauchen der modifizierten Elektrode für 2 Stunden in eine 50 U/ml Lösung komplexiert. Nach der β -Galactosidase-Streptavidin Modifizierung wurde die Elektrode 10 min in 0.1 mol/l Natriumpufferlösung gespült und anschließend in eine Meßzelle gespannt.

Figur 3 zeigt sogenannte Nyquist-Plots bei einem Potential von 50 mV, einer Amplitude von 10 mV und einem Frequenzbereich zwischen 2×10^{-3} Hz und 1×10^6 Hz, gemessen als Zweipol-Impedanz. Kurve I repräsentiert die mit SH-Biotin modifizierte Elektrode, Kurve II die gleiche Elektrode nach zusätzlicher Komplexierung des SH-Biotin mit β -Galactosidase-Streptavidin. Die Änderung der Impedanz zeigt die Störung des Dielektrikums zwischen den Elektroden durch das komplexierte Molekül und repräsentiert außerdem eine vollzogene Bindung zwischen dem Biotin und dem Streptavidin-Enzym-Komplex.

Das Enzym β -Galactosidase am Streptavidin wird unabhängig als kombinierter amperometrischer Nachweis der Bindung des β -Galactosidase-Streptavidins an das SH-Biotin genutzt. Dieser Nachweis wird mit der Funktion der β -Galactosidase, der enzymatischen Umsetzung von 5 mmol/l p-Aminophenyl- β -D-Galactopyranoside (p-APG) zu p-Aminophenol, über eine amperometrische Oxidation-Reduktion des p-Aminophenols durchgeführt.

Figur 4 zeigt den amperometrischen Nachweis von p-Aminophenol an den gleichen Elektroden mit einem Oxidationspotential von 250 mV und einem Reduktionspotential von -50 mV gegen eine Ag/AgCl-Referenzelektrode, nach Zugabe von 5 mmol/l p-APG in 0.1 mol/l Natriumpufferlösung in die Meßzelle. Die kontinuierliche Umsetzung von p-APG zu p-Aminophenol, welches durch den linearen Anstieg des Stromes repräsentiert wird, zeigt an, daß das Enzym die p-Aminophenolkonzentration in der Meßkammer erhöht.

Ansprüche:

1. Verfahren zum Detektieren von Molekülen oder Molekülkomplexen, wobei
 - 5 - eine Meßprobe mit einer Ultra-Mikroelektrodenanordnung in Kontakt gebracht wird, welche mindestens zwei Elektrodenstrukturen aufweist, die derartig zueinander angeordnet sind, daß die Abstände zwischen den verschiedenen Strukturen im Ultra-Mikrobereich liegen,
 - 10 - durch Anlegen eines elektrischen Potentials ein elektrisches Wechselfeld erzeugt wird und
 - die Strom- oder Potentialveränderungen gemessen werden, die durch in der Meßprobe vorhandene oder entstehende Spezies verursacht werden.
- 15 2. Verfahren nach Anspruch 1, worin die Feldveränderungen mit Hilfe der Impedanzspektroskopie gemessen werden.
- 20 3. Verfahren nach Anspruch 1 oder 2, worin die Verstimmung des elektrischen Feldes, die durch in der Meßprobe vorhandene oder entstehende Spezies entsteht, durch die Messung der kapazitiven und/oder der resistiven Anteile und/oder des Phasenwinkels zeitunabhängig oder zeitabhängig gemessen wird.
- 25 4. Verfahren nach einem der Ansprüche 1 bis 3, worin die Detektion der Moleküle oder Molekülkomplexe anhand ihrer Bindung oder Anlagerung oder Diffusion erfolgt.
- 30 5. Verfahren nach einem der Ansprüche 1 bis 4, wobei mehrere Elektrodenanordnungen überlagert angeordnet und die Kreuzungspunkte durch Isolationsschichten voneinander isoliert sind und die Messung sequentiell, parallel oder simultan erfolgt.

- 6 Verfahren nach einem der Ansprüche 1 bis 5, dadurch gekennzeichnet, daß das elektrische Wechselfeld mit einem Gleichstromanteil überlagert oder angeregt wird.
- 5 7. Verfahren nach Anspruch 6, wobei in der Meßprobe amperometrische Oxidationen oder Reduktionen oder Redox-Recycling von Molekülen mit elektrisch aktiven Gruppen oder von Redox-Mediatoren gemessen werden.
- 10 8. Verfahren nach einem der Ansprüche 1 bis 7, worin zu messende Spezies sich auf den aktiven Elektrodenflächen selbst anordnen und in gebundenem Zustand gemessen werden.
- 15 9. Verfahren nach einem der Ansprüche 1 bis 8, worin Moleküle auf den Elektrodenflächen durch Elektropolymerisation gebunden und in gebundenem Zustand gemessen werden.
- 20 10. Verfahren nach einem der Ansprüche 1 bis 9, wobei Moleküle in den Elektrodenzwischenräumen und/oder auf der Gesamtoberfläche der Elektroden durch physikalische oder chemische Bindung fixiert und gemessen werden.
- 25 11. Verfahren nach einem der Ansprüche 8 bis 10 wobei eine erste fixierte Molekülschicht eine Haftgruppe enthält, die selbst oder durch ein bifunktionelles Reagenz eine zweite Molekülschicht und diese gegebenenfalls weitere bindet und diese Ereignisse oder ihre Umkehr gemessen werden.
- 30 12. Verfahren nach Anspruch 11, worin die erste Molekülschicht komplexbindende Gruppen enthält, die ihren komplementären Bindungspartner binden, wobei diese Ereignisse oder ihre Umkehr gemessen werden.
- 35 13. Verfahren nach Anspruch 11 oder 12, worin die erste Molekülschicht ein Desoxyribonukleinsäure- oder ein Ribonukleinsäurebaustein ist, der durch Hybridisierung einen komplementären Molekülstrang bindet, wobei dieses Ereignis oder seine Umkehr gemessen werden.

14. Verfahren nach Anspruch 13, worin die Molekülanordnung einen weiteren Nucleinsäurebaustein oder ein komplexierendes oder einlagerndes Molekül bindet und dieses Ereignis oder seine Umkehr gemessen wird.
- 5 15. Verfahren nach einem der Ansprüche 1 bis 14, worin die Moleküle oder Molekülkomplexe detektiert werden, indem sie nach Größe und/oder Art unterschieden werden.
- 10 16. Verfahren nach einem der Ansprüche 1 bis 15, worin die aktiven Elektrodenflächen aus Gold, Platin, Iridium oder anderen Edelmetallen, aus Kohlenstoffmaterialien oder aus anderen leitenden Materialien oder aus Kombinationen-hieraus bestehen.
- 15 17. Verfahren nach einem der Ansprüche 1 bis 16, worin die Elektroden auf Siliciumverbindungen, Glas, Keramik, organische Polymere oder andere isolierende Materialien, aufgebracht oder darin eingelegt sind.
- 20 18. Verfahren nach einem der Ansprüche 1 bis 17, worin die Elektroden durch Beschichtung auf einem Substrat oder Einbettung in ein solches als Bänder oder Streifen oder kreisförmige Strukturen oder interdigitale Anordnungen im Mikrometer- oder Submikrometerabstand zueinander angeordnet sind.
- 25 19. Verfahren nach einem der Ansprüche 1 bis 18, worin die Elektroden zumindest teilweise als mehrlagige und voneinander isolierte und ggf. sich kreuzende Strukturen angeordnet sind.
- 30 20. Verfahren nach einem der Ansprüche 1 bis 19, worin die aktiven Elektrodenflächen über isolierte Zuleitungen und/oder elektronische Komponenten einzeln oder in Gruppen mit Gleich- und/oder Wechselstrom beaufschlagt werden können.
- 35

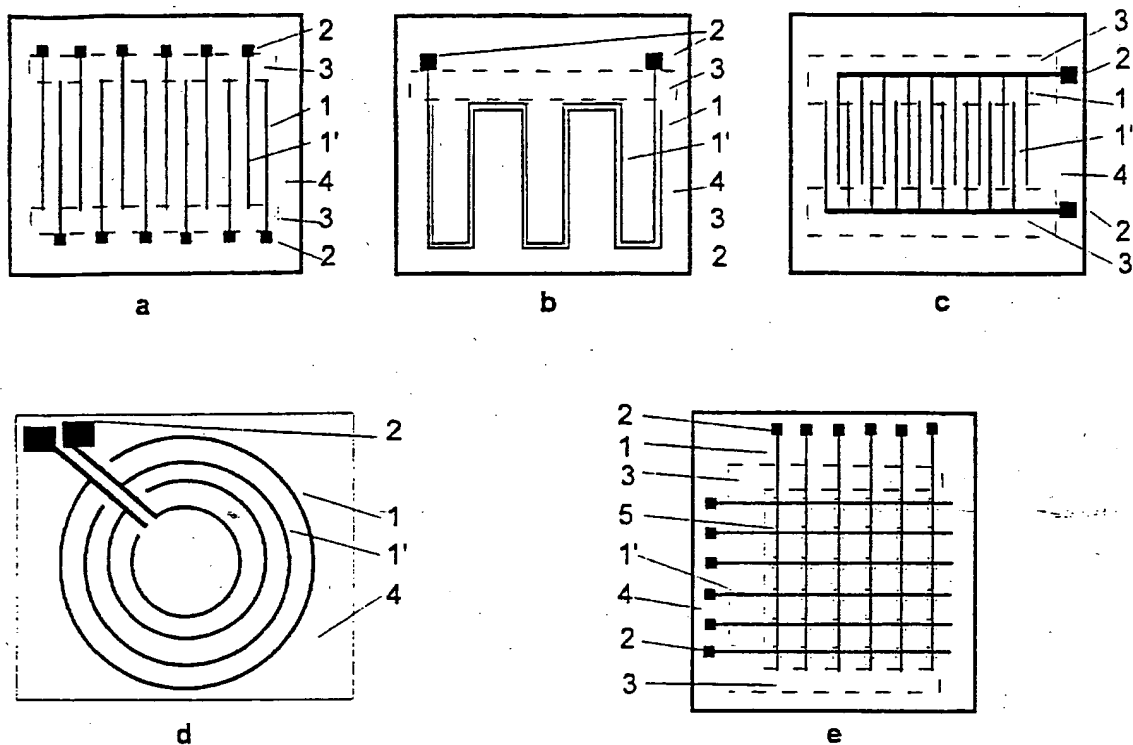


Fig. 1

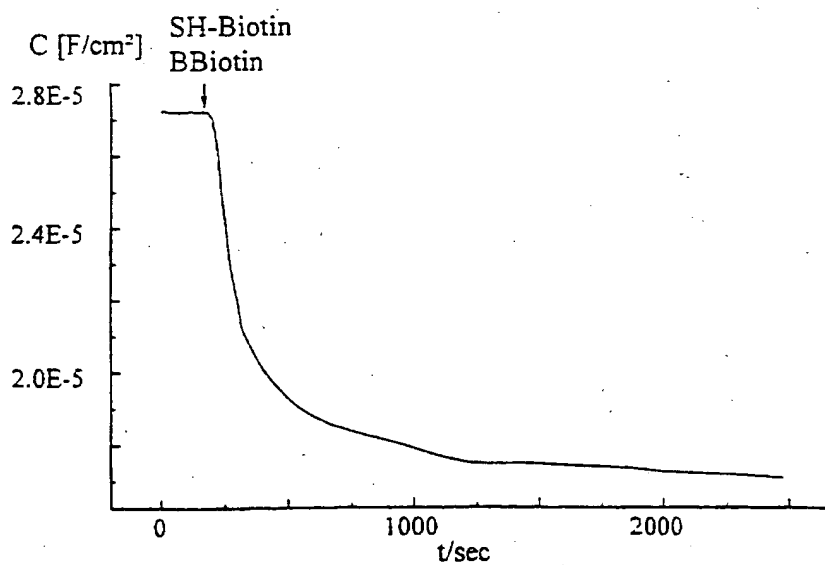
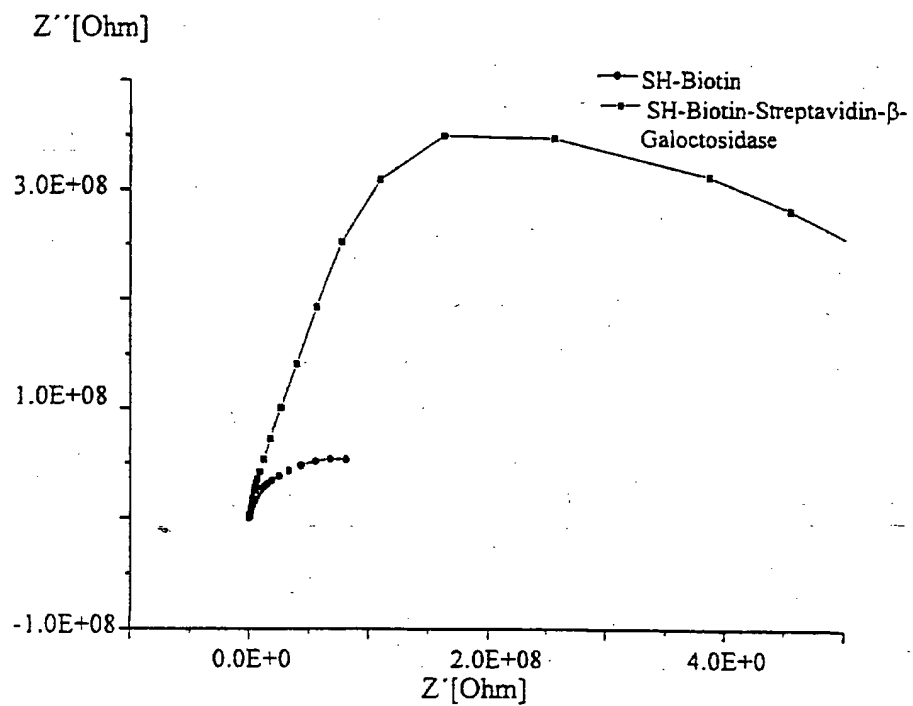
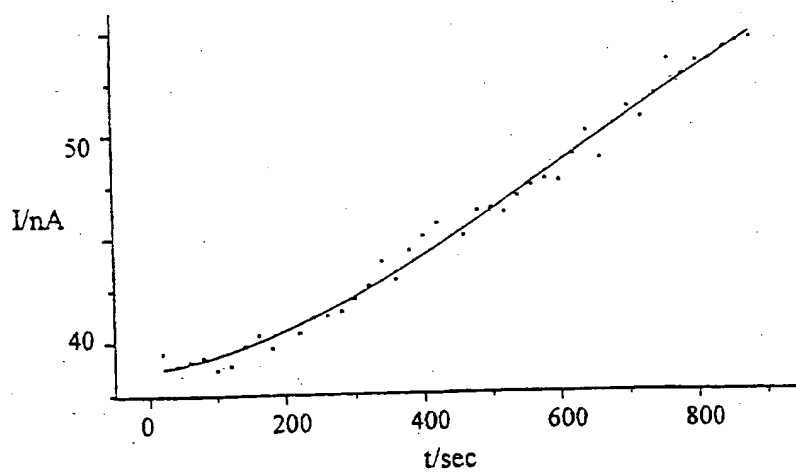


Fig. 2

**Fig. 3****Fig. 4**

INTERNATIONAL SEARCH REPORT

International Application No.

PCT/DE 97/00494

A. CLASSIFICATION OF SUBJECT MATTER
IPC 6 G01N27/12 G01N33/543

According to International Patent Classification (IPC) or to both national classification and IPC

B. FIELDS SEARCHED

Minimum documentation searched (classification system followed by classification symbols)

IPC 6 G01N

Documentation searched other than minimum documentation to the extent that such documents are included in the fields searched

Electronic data base consulted during the international search (name of data base and, where practical, search terms used)

C. DOCUMENTS CONSIDERED TO BE RELEVANT

Category	Citation of document, with indication, where appropriate, of the relevant passages	Relevant to claim No.
X	EP 0 299 780 A (STANFORD RES INST INT) 18 January 1989	1
Y	see page 5, line 4-16 see page 11, line 15-26	2-4, 6
A	US 5 491 097 A (RIBI HANS O ET AL) 13 February 1996 see the whole document	1-20
A	WO 94 29708 A (FRAUNHOFER GES FORSCHUNG ;HINTSCHE RAINER (DE); PAESCHKE MANFRED ()) 22 December 1994 see the whole document	1-20

-/--

☒ Further documents are listed in the continuation of box C.

☒ Patent family members are listed in annex.

* Special categories of cited documents:

- *A* document defining the general state of the art which is not considered to be of particular relevance
- *E* earlier document but published on or after the international filing date
- *L* document which may throw doubts on priority claim(s) or which is cited to establish the publication date of another citation or other special reason (as specified)
- *O* document referring to an oral disclosure, use, exhibition or other means
- *P* document published prior to the international filing date but later than the priority date claimed

- *T* later document published after the international filing date or priority date and not in conflict with the application but cited to understand the principle or theory underlying the invention
- *X* document of particular relevance; the claimed invention cannot be considered novel or cannot be considered to involve an inventive step when the document is taken alone
- *Y* document of particular relevance; the claimed invention cannot be considered to involve an inventive step when the document is combined with one or more other such documents, such combination being obvious to a person skilled in the art.
- *Z* document member of the same patent family

Date of the actual completion of the international search

14 July 1997

Date of mailing of the international search report

01 Dec 97

Name and mailing address of the ISA

European Patent Office, P.B. 5818 Patentlaan 2
NL - 2280 HV Rijswijk
Tel. (+31-70) 340-2040, Tx. 31 651 cpo nl,
Fax (+31-70) 340-3016

Authorized officer

Mueller, T

INTERNATIONAL SEARCH REPORT

International Application No.

PCT/DE 97/00494

C.(Continuation) DOCUMENTS CONSIDERED TO BE RELEVANT

Category	Citation of document, with indication, where appropriate, of the relevant passages	Relevant to claim No.
A	SENSORS AND ACTUATORS B, vol. B28, no. 2, 1 August 1995, pages 85-94, XP000539269 KNICHEL M ET AL: "UTILIZATION OF A SELF-ASSEMBLED PEPTIDE MONOLAYER FOR AN IMPEDIMETRIC IMMUNOSENSOR" see the whole document ---	12
Y	DE 32 28 542 A (SIEMENS AG) 2 February 1984 see page 8, line 15 - page 11, line 3 ---	2-4,6
A	NTT REVIEW, vol. 8, no. 2, March 1996, JAPAN, pages 77-80, XP002035202 MORITA M. NIWA O: "Electrochemical Detection using Interdigitated Array Carbon Microelectrodes" see the whole document -----	1-20

INTERNATIONAL SEARCH REPORT

information on patent family members

Inter nal Application No

PCT/DE 97/00494

Patent document cited in search report	Publication date	Patent family member(s)	Publication date
EP 0299780 A	18-01-89	US 4900405 A	13-02-90
		JP 1088354 A	03-04-89
US 5491097 A	13-02-96	US 5156810 A	20-10-92
		US 5571568 A	05-11-96
		US 5622872 A	22-04-97
		US 5427915 A	27-06-95
		US 5268305 A	07-12-93
		AT 145064 T	15-11-96
		CA 2019039 A	15-12-90
		DE 69029060 D	12-12-96
		DE 69029060 T	30-04-97
		EP 0402917 A	19-12-90
		JP 3128449 A	31-05-91
WO 9429708 A	22-12-94	DE 4318519 A	08-12-94
		AT 149686 T	15-03-97
		DE 59401964 D	10-04-97
		EP 0701691 A	20-03-96
DE 3228542 A	02-02-84	EP 0101880 A	07-03-84
		US 4919770 A	24-04-90

INTERNATIONALER RECHERCHENBERICHT

Internationales Aktenzeichen

PCT/DE 97/00494

A. KLASSIFIZIERUNG DES ANMELDUNGSGEGENSTANDES
IPK 6 G01N27/12 G01N33/543

Nach der Internationalen Patentklassifikation (IPK) oder nach der nationalen Klassifikation und der IPK

B. RECHERCHIERTE GEBIETE

Recherchierter Mindestprüfstoff (Klassifikationssystem und Klassifikationssymbole)

IPK 6 G01N

Recherchierte aber nicht zum Mindestprüfstoff gehörende Veröffentlichungen, soweit diese unter die recherchierten Gebiete fallen

Während der internationalen Recherche konsultierte elektronische Datenbank (Name der Datenbank und evtl. verwendete Suchbegriffe)

C. ALS WESENTLICH ANGESEHENE UNTERLAGEN

Kategorie	Bezeichnung der Veröffentlichung, soweit erforderlich unter Angabe der in Betracht kommenden Teile	Betr. Anspruch Nr.
X	EP 0 299 780 A (STANFORD RES INST INT) 18. Januar 1989	1
Y	siehe Seite 5, Zeile 4-16 siehe Seite 11, Zeile 15-26	2-4,6
A	US 5 491 097 A (RIBI HANS O ET AL) 13. Februar 1996 siehe das ganze Dokument	1-20
A	WO 94 29708 A (FRAUNHOFER GES FORSCHUNG ;HINTSCHE RAINER (DE); PAESCHKE MANFRED ()) 22. Dezember 1994 siehe das ganze Dokument	1-20
	--- -/-	

☒ Weitere Veröffentlichungen sind der Fortsetzung von Feld C zu entnehmen

☒ Siehe Anhang Patentfamilie

* Besondere Kategorien von angegebenen Veröffentlichungen :

- * "A" Veröffentlichung, die den allgemeinen Stand der Technik definiert, aber nicht als besonders bedeutsam anzusehen ist
- * "E" älteres Dokument, das jedoch erst am oder nach dem internationalen Anmeldedatum veröffentlicht worden ist
- * "L" Veröffentlichung, die geeignet ist, einen Prioritätsanspruch zweifelhaft erscheinen zu lassen, oder durch die das Veröffentlichungsdatum einer anderen im Recherchenbericht genannten Veröffentlichung belegt werden soll oder die aus einem anderen besonderen Grund angegeben ist (wie ausgeführt)
- * "O" Veröffentlichung, die sich auf eine mündliche Offenbarung, eine Benutzung, eine Ausstellung oder andere Maßnahmen bezieht
- * "P" Veröffentlichung, die vor dem internationalen Anmeldedatum, aber nach dem beanspruchten Prioritätsdatum veröffentlicht worden ist

* "T" Spätere Veröffentlichung, die nach dem internationalen Anmeldedatum oder dem Prioritätsdatum veröffentlicht worden ist und mit der Anmeldung nicht kollidiert, sondern nur zum Verständnis des der Erfindung zugrundeliegenden Prinzips oder der ihr zugrundeliegenden Theorie angegeben ist

* "X" Veröffentlichung von besonderer Bedeutung, die beanspruchte Erfindung kann allein aufgrund dieser Veröffentlichung nicht als neu oder auf erfinderischer Tätigkeit beruhend betrachtet werden

* "Y" Veröffentlichung von besonderer Bedeutung, die beanspruchte Erfindung kann nicht als auf erfinderischer Tätigkeit beruhend betrachtet werden, wenn die Veröffentlichung mit einer oder mehreren anderen Veröffentlichungen dieser Kategorie in Verbindung gebracht wird und diese Verbindung für einen Fachmann naheliegend ist

* "&" Veröffentlichung, die Mitglied derselben Patentfamilie ist

Datum des Abschlusses der internationalen Recherche

14. Juli 1997

Abschließdatum des internationalen Recherchenberichts

01.08.97

Name und Postanschrift der Internationalen Recherchenbehörde
Europäisches Patentamt, P.B. 5818 Patentlaan 2
NL - 2280 HV Rijswijk
Tel. (+ 31-70) 340-2040, Tx. 31 651 epo nl,
Fax (+ 31-70) 340-3016

Bevollmächtigter Bediensteter

Mueller, T

INTERNATIONALER RECHERCHENBERICHT

Inte: nales Aktenzeichen

PCT/DE 97/00494

C/(Fortsetzung) ALS WESENTLICH ANGESEHENE UNTERLAGEN		
Kategorie	Bezeichnung der Veröffentlichung, soweit erforderlich unter Angabe der in Betracht kommenden Teile	Betr. Anspruch Nr.
A	SENSORS AND ACTUATORS B, Bd. B28, Nr. 2, 1. August 1995, Seiten 85-94, XP000539269 KNICHEL M ET AL: "UTILIZATION OF A SELF-ASSEMBLED PEPTIDE MONOLAYER FOR AN IMPEDIMETRIC IMMUNOSENSOR" siehe das ganze Dokument ---	12
Y	DE 32 28 542 A (SIEMENS AG) 2. Februar 1984 siehe Seite 8, Zeile 15 - Seite 11, Zeile 3 ---	2-4,6
A	NTT REVIEW, Bd. 8, Nr. 2, März 1996, JAPAN, Seiten 77-80, XP002035202 MORITA M. NIWA O: "Electrochemical Detection using Interdigitated Array Carbon Microelectrodes" siehe das ganze Dokument -----	1-20

INTERNATIONALER RECHERCHENBERICHT

Angaben zu Veröffentlichungen, die zur selben Patentfamilie gehören

Internationales Aktenzeichen

PCT/DE 97/00494

Im Recherchenbericht angeführtes Patentdokument	Datum der Veröffentlichung	Mitglied(er) der Patentfamilie	Datum der Veröffentlichung
EP 0299780 A	18-01-89	US 4900405 A	13-02-90
		JP 1088354 A	03-04-89

US 5491097 A	13-02-96	US 5156810 A	20-10-92
		US 5571568 A	05-11-96
		US 5622872 A	22-04-97
		US 5427915 A	27-06-95
		US 5268305 A	07-12-93
		AT 145064 T	15-11-96
		CA 2019039 A	15-12-90
		DE 69029060 D	12-12-96
		DE 69029060 T	30-04-97
		EP 0402917 A	19-12-90
		JP 3128449 A	31-05-91

WO 9429708 A	22-12-94	DE 4318519 A	08-12-94
		AT 149686 T	15-03-97
		DE 59401964 D	10-04-97
		EP 0701691 A	20-03-96

DE 3228542 A	02-02-84	EP 0101880 A	07-03-84
		US 4919770 A	24-04-90

PCT

WELTORGANISATION FÜR GEISTIGES EIGENTUM
Internationales Büro



INTERNATIONALE ANMELDUNG VERÖFFENTLICHT NACH DEM VERTRAG ÜBER DIE
INTERNATIONALE ZUSAMMENARBEIT AUF DEM GEBIET DES PATENTWESENS (PCT)

(51) Internationale Patentklassifikation ⁵ : G01N 27/30, 27/28, 27/49	A1	(11) Internationale Veröffentlichungsnummer: WO 94/29708 (43) Internationales Veröffentlichungsdatum: 22. December 1994 (22.12.94)
---	----	--

(21) Internationales Aktenzeichen: PCT/DE94/00598
(22) Internationales Anmeldedatum: 21. Mai 1994 (21.05.94)
(30) Prioritätsdaten:
P 43 18 519.3 3. Juni 1993 (03.06.93) DE
(71) Anmelder (für alle Bestimmungsstaaten ausser US):
FRAUNHOFER-GESELLSCHAFT ZUR FÖRDERUNG
DER ANGEWANDTEN FORSCHUNG E.V. [DE/DE];
Leonrodstrasse 54, D-80636 München (DE).
(72) Erfinder; und
(75) Erfinder/Anmelder (nur für US): HINTSCHE, Rainer
[DE/DE]; Schwedter Strasse 14, D-10199 Berlin (DE).
PAESCHKE, Manfred [DE/DE]; An der Wildbahn
59, D-16352 Basdorf (DE). SCHNAKENBERG, Uwe
[DE/DE]; Birkenstrasse 10, D-10559 Berlin (DE). WOL-
LENBERGER, Ulla [DE/DE]; Ossietzkystrasse 9, D-13187
Berlin (DE).

(81) Bestimmungsstaaten: US, europäisches Patent (AT, BE, CH,
DE, DK, ES, FR, GB, GR, IE, IT, LU, MC, NL, PT, SE).
Veröffentlicht
Mit internationalem Recherchenbericht.

(54) Title: ELECTROCHEMICAL SENSOR

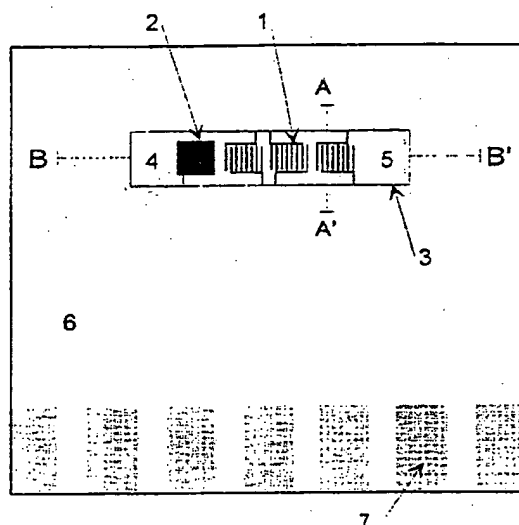
(54) Bezeichnung: ELEKTROCHEMISCHER SENSOR

(57) Abstract

The invention relates to an electrochemical sensor with interdigital micro-electrodes (1) with structure widths in the sub- μ m range. With a twin or multi-pair array of the interdigital micro-electrodes on a substrate (8), the electrochemical detection of molecules with high sensitivity is made possible and further uses for the detection of chemical reaction cycles are made available. The electrodes may be arranged in a micro-channel applied to the substrate having a constant small volume of a few nanolitres. The electrochemical sensor of the invention is suitable for the multiple measurement of the same species of molecule or as a multi-sensitive sensor in chemical analysis and process control in various fields such as biotechnology, environmental protection or health.

(57) Zusammenfassung

Die Erfindung betrifft einen elektrochemischen Sensor mit interdigitalen Mikroelektroden (1), die Strukturbreiten im sub- μ m-Bereich aufweisen. Durch arrayförmige Anordnung zweier oder mehrerer Paare der interdigitalen Mikroelektroden auf einem Substrat (8) werden die elektrochemische Detektion von Molekülen mit hoher Nachweisempfindlichkeit ermöglicht und erweiterte Einsatzmöglichkeiten zur Erfassung chemischer Reaktionsabläufe zur Verfügung gestellt. Die Elektroden können in einem auf das Substrat aufgetragenen Mikrokanal angeordnet sein, der ein konstantes, kleines Volumen von wenigen Nanolitern aufweist. Der erfindungsgemäße elektrochemische Sensor ist zur Vielfachmessung der gleichen Molekülspezies oder auch als multisensitiver Sensor in der chemischen Analytik und Prozeßkontrolle auf verschiedenen Gebieten wie Biotechnologie, Umweltschutz oder Gesundheitswesen einsetzbar.



LEDIGLICH ZUR INFORMATION

Codes zur Identifizierung von PCT-Vertragsstaaten auf den Kopfbögen der Schriften, die internationale Anmeldungen gemäss dem PCT veröffentlichen.

AT	Österreich	GA	Gabon	MR	Mauretanien
AU	Australien	GB	Vereinigtes Königreich	MW	Malawi
BB	Barbados	GE	Georgien	NE	Niger
BE	Belgien	GN	Guinea	NL	Niederlande
BF	Burkina Faso	GR	Griechenland	NO	Norwegen
BG	Bulgarien	HU	Ungarn	NZ	Neuseeland
BJ	Benin	IE	Irland	PL	Polen
BR	Brasilien	IT	Italien	PT	Portugal
BY	Belarus	JP	Japan	RO	Rumänien
CA	Kanada	KE	Kenya	RU	Russische Föderation
CF	Zentrale Afrikanische Republik	KG	Kirgisistan	SD	Sudan
CG	Kongo	KP	Demokratische Volksrepublik Korea	SE	Schweden
CH	Schweiz	KR	Republik Korea	SI	Slowenien
CI	Côte d'Ivoire	KZ	Kasachstan	SK	Slowakei
CM	Kamerun	LI	Liechtenstein	SN	Senegal
CN	China	LK	Sri Lanka	TD	Tschad
CS	Tschechoslowakei	LU	Luxemburg	TG	Togo
CZ	Tschechische Republik	LV	Lettland	TJ	Tadschikistan
DE	Deutschland	MC	Monaco	TT	Trinidad und Tobago
DK	Dänemark	MD	Republik Moldau	UA	Ukraine
ES	Spanien	MG	Madagaskar	US	Vereinigte Staaten von Amerika
FI	Finnland	ML	Mali	UZ	Usbekistan
FR	Frankreich	MN	Mongolei	VN	Vietnam

BESCHREIBUNG

ELEKTROCHEMISCHER SENSOR

Technisches Gebiet

Die Erfindung betrifft einen elektrochemischen Sensor nach dem Oberbegriff des Anspruchs 1.

Elektrochemische Sensoren mit interdigitalen (d.h. fingerartig ineinandergreifenden) Mikroelektroden sind für die chemische Analytik und Prozeßkontrolle auf verschiedenen Gebieten wie Biotechnologie, Umweltschutz, Gesundheitswesen einsetzbar. Sie weisen kleine Diffusionslängen für elektrochemisch aktive Moleküle auf, da die Abstände zwischen den einzelnen fingerartigen Elektrodenbereichen im μm - oder sub- μm -Bereich liegen.

Stand der Technik

Bisher bekannt sind elektrochemische Sensoren mit miniaturisierten planaren Elektroden mit Geometrien oberhalb von $2\ \mu\text{m}$. Sie werden in Dünnschichttechnologie hergestellt und als Transduktoren zur Detektion von chemischen oder biochemischen Substanzen verwendet.

Mit Elektrodengeometrien zwischen 20 und $100\ \mu\text{m}$ werden nur Detektionseigenschaften der Elektroden erreicht, wie man sie auch bei konventionellen Elektroden aus dünnen Drähten findet (vgl. M. Suda et al., Proceedings Second World Congress on Biosensors, Genf, Schweiz 1992, p. 400; N.F. Sheppard, Jr. et al., Anal. Chem. 1993, 65, 1199 - 1202).

Aus L.D. Watson (Biosensors 3, 1987/88, 101-115) sind Anordnungen mit zwei parallelen und $5\ \mu\text{m}$ breiten Metaldünnschichtbändern zur Leitfähigkeitsmessung bekannt.

Für die Beschreibung von Spannungsprofilen nutzten T. Matsue et al. (Anal. Chem. 62, 1990, 407-409) eine Anordnung von 16 Elektroden mit 1 mm Länge und 0,1 mm Breite.

Eine Anordnung von sphärischen Elektroden mit Mikrometerabmessungen in der Isolierung auf einer Metallfläche wird von B. Ross et al. (Sensors & Actuators B7, 1992, 758-762) beschrieben. Durch die elektrisch parallel miteinander verbundenen Mikroelektroden entsteht dabei nur ein Meßsignal bei voltammetrischen und chronoamperometrischen Messungen.

I. Fritsch-Faules et al. (Anal. Chem. 64, 1992, 1118-1127) verwenden eine Anordnung mit 4 μm breiten und 8 μm voneinander entfernten Elektroden für die Bestimmung von Konzentrationsprofilen von Redoxzentren in Polymerfilmen.

Ein elektrochemischer Sensor mit einem Paar interdigitaler Mikroelektroden ist aus O. Niwa et al. (Anal. Chem. 62, 1990, 447-452) bekannt. An den Mikroelektroden dieses Sensors mit Strukturbreiten zwischen 0,75 und 10 μm wurden erstmals Verstärkungseffekte durch elektrochemisches Rezyklisieren von reversiblen Redoxmolekülen aufgezeigt.

Alle beschriebenen Elektroden wurden jeweils in stationären Meßverfahren eingesetzt.

Darstellung der Erfindung

Der Erfindung liegt die Aufgabe zugrunde, einen elektrochemischen Sensor anzugeben, der die elektrochemische Detektion von Molekülen mit höherer Nachweisempfindlichkeit ermöglicht und erweiterte Einsatzmöglichkeiten zur Erfassung chemischer Reaktionsabläufe bietet.

Die erfindungsgemäße Lösung dieser Aufgabe ist in Anspruch 1 angegeben. Weiterbildungen und besondere Ausgestaltungen der Erfindung sind Gegenstand der Unteransprüche.

Erfindungsgemäß weist der elektrochemische Sensor nach Anspruch 1 zwei oder mehr Paare interdigitaler Mikroelektroden mit Strukturbreiten unter 1 μm auf, die als Mikroelektrodenarray auf einem Substrat angeordnet sind. Die einzelnen Paare sind unabhängig voneinander mit elektrischen Potentialen be-

aufschlagbar, und die Meßeffekte an den einzelnen Elektroden sind unabhängig voneinander ableitbar. Unter Meßeffekten sind hier insbesondere amperometrische, potentiometrische oder impedimetrische Effekte zu verstehen. Vorzugsweise wird ein planares Substrat aus Glas, Saphir, Silizium oder Polymeren verwendet, wobei die Elektroden in Planartechnologie aufgebracht werden. Durch die Feinstrukturierung der Elektroden wird erreicht, daß die Abstände zwischen den interdigitalen, d.h. fingerartig angeordneten Mikroelektroden (z.B. Abstände von ca. 700 nm) klein werden gegenüber den Entfernungen, die nachzuweisende Moleküle während der Meßzeit zurücklegen. Dies ermöglicht es, das gleiche Molekül mehrfach elektrochemisch zu erfassen, z.B. es wiederholt zu oxidieren und zu reduzieren, bevor es aus dem Elektrodenbereich wegdiffundiert ist.

Auf diese Weise erreicht man besonders vorteilhafte Verstärkungseffekte. Die erfindungsgemäße mehrfache Anordnung dieserart feinstrukturierter Elektrodenpaare führt in vorteilhafter Weise zur Multiplikation des eben beschriebenen Verstärkungseffektes, indem mit geeigneter Multielektrodenmeßtechnik (z.B. mit einem rechnergestützten Multipotentiometer) sowohl simultane Messungen als auch die Wiedererfassung von Molekülspezies, die vorher an einem benachbarten interdigitalen Mikroelektrodenpaar erzeugt wurden, realisiert werden. Simultane Messung und Wiedererfassung führen zu einer signifikanten Verbesserung der analytischen Nachweisempfindlichkeit.

Zusätzliche vorteilhafte Einsatzmöglichkeiten des erfindungsgemäßen Sensors sind weiter unten beschrieben.

Die Mikroelektroden bestehen gemäß Anspruch 2 vorzugsweise aus dünnen Schichten von Edelmetallen und/oder potentialbildenden Metalloxiden (z.B. Silber-Silberhalogenid) oder Metallsalzen. Diese dünnen Schichten sind als Dünnschichtelektroden so in die Substratoberfläche eingelegt bzw. eingegraben, daß eine Planarisierung der Oberfläche und gleichzeitig eine mechanische Stabilisierung der Elektroden erreicht wird. Durch die Planarisierung wird die Diffusionscharakteristik zwischen zwei benachbarten Elektroden optimiert.

Eine besonders vorteilhafte Weiterbildung des erfindungsgemäßen Sensors besteht nach Anspruch 3 darin, daß sich die aktiven Flächen der Mikroelektroden in einem Mikrokanal mit Zu- und Abflußöffnung befinden, der auf das Substrat

aufgebracht ist. Der Mikrokanal kann z.B. ein Kanal oder Graben aus geätztem oder laserstrukturiertem Silizium oder Polymeren sein, der auf das Substrat aufgeklebt oder gebondet ist. Das gesamte Mikroelektrodenarray ist somit in einem definierten und konstanten Raum geringen Volumens, dem erfindungsgemäßen Mikrokanal, angeordnet. Der besondere Vorteil dieser Anordnung ergibt sich aus dem konstanten und kleinen Volumen von wenigen Nanolitern, das die Mikroelektroden umgibt und hochempfindlich kleinste Veränderungen der zu untersuchenden Substanz zu messen gestattet. Bei in Kanalrichtung in Reihe angeordneten interdigitalen Mikroelektrodenpaaren (die fingerartigen Elektrodenbereiche sind senkrecht zur Kanalrichtung angeordnet) ergibt sich die Möglichkeit, gleichzeitig oder zeitversetzt an verschiedenen Stellen des Mikrokanals zu messen.

Als besondere Ausgestaltung ist nach Anspruch 4 der Mikrokanal als mechanisches Hilfsmittel zur Immobilisierung oder Rückhaltung von chemischen oder biochemischen Komponenten ausgebildet, indem z.B. durch schräge oder überstehende Kanalwände Polymerfilme mit immobilisierten Biokomponenten fixiert werden können. Durch siliziumgeätzte Gitter gelingt auch die Retention von chemisch beladenen Mikrokugeln, wobei der Mikrokanal in diesem Fall als Reaktorgefäß dient.

Nach Anspruch 5 sind auf dem Substrat zusätzlich zu den Mikroelektrodenarrays, z.B. als umgebende Fläche, weitere flächige Elektroden als Arbeits- oder Bezugselektroden angeordnet.

Eine Weiterbildung des erfindungsgemäßen elektrochemischen Sensors ist in Anspruch 6 angegeben. Die Weiterbildung betrifft die flüssigkeitsresistente Isolation der Leiterbahnen, die die Mikroelektroden mit Kontaktflächen am Rand des Substrats verbinden, durch eine isolierende Schicht, vorzugsweise aus Siliziumoxid, Siliziumnitrid oder Photolacken. Die isolierende Schicht ist so aufgebracht, daß die aktiven Flächen der Mikroelektroden für das analytische Medium und die Kontaktflächen für elektrische Kontaktierungen zugänglich bleiben.

Der erfindungsgemäße elektrochemische Sensor hat eine Vielzahl von Einsatzmöglichkeiten. So läßt er sich z.B. zur simultanen Vielfachmessung der gleichen Molekülspezies einsetzen. Wie in Anspruch 7 dargelegt, können durch Vielfachmessung des gleichen Meßeffektes mit der Mehrfachanordnung der interdigitalen Mikroelektroden die amperometrischen, potentiometrischen oder impedimetrischen Meßeffekte an den einzelnen Mikroelektroden ausgemittelt werden. Jeder Meßeffekt wird entsprechend der Zahl n der Mikroelektroden n -fach gemessen und somit gemäß der Quadratwurzel aus n das Signal-Rausch-verhältnis bzw. die Empfindlichkeit der Gesamtmessung verbessert.

Eine weitere Verwendungsmöglichkeit des erfindungsgemäßen Sensors besteht gemäß Anspruch 8 in der gleichzeitigen oder zeitversetzten Detektion unterschiedlicher elektrochemischer Reaktionen oder zur Detektion des zeitlichen Verlaufs der gleichen oder unterschiedlicher elektrochemischer Reaktionen. Durch gleichzeitiges oder zeitversetztes Anlegen unterschiedlicher Potentiale an die einzelnen Mikroelektroden können verschiedene elektrochemische Prozesse, die an den jeweiligen Elektroden ablaufen, gleichzeitig oder zeitversetzt detektiert werden. Zeitversetzte Applikation der Potentiale an räumlich eng benachbarten Mikroelektroden bietet außerdem die vorteilhafte Möglichkeit, schnelle Reaktionen zeitlich verfolgen zu können. Das Meßverfahren der Puls polarographie kann durch zeitlich alternierendes Anlegen der Potentiale an die Mikroelektroden ebenfalls angewendet werden.

Nach Anspruch 9 läßt sich der erfindungsgemäße Sensor zur Messung der Strömungsgeschwindigkeit einer analytischen Probe, der zeitlichen Probenveränderung oder von Durchmischungseffekten der Probe verwenden, indem elektrochemisch aktive Moleküle der Probe an verschiedenen Elektroden durch örtlich und/oder zeitlich versetzte Detektion gemessen werden. Ein wesentlicher Vorteil ergibt sich bei der Messung, wenn die Mikroelektroden in einem Mikrokanal gemäß Anspruch 3 mit definiertem und konstantem Volumen angeordnet sind. Vorteilhaft wird dabei an einer Elektrode eine Spezies erzeugt und an einer anderen stömungsabhängig gemessen. Durch das konstante Volumen können bei gestopptem Fluß auch die Probenveränderung mit der Zeit oder Durchmischungseffekte verfolgt werden.

Eine vorteilhafte Verwendung des erfindungsgemäßen Sensors besteht nach Anspruch 10 darin, die Aktivität von Enzymen, die bei Einsatz geeigneter Enzymsubstrate die Freisetzung eines elektrochemisch reversiblen Produktes katalysieren, mit hoher Empfindlichkeit nachzuweisen, indem eine Mikroelektrode eines interdigitalen Mikroelektrodenpaares so polarisiert wird, daß das reduzierte Reaktionsprodukt oxidiert wird, und die andere Mikroelektrode des gleichen interdigitalen Mikroelektrodenpaares so polarisiert wird, daß das oxidierte Reaktionsprodukt reduziert wird. Damit kann die Freisetzung reversibel oxidierbarer und reduzierbarer Produkte, insbesondere hydrolytischer Enzymreaktionen, sehr empfindlich durch die mehrfache Umsetzung des Produktes der Enzymreaktion detektiert werden. Dieser Einsatz des erfindungsgemäßen Sensors erlaubt die Bestimmung von Enzymsubstraten mit hoher Empfindlichkeit und ist für den hochempfindlichen Nachweis von Enzymen geeignet.

Das Enzym kann z.B. auch selbst Analyt sein oder als Marker in Immunotests oder DNA-Hybridisierungsmethoden dienen. Hierbei werden das oder die Enzyme in gelöster Form extern inkubiert oder dem Elektrodenraum (z.B. Mikrokanal) zugeführt oder sind bereits immobilisiert im Mikroreaktionsraum angeordnet.

Die erfindungsgemäße Anordnung wird im folgenden anhand der Ausführungsbeispiele und der Zeichnungen näher erläutert.

Dabei zeigen:

Figur 1 schematisch ein Beispiel des elektrochemischen Sensors,

Figur 2 schematisch einen Querschnitt (A-A') und einen Längsschnitt (B-B') durch die Elektrodenanordnung des elektrochemischen Sensors aus Fig. 1 mit aufgebrachtem Mikrokanal (in Fig. 1 nicht gezeigt),

Figur 3 Meßkurven der Oxidation von Ferrocyanid, und

Figur 4 Meßkurven des Nachweises von p-Aminophenol.

Ausführungsbeispiel

Ein Ausführungsbeispiel für den erfindungsgemäßen elektrochemischen Sensor ist in Figur 1 gezeigt. Die interdigitalen Mikroelektroden 1 sind hier paarweise in einer Reihe gemeinsam mit der Referenzelektrode 2 auf einem planaren Silizium-Chip 8 angeordnet. Die Leiterbahnen von den Mikroelektroden 1 und der Referenzelektrode 2 zu den elektrischen Kontaktflächen 7 sind durch eine isolierende Schicht 6 abgedeckt.

Ein Querschnitt entlang der Achse A-A' und ein Längsschnitt entlang der Achse B-B' aus Figur 1 ist in Figur 2 mit aufgesetztem Mikrokanal 3 gezeigt. Der Mikrokanal 3 besteht in diesem Beispiel aus einem Silizium-Chip 9 mit anisotrop geätztem Graben, der auf den die Mikroelektroden 1 enthaltenden Silizium-Chip 8 aufgeklebt ist. Zwischen den beiden Silizium-Chips 8 und 9 befindet sich die Kleb- bzw. Dichtungsschicht 10. Zu- und Abflußöffnungen 4 und 5 des Mikrokanals 3 sind im Längsschnitt zu erkennen.

Figur 3 zeigt mit dem erfindungsgemäßen Sensor aufgenommene Meßkurven der Oxidation von Ferrocyano. Die einzelnen Maxima ergeben sich nach Zugabe von 62, 124, 250 und 500 $\mu\text{mol/l}$ Ferrocyano. Dargestellt sind die simultan erfaßten Meßkurven ($I(t)$) jeder einzelnen von vier Mikroelektroden (el.1, el.2, el.3, el.4), die Meßkurve der Parallelschaltung der vier Elektroden (parallel el.1-4) und die ausgemittelte Meßkurve aus der Simultanmessung mit den vier Elektroden (average el.1-4). Das geringere Signal-Rauschverhältnis bei der mit dem erfindungsgemäßen Sensor möglichen simultanen Vielfachmessung ist deutlich zu erkennen.

Der Verstärkungseffekt der interdigitalen Mikroelektrodenanordnung ist in Figur 4 am Beispiel von Meßkurven ($I(t)$) des Nachweises von p-Aminophenol mit wiederholter Oxidation/Reduktion an einem interdigitalen Mikroelektrodenpaar (A(Ox) und A'(Red)) dargestellt. Zum Vergleich dazu ist eine Meßkurve (B(Ox)) gezeigt, die bei konventioneller Oxidation (zweite Elektrode ohne Funktion) am gleichen Elektrodenpaar gemessen wurde. (a, b: jeweils Zugabe von 50 $\mu\text{mol/l}$ p-Aminophenol). Die deutlichen Unterschiede in der Signalthöhe zeigen den Vorteil der interdigitalen Mikroelektrodenanordnung.

Im folgenden werden zwei Ausführungsbeispiele zur Verwendung des erfindungsgemäßen elektrochemischen Sensors angegeben.

Das erste Ausführungsbeispiel betrifft die empfindliche Bestimmung der Aktivität von alkalischer Phosphatase. Der in den Figuren 1 und 2 gezeigte elektrochemische Sensor wird in ein Fließsystem eingesetzt. Mit einem Multipotentiostaten wird eine Elektrode eines interdigitalen Elektrodenpaares gegenüber einer Silber/Silberchlorid (gesättigte KCl) - Referenzelektrode (im Abfluß positioniert) auf 250 mV polarisiert. An die jeweils andere Elektrode des Elektrodenpaares wird ein Potential von -50 mV angelegt. In gleicher Weise werden an alle anderen Elektrodenpaare des interdigitalen Mikroelektrodenarrays unabhängig voneinander die entsprechenden anodischen oder kathodischen Potentiale gelegt. Die Meßlösung, bestehend aus 0,1 mol/l Phosphatpufferlösung (pH 7,0) mit 0,1 mol/l KCl, wird mit 0,8 ml/min Fließgeschwindigkeit durch die Elektrodenmikrokammer (Mikrokanal) geführt. Die Grundströme jeder Elektrode werden simultan aber unabhängig voneinander abgeleitet. Nach Injektion von 1 µmol/l p-Aminophenol werden an jeder einzelnen Anode die Erhöhung der Oxidationsströme und an jeder einzelnen Kathode die Veränderung der Reduktionsströme registriert (zum Vergleich siehe Figur 1). Die Meßdaten werden rechnerisch zu rauschverminderten gemittelten Meßsignalen verarbeitet. Durch Registrierung und Verarbeitung der Stromänderung nach Injektion von 2, 5 und 10 µmol/l p-Aminophenol wird eine Eichkurve erstellt. Gleichzeitig werden in externen temperierten Meßgefäßen Proben mit alkalischer Phosphatase mit 5 mmol/l p-Aminophenylphosphat in 1 mol/l Diethanolamin-Puffer (pH 9,8; mit 0,5 mmol/l MgCl_2 , 37°C) inkubiert. Nach 1 Minute Inkubationszeit werden 100 µl der Reaktionslösung in den fließenden Puffer der Meßanordnung injiziert. Die Veränderung der amperometrischen Elektrodensignale wird wie oben beschrieben einzeln abgeleitet und verarbeitet. Die Enzymaktivität der Meßprobe, definiert als Bildungsgeschwindigkeit von p-Aminophenol aus p-Aminophenylphosphat (1 U = 1 µmol/min), wird mit Hilfe der zuvor erstellten Eichkurve berechnet.

Im zweiten Ausführungsbeispiel wird die Aktivität von alkalischer Phosphatase, die auf einem mikrodispersen Träger immobilisiert ist, mit der im vorhergehenden Ausführungsbeispiel beschriebenen Meßanordnung bestimmt. Die Träger werden dazu in der beschriebenen Mikrokammer durch ein geätztes Siliziumgitter zurückgehalten. Nach der p-Aminophenylphosphat-Zugabe erfolgt die Registrierung der Bildung von p-Aminophenol. Die Messung, Eichung und Auswertung erfolgt analog zum vorhergehenden Ausführungsbeispiel.

PATENTANSPRÜCHE

1. Elektrochemischer Sensor mit interdigitalen Mikroelektroden (1), die Strukturbreiten im sub- μm -Bereich aufweisen,
dadurch gekennzeichnet,
daß auf einem Substrat (8) zwei oder mehr Paare der interdigitalen Mikroelektroden (1) als Mikroelektrodenarray angeordnet sind, wobei die einzelnen Paare unabhängig voneinander mit elektrischen Potentialen beaufschlagbar, und die Meßeffekte an den einzelnen Elektroden unabhängig voneinander ableitbar sind.
2. Elektrochemischer Sensor nach Anspruch 1,
dadurch gekennzeichnet,
daß die Mikroelektroden aus dünnen Schichten von Edelmetallen und/oder potentialbildenden Metalloxiden oder Metallsalzen bestehen, die so in die Substratoberfläche eingegraben sind, daß sich eine ebene Oberfläche ergibt.
3. Elektrochemischer Sensor nach Anspruch 1 oder 2,
dadurch gekennzeichnet,
daß sich die aktiven Flächen der Mikroelektroden in einem Mikrokanal 3 mit Zu- und Abflußöffnung (4, 5) befinden, der auf das Substrat aufgebracht ist.
4. Elektrochemischer Sensor nach einem der Ansprüche 1 bis 3,
dadurch gekennzeichnet,
daß der Mikrokanal so ausgebildet ist, daß er als mechanisches Hilfsmittel für die Immobilisierung von chemisch oder biologisch aktiven Substanzen genutzt werden kann.

5. Elektrochemischer Sensor nach einem der Ansprüche 1 bis 4,
dadurch gekennzeichnet,
daß auf dem Substrat zusätzlich weitere flächige Elektroden (2) als Arbeits- oder Bezugselektroden angeordnet sind.
6. Elektrochemischer Sensor nach einem der Ansprüche 1 bis 5,
dadurch gekennzeichnet,
daß Leiterbahnen, die von den Mikroelektroden zu Kontaktflächen führen, durch eine isolierende Schicht, vorzugsweise aus Siliziumoxid oder Siliziumnitrid oder Photolacken, so bedeckt sind, daß nur die aktiven Mikroelektrodenflächen für analytische Medien und die Kontaktflächen für elektrische Kontaktierungen offen zugänglich sind.
7. Verwendung des elektrochemischen Sensors nach einem der Ansprüche 1 bis 6 zur Vielfachmessung des gleichen Meßeffektes, wobei die Mehrfachanordnung der interdigitalen Mikroelektroden zur Ausmittlung der amperometrischen, potentiometrischen oder impedimetrischen Meßeffekte an den einzelnen Mikroelektroden genutzt wird.
8. Verwendung des elektrochemischen Sensors nach einem der Ansprüche 1 bis 6 zur gleichzeitigen oder zeitversetzten Detektion unterschiedlicher elektrochemischer Reaktionen oder zur Detektion des zeitlichen Verlaufs der gleichen oder unterschiedlicher elektrochemischer Reaktionen, indem an die einzelnen Mikroelektroden gleichzeitig oder zeitversetzt und/oder zeitlich alternierend unterschiedliche Potentiale angelegt werden.
9. Verwendung des elektrochemischen Sensors nach einem der Ansprüche 1 bis 6 zur Messung der Strömungsgeschwindigkeit einer analytischen Probe, der zeitlichen Probenveränderung oder von Durchmischungseffekten, indem elektrochemisch aktive Moleküle der Probe an verschiedenen Elektroden durch örtlich und/oder zeitlich versetzte Detektion gemessen werden.

10. Verwendung des elektrochemischen Sensors nach einem der Ansprüche 1 bis 6 zum Nachweis der Aktivität von Enzymen mit hoher Empfindlichkeit, die bei Einsatz geeigneter Enzymsubstrate die Freisetzung eines elektrochemisch reversiblen Produktes katalysieren, indem eine Mikroelektrode eines interdigitalen Mikroelektrodenpaares so polarisiert wird, daß das reduzierte Reaktionsprodukt oxidiert wird, und die andere Mikroelektrode des gleichen interdigitalen Mikroelektrodenpaares so polarisiert wird, daß das oxidierte Reaktionsprodukt reduziert wird.

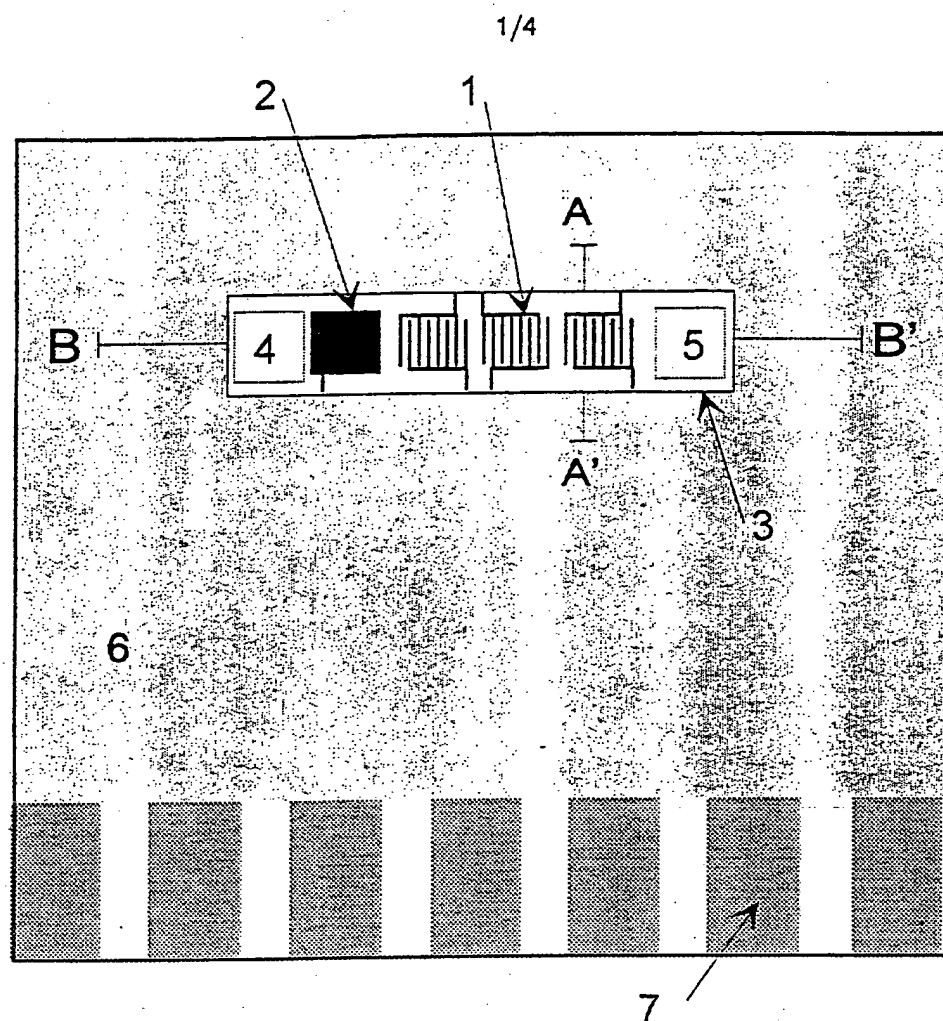


FIG.1

2/4

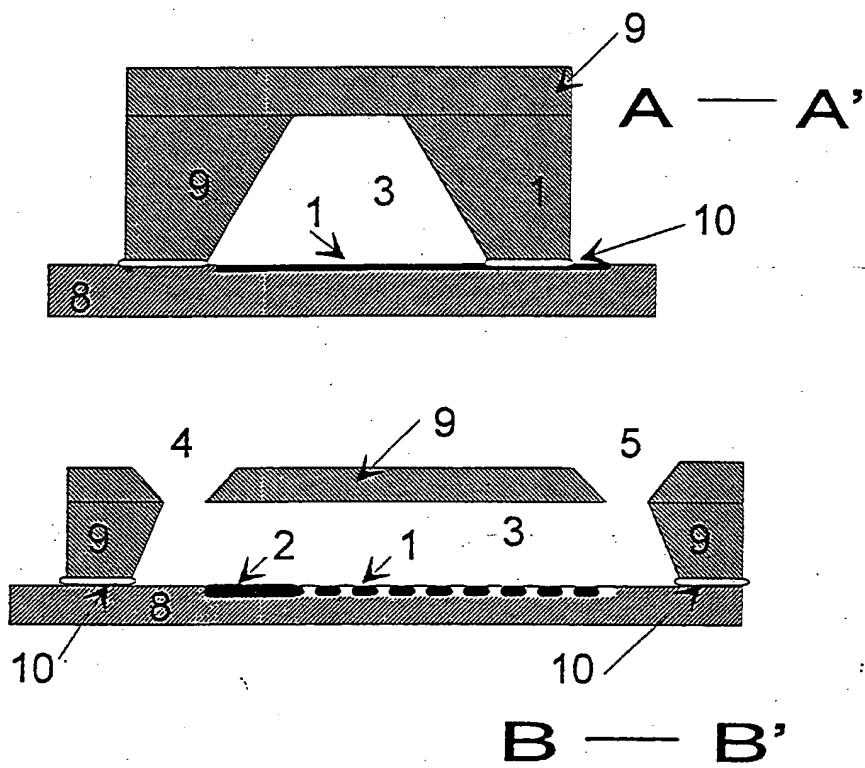


FIG. 2

3/4

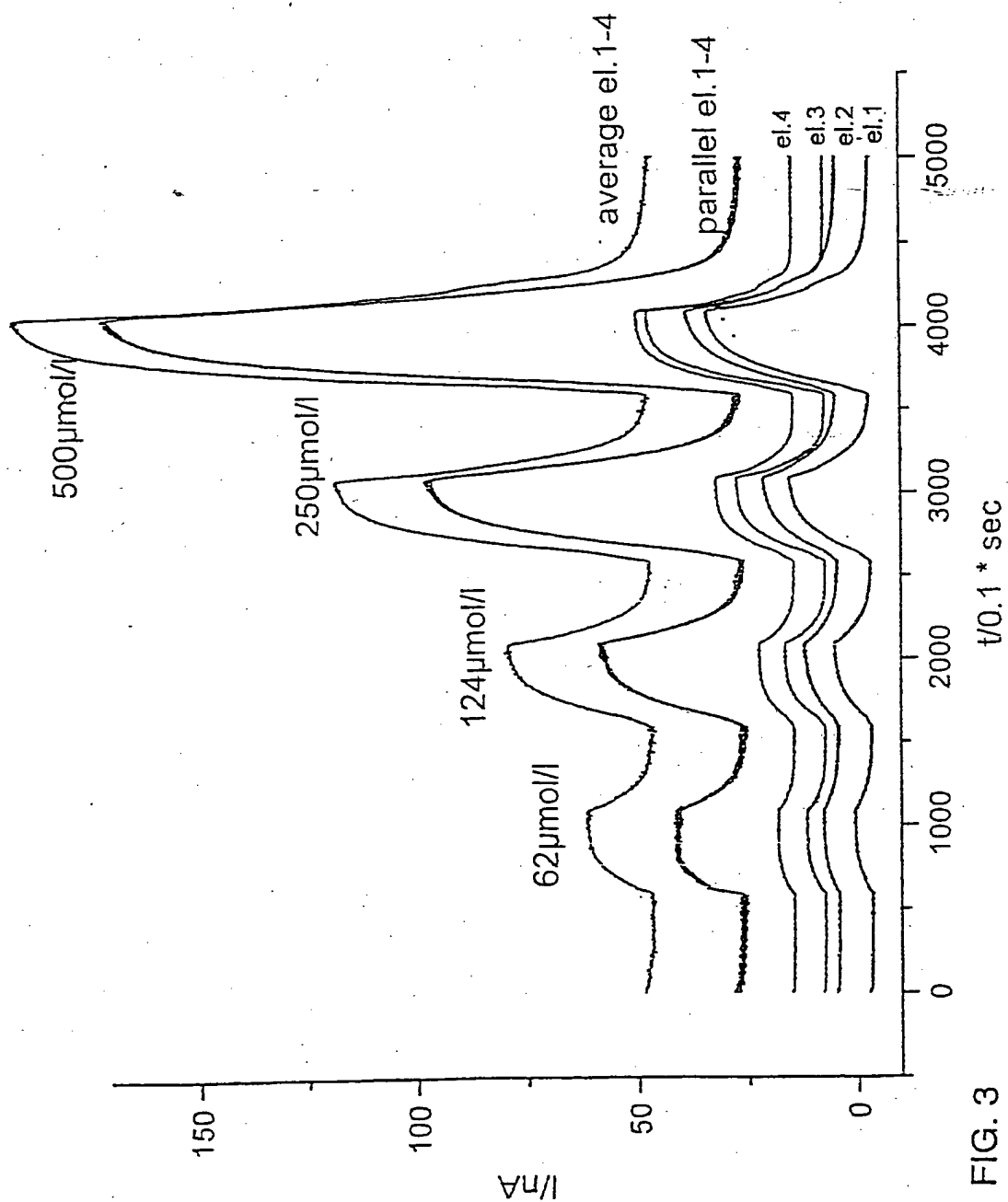


FIG. 3

4/4

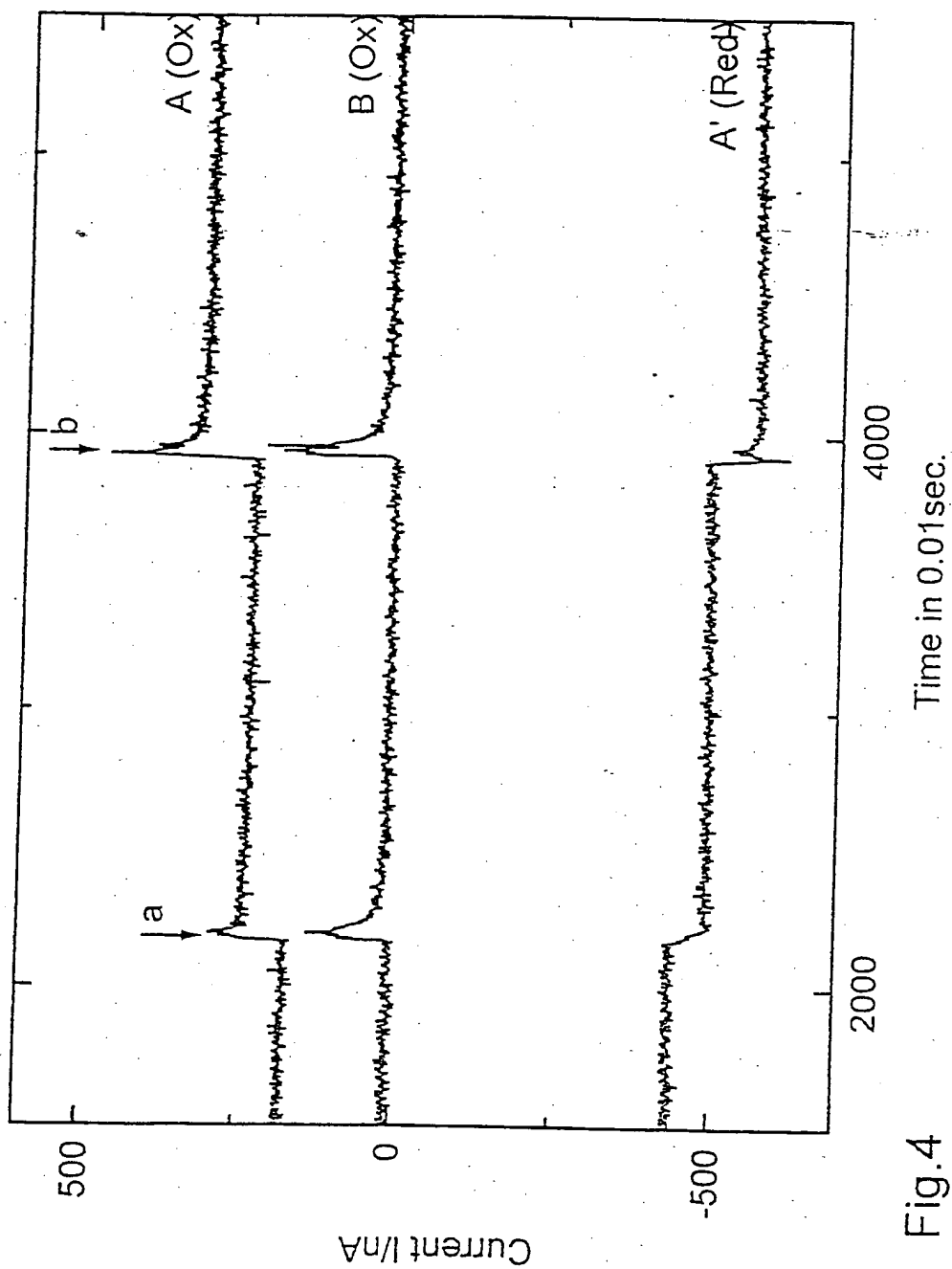


Fig.4

INTERNATIONAL SEARCH REPORT

Intern al Application No

PCT/DE 94/00598

A. CLASSIFICATION OF SUBJECT MATTER

IPC 5 G01N27/30 G01N27/28 G01N27/49

According to International Patent Classification (IPC) or to both national classification and IPC

B. FIELDS SEARCHED

Minimum documentation searched (classification system followed by classification symbols)

IPC 5 G01N

Documentation searched other than minimum documentation to the extent that such documents are included in the fields searched

Electronic data base consulted during the international search (name of data base and, where practical, search terms used)

C. DOCUMENTS CONSIDERED TO BE RELEVANT

Category *	Citation of document, with indication, where appropriate, of the relevant passages	Relevant to claim No.
X	WO,A,90 15323 (SRI INTERNATIONAL) 13 December 1990	1,2,6-8
Y	see the whole document ---	3-8,10
Y	WO,A,93 06237 (ALLAGE ASSOCIATES, INC.) 1 April 1993 see the whole document ---	4-8,10
Y	SENSORS AND ACTUATORS, vol.15, no.4, December 1988, LAUSANNE CH pages 337 - 345 SINCLAIR YEE, ET AL. 'MINIATURE LIQUID JUNCTION REFERENCE ELECTRODE WITH MICROMACHINED SILICON CAVITY' see the whole document --- -/--	3-8,10

☒ Further documents are listed in the continuation of box C.☒ Patent family members are listed in annex.

* Special categories of cited documents :

"A" document defining the general state of the art which is not considered to be of particular relevance

"E" earlier document but published on or after the international filing date

"L" document which may throw doubts on priority claim(s) or which is cited to establish the publication date of another citation or other special reason (as specified)

"O" document referring to an oral disclosure, use, exhibition or other means

"P" document published prior to the international filing date but later than the priority date claimed

"T" later document published after the international filing date or priority date and not in conflict with the application but cited to understand the principle or theory underlying the invention

"X" document of particular relevance; the claimed invention cannot be considered novel or cannot be considered to involve an inventive step when the document is taken alone

"Y" document of particular relevance; the claimed invention cannot be considered to involve an inventive step when the document is combined with one or more other such documents, such combination being obvious to a person skilled in the art.

"&" document member of the same patent family

Date of the actual completion of the international search

6 September 1994

Date of mailing of the international search report

05.10.94

Name and mailing address of the ISA

European Patent Office, P.B. 5818 Patentlaan 2
NL - 2280 HV Rijswijk
Tel. (+31-70) 340-2040, Tx. 31 651 epo nl,
Fax (+31-70) 340-3016

Authorized officer

Bosma, R

INTERNATIONAL SEARCH REPORT

Intern: al Application No

PCT/DE 94/00598

C.(Continuation) DOCUMENTS CONSIDERED TO BE RELEVANT		
Category *	Citation of document, with indication, where appropriate, of the relevant passages	Relevant to claim No.
A	ANALYTICAL CHEMISTRY, vol.62, 1990, COLUMBUS US pages 407 - 409 TOMOKAZU MATSUE, ET AL. 'MULTICHANNEL ELECTROCHEMICAL DETECTION SYSTEM FOR FLOW ANALYSIS' see the whole document ----	1-10
A	ANALYTICAL CHEMISTRY, vol.64, 1992, COLUMBUS US pages 1118 - 1127 I. FRITSCH-FAULES, ET AL. 'USE OF MICROELECTRODE ARRAYS TO DETERMINE CONCENTRATION PROFILES OF REDOX CENTERS IN POLYMER FILMS' cited in the application see the whole document ----	1-3
A	ANALYTICAL CHEMISTRY, vol.62, 1990, COLUMBUS US pages 447 - 452 OSAMU NIWA, ET AL. 'ELECTROCHEMICAL BEHAVIOR OF REVERSIBLE REDOX SPECIES AT INTERDIGITATED ARRAY ELECTRODES WITH DIFFERENT GEOMETRIES: CONSIDERATION OF REDOX CYCLING AND COLLECTION EFFICIENCY' cited in the application see the whole document -----	1

INTERNATIONAL SEARCH REPORT

information on patent family members

International Application No

PCT/DE 94/00598

Patent document cited in search report	Publication date	Patent family member(s)	Publication date
WO-A-9015323	13-12-90	NONE	
WO-A-9306237	01-04-93	US-A- 5312762	17-05-94

INTERNATIONALER RECHERCHENBERICHT

Internationales Aktenzeichen

PCT/DE 94/00598

A. KLASSIFIZIERUNG DES ANMELDUNGSGEGENSTANDES

IPK 5 G01N27/30 G01N27/28 G01N27/49

Nach der Internationalen Patentklassifikation (IPK) oder nach der nationalen Klassifikation und der IPK

B. RECHERCHIERTE GEBIETE

Recherchierter Mindestprüfstoff (Klassifikationssystem und Klassifikationssymbole)

IPK 5 G01N

Recherchierte aber nicht zum Mindestprüfstoff gehörende Veröffentlichungen, soweit diese unter die recherchierten Gebiete fallen

Während der internationalen Recherche konsultierte elektronische Datenbank (Name der Datenbank und evtl. verwendete Suchbegriffe)

C. ALS WESENTLICH ANGESEHENE UNTERLAGEN

Kategorie	Bezeichnung der Veröffentlichung, soweit erforderlich unter Angabe der in Betracht kommenden Teile	Betr. Anspruch Nr.
X	WO,A,90 15323 (SRI INTERNATIONAL) 13. Dezember 1990	1,2,6-8
Y	siehe das ganze Dokument ---	3-8,10
Y	WO,A,93 06237 (ALLAGE ASSOCIATES, INC.) 1. April 1993	4-8,10
	siehe das ganze Dokument ---	
Y	SENSORS AND ACTUATORS, Bd.15, Nr.4, Dezember 1988, LAUSANNE CH Seiten 337 - 345 SINCLAIR YEE, ET AL. 'MINIATURE LIQUID JUNCTION REFERENCE ELECTRODE WITH MICROMACHINED SILICON CAVITY' siehe das ganze Dokument ---	3-8,10
	--- -/--	



Weitere Veröffentlichungen sind der Fortsetzung von Feld C zu entnehmen



Siehe Anhang Patentfamilie

* Besondere Kategorien von angegebenen Veröffentlichungen :

"A" Veröffentlichung, die den allgemeinen Stand der Technik definiert, aber nicht als besonders bedeutsam anzusehen ist

"E" älteres Dokument, das jedoch erst am oder nach dem internationalen Anmeldedatum veröffentlicht worden ist

"L" Veröffentlichung, die geeignet ist, einen Prioritätsanspruch zweifelhaft erscheinen zu lassen, oder durch die das Veröffentlichungsdatum einer anderen im Recherchenbericht genannten Veröffentlichung belegt werden soll oder die aus einem anderen besonderen Grund angegeben ist (wie ausgeführt)

"O" Veröffentlichung, die sich auf eine mündliche Offenbarung, eine Benutzung, eine Ausstellung oder andere Maßnahmen bezieht

"P" Veröffentlichung, die vor dem internationalen Anmeldedatum, aber nach dem beanspruchten Prioritätsdatum veröffentlicht worden ist

"T" Spätere Veröffentlichung, die nach dem internationalen Anmeldedatum oder dem Prioritätsdatum veröffentlicht worden ist und mit der Anmeldung nicht kollidiert, sondern nur zum Verständnis des der Erfindung zugrundeliegenden Prinzips oder der ihr zugrundeliegenden Theorie angegeben ist

"X" Veröffentlichung von besonderer Bedeutung, die beanspruchte Erfindung kann allein aufgrund dieser Veröffentlichung nicht als neu oder auf erfinderischer Tätigkeit beruhend betrachtet werden

"Y" Veröffentlichung von besonderer Bedeutung, die beanspruchte Erfindung kann nicht als auf erfinderischer Tätigkeit beruhend betrachtet werden, wenn die Veröffentlichung mit einer oder mehreren anderen Veröffentlichungen dieser Kategorie in Verbindung gebracht wird und diese Verbindung für einen Fachmann nabeliegend ist

"&" Veröffentlichung, die Mitglied derselben Patentfamilie ist

Datum des Abschlusses der internationalen Recherche

6. September 1994

Absendedatum des internationalen Recherchenberichts

05.10.94

Name und Postanschrift der internationalen Recherchenbehörde

Europäisches Patentamt, P.B. 5818 Patentlaan 2
NL - 2280 HV Rijswijk
Tel. (+31-70) 340-2040, Tx. 31 651 epo nl,
Fax (+31-70) 340-3016

Bevollmächtigter Bediensteter

Bosma, R

C.(Fortsetzung) ALS WESENTLICH ANGESEHENE UNTERLAGEN		
Kategorie*	Bezeichnung der Veröffentlichung, soweit erforderlich unter Angabe der in Betracht kommenden Teile	Betr. Anspruch Nr.
A	ANALYTICAL CHEMISTRY, Bd.62, 1990, COLUMBUS US Seiten 407 - 409 TOMOKAZU MATSUE, ET AL. 'MULTICHANNEL ELECTROCHEMICAL DETECTION SYSTEM FOR FLOW ANALYSIS' siehe das ganze Dokument ---	1-10
A	ANALYTICAL CHEMISTRY, Bd.64, 1992, COLUMBUS US Seiten 1118 - 1127 I. FRITSCH-FAULES, ET AL. 'USE OF MICROELECTRODE ARRAYS TO DETERMINE CONCENTRATION PROFILES OF REDOX CENTERS IN POLYMER FILMS' in der Anmeldung erwähnt siehe das ganze Dokument ---	1-3
A	ANALYTICAL CHEMISTRY, Bd.62, 1990, COLUMBUS US Seiten 447 - 452 OSAMU NIWA, ET AL. 'ELECTROCHEMICAL BEHAVIOR OF REVERSIBLE REDOX SPECIES AT INTERDIGITATED ARRAY ELECTRODES WITH DIFFERENT GEOMETRIES: CONSIDERATION OF REDOX CYCLING AND COLLECTION EFFICIENCY' in der Anmeldung erwähnt siehe das ganze Dokument -----	1

INTERNATIONALER RECHERCHENBERICHT

Angaben zu Veröffentlichungen, die zur selben Patentfamilie gehören

Internationales Aktenzeichen

PCT/DE 94/00598

Im Recherchenbericht angeführtes Patentdokument	Datum der Veröffentlichung	Mitglied(er) der Patentfamilie	Datum der Veröffentlichung
WO-A-9015323	13-12-90	KEINE	
WO-A-9306237	01-04-93	US-A- 5312762	17-05-94

**Electrodeposited Iridium Oxide pH
Electrode for Measurement of
Extracellular Myocardial Acidosis during
Acute Ischemia**

Sayed A. M. Marzouk, Stefan Ufer, and Richard P. Buck

Department of Chemistry, University of North Carolina, Chapel Hill,
North Carolina 27599-3290

Timothy A. Johnson, Larry A. Dunlap, and Wayne E. Cascio

Department of Medicine, University of North Carolina, Chapel Hill,
North Carolina 27599-7075

**ANALYTICAL[®]
CHEMISTRY**

Reprinted from
Volume 70, Number 23, Pages 5054-5061

Anal. Chem. 1998, 70, 5054-5061

Electrodeposited Iridium Oxide pH Electrode for Measurement of Extracellular Myocardial Acidosis during Acute Ischemia

Sayed A. M. Marzouk,[†] Stefan Ufer, and Richard P. Buck*

Department of Chemistry, University of North Carolina, Chapel Hill, North Carolina 27599-3290

Timothy A. Johnson, Larry A. Dunlap, and Wayne E. Cascio

Department of Medicine, University of North Carolina, Chapel Hill, North Carolina 27599-7075

In the present paper, fabrication, characterization, and physiological applications of a solid-state pH electrode are described. The pH sensing layer was based on an anodic electrodeposited iridium oxide film (AEIROF). Sputtered platinum electrodes (1 mm diameter) fabricated on flexible Kapton films or platinum wires were used as planar or cylindrical supports. Each electrode site was coated with Nafion to attenuate the interference of anionic redox species and to protect the electrode surface during in vivo measurements. Performance of the AEIROF was evaluated, for the first time, as a pH electrode and proved to have a slightly super-Nernstian response with slope of -63.5 ± 2.2 mV/pH unit for both wire and planar sputtered platinum electrodes. Linear pH responses were obtained in the pH range 2–10. The electrodes have a working lifetime of at least 1 month with accuracy of about 0.02 pH unit and fast response time. The electrodes showed very low sensitivities for different species, such as Na^+ , K^+ , Li^+ , NH_4^+ , Ca^{2+} , Mg^{2+} , dissolved oxygen, lactate, ascorbate, and urate, which are important for physiological applications. The electrodes were applied in extracellular pH measurements during brief regional ischemia in a swine heart and no-flow ischemia in an isolated rabbit papillary muscle. A first report on extracellular pH, K^+ , and lactate simultaneous measurements during no-flow ischemia using the AEIROF pH electrode and the previously described K^+ and lactate electrodes is presented as well.

Intracellular and extracellular pH contribute importantly to the control of many critical physiological processes. As such, intracellular and extracellular pH values are tightly regulated despite changes in metabolic conditions that alter the production or transport of protons. One condition of significant clinical importance is myocardial ischemia. Myocardial ischemia results in cellular K^+ loss and net accumulation of protons. This myocardial acidosis was partially explained by the production and accumulation of lactic acid during anaerobic glycolysis. The electrophysiological

consequences of tissue acidification and extracellular K^+ accumulation include depressed membrane excitability, alterations in impulse propagation, and the initiation and maintenance of ventricular arrhythmias. These arrhythmias frequently accompany myocardial ischemia in humans and contribute to the high mortality rate associated with myocardial infarction. Despite the clinical importance of this condition, the relationship among cellular K^+ loss, tissue acidosis, and lactate transport in ischemic ventricular myocardium is not fully understood.^{1–3} To address this relationship, simultaneous measurements of extracellular pH, lactate, and K^+ are necessary. A goal of our laboratory is to realize simultaneous measurements of these ionic species with sufficient temporal and spatial resolution to address mechanisms of H^+ , lactate, and K^+ efflux.

Our prior accomplishments toward the goal of simultaneous measurements of these ionic species were, first, development of potentiometric sensor arrays sensitive for pH and K^+ which were employed in the perfused in situ swine heart,⁴ and second, development of two types of amperometric biosensors that were used successfully for continuous measurements of extracellular lactate accumulation in ischemic rabbit ventricular myocardium.^{5,6} Ideally, the sensors should be of very small size to allow spatial resolution and to minimize distortion of the tissue which is necessary for reliable physiological measurements. Moreover, miniaturization of the sensors allows incorporation of the three sensors into the limited available space around the isolated papillary muscle, which has been identified as a useful complementary technique^{7,8} for the whole heart in vivo measurements. Size reduction of the previously described lactate sensor⁶ by 40% has been accomplished. However, further size reduction of the potentiometric planar array pH and K^+ sensors constructed on

- (1) Wilde, A. A. M.; Alesnes, G. *Cardiovasc. Res.* 1995, 29, 1–15.
- (2) Weiss, J. N.; Shih, R.-C. *Cardiovasc. Res.* 1994, 28, 1125–1132.
- (3) Shih, R.-C.; Goel, J. L.; Stuart, J. S.; Weiss, J. N. *Circ. Res.* 1994, 74, 829.
- (4) Cosofret, V. V.; Erdosy, M.; Johnson, T. A.; Buck, R. P.; Ash, R. B.; Neuman, M. R. *Anal. Chem.* 1995, 67, 1647–1653.
- (5) Marzouk, S. A.; Cosofret, V. V.; Buck, R. P.; Yang, H.; Cascio, W. E.; Hassan, S. S. M. *Talanta* 1997, 44, 1527–1541.
- (6) Marzouk, S. A.; Cosofret, V. V.; Buck, R. P.; Yang, H.; Cascio, W. E.; Hassan, S. S. M. *Anal. Chem.* 1997, 69, 2646–2652.
- (7) Kleber, A. G.; Hegger, C. B. *J. Physiol.* 1987, 385, 307–324.
- (8) Kleber, A. G.; Hegger, C. B.; Janse M. J. *Circ. Res.* 1987, 61, 271–279.

[†] On leave from the Department of Chemistry, Ain Shams University, Cairo, Egypt.

Kapton support was limited by the manual deposition of the membrane cocktail, weaker adhesion to the support as the membrane contact area is diminished, and high impedance. Further miniaturization of, at least, pH sensors can be accomplished by replacing the polymeric membrane electrode by a solid-state analogue.

The pH-sensing capability of metal-metal oxide electrodes has been well documented.⁹⁻¹⁸ Iridium oxide electrodes, in particular, are very attractive candidates because they show (i) potential stability in aqueous solutions over a wide range of temperature and pressure, (ii) a wide pH response range, (iii) a fast response, and (iv) the lowest sensitivity to the redox interference, and (v) they are not sensitive to stirring.^{11,12,18} Available literature techniques to construct the IrO₂ pH electrodes include high-temperature oxidation of iridium wetted with NaOH,¹¹ high-temperature treatment of iridium in molten potassium nitrate,¹⁰ thermal decomposition of an iridium salt,^{15,19} anodic activation of Ir substrates in sulfuric acid,^{14,16,17} and direct IrO₂ coating by reactive sputtering.^{18,20,21} The last approach is advantageous in terms of its sufficient processing flexibility to be compatible with multiple probe microelectrode fabrication, and it is not constrained to the use of expensive iridium substrates. Unfortunately, Ir or IrO₂ sputtering was not a practical option owing to the high cost of the iridium target.

An obvious alternative is to electroplate iridium on either Kapton-based gold or platinum electrodes, followed by electrochemical activation to form the pH-sensing IrO₂ layer.^{14,16,17} However, this approach is not satisfactory because, unlike iridium metal, an electroplated Ir layer undergoes dissolution during the electrochemical activation rather than the desirable oxide growth.²² Cukman et al.^{22,23} have used electroplated ruthenium-iridium coatings to prepare stable electrodes for oxygen evolution reaction. Electrochemical activation of these coatings resulted in a net IrO₂ growth, as indicated by its electrochromic properties and cyclic voltammetric behavior. The mild conditions of this approach are suitable for the planar Kapton supports. However, preliminary investigation showed that the electrodes could be easily damaged during the electrochemical activation. The recently described²⁴

screen-printed pH electrode, prepared by simple incorporation of ruthenium oxide into the printing carbon ink, suffers from severe redox interferences, which limits its use in our present application.

On the other hand, Yamanaka has described an interesting approach²⁵ for direct anodic deposition of IrO₂ film (AEIROF) on indium-tin oxide transparent electrodes as an alternative to reactive sputtering to prepare an IrO₂-based electrochromic device. Despite the simplicity and the mild conditions of this method, the AEIROF coating has not been investigated as a pH sensor to date. We adapted this one-step process to form an IrO₂ layer directly on wire and sputtered planar Pt electrodes for miniature pH sensor fabrication. Similar to IrO₂ reactive sputtering, this approach provides several advantages: (i) it eliminates the need for sputtered or electrodeposited Ir as electrode support, (ii) it eliminates high-temperature treatment, which is inappropriate for the polymeric Kapton supports, (iii) it eliminates the electrochemical activation step when Ir is used as base electrode, and (iv) it provides the capability of fabricating planar sensor arrays. This approach is superior to the sputtering techniques in terms of cost and convenience and is suitable for preparing, not only planar electrodes but other geometries as well, e.g., wire electrodes. The objectives of this work were to investigate for the first time the use of these anodic electrodeposited iridium oxide films as a coating for pH sensor electrodes and to realize for the first time the required simultaneous extracellular pH, K⁺, and lactate measurements for cardiac physiology studies using the AEIROF pH and the previously described K⁺^{26,27} and lactate electrodes.⁶ The results show the usefulness of the AEIROF as a reliable pH sensor and the versatility of this approach to prepare planar and wire sensors. Results obtained for in situ extracellular pH measurements in a swine heart and during no-flow ischemia in an isolated rabbit papillary muscle are presented. Brief results for the first simultaneous extracellular potentiometric pH and K⁺ and amperometric lactate measurements in ischemic rabbit papillary muscle are presented as well.

EXPERIMENTAL SECTION

Materials and Reagents. Iridium tetrachloride of 99.95% purity and graphite rods, 3.05 mm in diameter of Ultra F purity were purchased from Alfa (Ward Hill, MA). Platinum wire, 1.0 mm in diameter, of 99.9% purity, oxalic acid dihydrate, Nafion solution (5 wt %), and 4-(2-hydroxyethyl)-1-piperazineethanesulfonic acid (HEPES) were purchased from Aldrich Chemical Co. (Milwaukee, WI). All other chemicals were of the analytical reagent grade. All solutions were prepared with water from a Barnstead Nanopure II system.

Apparatus. A Princeton Applied Research model 363 potentiostat/galvanostat was used for the controlled-current deposition of the iridium oxide layer. A Princeton Applied Research model 175 universal programmer was coupled for potential scanning experiments. Unless otherwise stated, all potentiometric measurements were made at room temperature in an air-conditioned laboratory at 22.5 ± 0.5 °C using either an Orion ion analyzer, model EA 920, or an Orion pH/mV meter (model 720 A) connected to a data acquisition system controlled by an IBM-compatible 486DX-33 computer. The software used for the data handling was written by C. Mundt at North Carolina State

- (9) Stock, J. T.; Purdy, W. C.; Garcia, L. M. *Chem. Rev.* 1958, 58, 611-626.
- (10) Dobson, J. V.; Sordin, R. P.; Thirsk, H. R. *Electrochim. Acta* 1976, 21, 527-533.
- (11) Papeschi, G.; Bordi, S.; Beni, C.; Ventura, L. *Biochim. Biophys. Acta* 1976, 453, 192-199.
- (12) Liu, C.-C.; Bocchicchio, B. C.; Overmyer, P. A.; Neuman, M. R. *Science* 1980, 207, 188-189.
- (13) Fog, A.; Buck, R. P. *Sens. Actuators* 1984, 5, 137-146.
- (14) Burke, L. D.; Mulcahy, J. K.; Whelan, D. P. *J. Electroanal. Chem.* 1984, 163, 117-128.
- (15) Kinoshita, K.; Madou, M. J. *J. Electrochem. Soc.* 1984, 131, 1089-1094.
- (16) Kinoshita, E.; Ingman, F.; Edwall, G.; Thulin, S.; Glab, S. *Talanta* 1986, 33, 125-134.
- (17) Hitchman, M. L.; Ramanathan, S. *Analyst* 1988, 113, 35-39.
- (18) Kinlen, P. J.; Heider, J. E.; Hubbard, D. E. *Sens. Actuators* 1994, B 22, 13-25.
- (19) Ardizzone, S.; Carugati, A.; Trasatti, S. *J. Electroanal. Chem.* 1981, 126, 287-292.
- (20) Katsube, T.; Lauks, L.; Zemel, J. N. *Sens. Actuators* 1982, 2, 339-410.
- (21) Kato, A.; Konno, Y.; Yanagida, Y.; Yamasato, M.; Taguchi, T.; Motohashi, R. *Anal. Sci.* 1991, 7, 1577-1580.
- (22) Vukovic, M.; Cukman, D.; Milun, M.; Atanasoska, L. D.; Atanasoski, R. T. *J. Electroanal. Chem.* 1992, 330, 663-673.
- (23) Cukman, D.; Vukovic, M.; Milun, M. *J. Electroanal. Chem.* 1995, 389, 209-213.
- (24) Koncki, R.; Mascini, M. *Anal. Chim. Acta* 1997, 351, 143-149.

(25) Yamanaka, K. *Jpn. J. Appl. Phys.* 1989, 28, 632-637.

University, using the labVIEW for Windows development System (National Instruments, Inc.). As a reference electrode, a double-junction Ag/AgCl electrode (Orion model 90-02) was used throughout the in vitro measurements. The outer compartment of the reference electrode was filled with 10% KNO₃.

Wafer Fabrication. Our standard procedure⁴ for the fabrication of sputtered circular disk gold electrodes on flexible polyimide Kapton substrates was modified for the platinum electrode fabrication. This change is caused by incompatibility of Ti/Pt films with wet etching procedures. A lift-off step in combination with negative photoresist was used for the patterning of the metal instead of a positive system for wet etching of Cr/Au films. Changing to a negative photoresist allows us to employ the same phototools for the photoresist exposure (UV lithography) as before. After sputtering 30 nm of Ti, followed by 200 nm of Pt, the patterned layer of photoresist underneath the two metal films was removed by submerging the wafer in acetone. The same photodefinable polyimide as described before⁴ served as a top encapsulation layer to define the electrode sites and bonding pads. All electrode substrates were fabricated at the NSF Engineering Research Center for Advanced Electronic Materials Processing and the Biomedical Microsensors Laboratory, which are both located at North Carolina State University, Raleigh, NC.

Wire Electrodes. Platinum wire, 1.0 mm in diameter, was cut into pieces (10 mm). Each piece was connected to insulated copper wire, and the active tip (~2 mm) was defined using Teflon tape. Epoxy was not used in order to avoid contamination of the electrodeposition solution.

Anodic Electrodeposition of Iridium Oxide Film. Anodic electrodeposition of iridium oxide film was performed according to the method described by Yamanaka.²⁵ The deposition solution was prepared as follows. A 75-mg portion of iridium tetrachloride was dissolved in 50 mL of water. The solution was magnetically stirred for 30 min. A 0.5-mL aliquot of aqueous 30% hydrogen peroxide solution was added, and the resulting solution was stirred for 10 min. A 250-mg portion of oxalic acid dihydrate was added, and the solution was stirred again for 10 min. The pH of the solution was adjusted slowly to 10.5 by addition of small portions of anhydrous potassium carbonate. The resulting yellow solution was covered and left at room temperature for 2 days for stabilization. The anodic deposition was performed on the sputtered Pt disk electrodes and platinum wire electrodes. A 5-cm-diameter Pt mesh was used as cathode. The recommended current density (0.16 mA/cm²) for electrodeposition on iridium-oxine electrodes²⁵ proved to be inadequate for platinum. No deposits were observed after at least 20 min. However, a current density of 0.5–1 mA/cm² gave a blue deposit on sputtered platinum within 3 min. Deposits obtained by 6 min of deposition at 1 mA/cm² proved to be adequate. To complete the construction of the pH electrode, a 0.25-μL aliquot of 5% Nafion solution was deposited onto the electrode surface and air-dried for 10 min. The electrodes were individually cut and connected to electrical wire using conductive silver epoxy (Epoxy Technology) and heated at 100 °C for 1 h. The electrical connection was then insulated with silicone rubber (Dow Corning 3140 RTV). The electrodes were conditioned in tris buffer, pH 7.0, for 2 days to stabilize the potential readings. The construction of the planar electrode is shown in Figure 1. When Pt wire was used as electrode support,

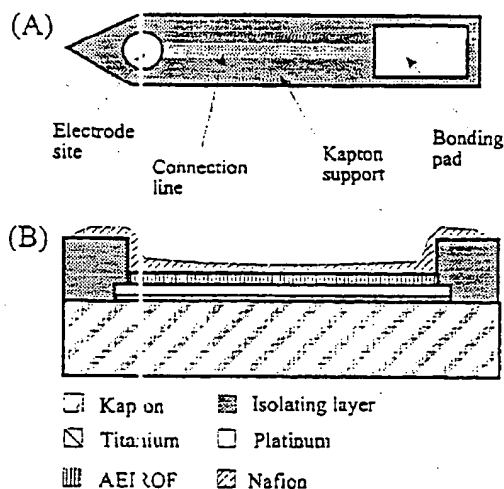


Figure 1. (A) Kapton-based planar single electrode. The edge was tapered to facilitate the electrode implantation in the myocardium. (B) Layer structure of the AEIROF-based planar pH electrode.

the deposition was carried out for 8 min at a current density of 2 mA/cm². The electrodes were coated with Nafion by dipping into 5% Nafion solution twice. The electrodes were allowed to dry between the two coatings. Heat treatment and conditioning were the same as described for the planar electrodes.

pH Measurements. The electrodes were evaluated for their pH responses in a series of buffer solutions in the pH range 2–10. The buffers were prepared by dropwise addition of 1 M solutions of HCl and NaOH to universal stock buffer solution having the following composition: 5 mM potassium hydrogen phthalate, 5 mM potassium dihydrogen phosphate, 5 mM tris(hydroxymethyl)aminomethane, 2.5 mM Borax, and 100 mM NaCl. Calibration curves covering only the physiological pH range were constructed by titrating 0.1 M phosphate buffer with 1 M HCl and 1 M NaOH between pH 6 and 8. The reproducibility of the pH responses in the pH range 2–9 was evaluated by changing the pH, randomly, by addition of 1 M HCl and 1 M NaOH to a tris buffer with 100 mM NaCl ion background [15 mM tris(hydroxymethyl)aminomethane–140 mM NaCl]. The pH values of all buffer solutions were determined with a calibrated Orion pH Ross electrode (model 81-02).

Electrode Selectivity. The selectivity of the AEIROF pH electrode was assessed under conditions relevant to the physiological applications. The iridium electrode, along with the Ag/AgCl double-junction reference electrode, was immersed in well-stirred 45-mL volume of 0.1 M tris buffer adjusted to pH 7.0 with HCl. After potential stabilization, a 5-mL aliquot of 1 M solution of NaCl, KCl, LiCl, NH₄Cl, or CaCl₂ prepared in 0.1 M tris buffer, pH 7.0, was added. The changes in millivolt reading were recorded. The effects of ascorbic, uric, and lactic acids were evaluated similarly using 0.1 M stock solution of ascorbic acid and lithium lactate prepared in 0.1 M Tris buffer and adjusted to pH 7.0. Milky suspension of 0.1 M sodium urate was obtained by brief sonication. The effect of dissolved oxygen was evaluated by allowing potential stabilization in tris buffer containing 100 mM NaCl as background. Nitrogen gas was bubbled for 15 min and then stopped for another 15 min. The potential readings were observed during changes of the oxygen tension.

Measurement of Extracellular pH in Ischemic Whole Swine Heart. All animal preparations were performed in accordance with accepted guidelines for the care and treatment of experimental animals at the University of North Carolina at Chapel Hill using established methods.^{28,29} Domestic swine ($n = 2$) weighing 30–35 kg were prepared for these studies using surgical and instrumentation techniques similar to those in a previous report.²⁹ The animals were tranquilized with Ketaset (20 mg/kg) and anesthetized with pentothal (25 mg/kg). A deep surgical plane was maintained using α -chloralose (25–50 mg kg⁻¹ h⁻¹). Mechanical ventilation and supplemental oxygen were supplied via an endotracheal tube and a Harvard ventilator. Monitored arterial blood gases were adjusted at the ventilator to maintain $pO_2 > 80$ mmHg, pCO_2 of 35–45 mmHg, and pH of 7.35–7.45. The heart was exposed via a median sternotomy and suspended in a pericardial cradle. The left anterior descending (LAD) coronary artery was dissected free from surrounding tissue midway along its length at a branch-free site and fitted with a polypropylene ligature. The extent of the ischemic zone was identified and marked by briefly occluding the LAD. The animal was heparinized (1000 units) and atrially paced (100–120 bpm).

The planar pH electrodes to be used for in situ measurements were glued back-to-back to Kapton-based Ag/AgCl reference electrodes. The reference electrodes were of the same diameter, i.e., 1 mm, and prepared from sputtered gold electrodes by electrochemical silver deposition and chloridization. As many as 10 pH electrodes were installed via plunge techniques to a midmyocardial depth (5–10 mm), well within the center of the ischemic region (≥ 10 mm), at the border zone of the identified ischemic boundary and at the normal zone. Immediately prior to insertion, electrodes were calibrated in vitro using 0.1 M phosphate buffer solutions, pH 8 and 6, containing 100 mM NaCl, respectively. The electrodes were recalibrated at the conclusion of the experiment following electrode removal. Following a 60-min stabilization period after electrode placement, each heart was subjected to four regional ischemic episodes of 10-min duration, separated by 50 min of reperfusion. Ischemia was induced by tightly securing the ligature around the LAD. The pH data were digitally collected following amplification ($\times 10$) and analogue filtration (0–1 Hz at -1 dB). Extracellular pH values were calculated for each electrode using its calibration slope and initial systemic pH values (IL blood gas analyzer). Data collection was suspended 10 min after reperfusion.

Measurement of Extracellular pH of Ischemic Rabbit Papillary Muscle. The experimental technique was described previously in detail.^{7,8} In brief, New Zealand white rabbits ($n = 6$) were anticoagulated with heparin (200 units/kg, iv) and anesthetized with sodium pentothal (40–50 mg/kg, iv). In each case, the heart was rapidly excised and arrested in cold Tyrode's solution. The atria and left ventricle (LV) free wall were removed, and the left ventricular septal surface of the tissue was pinned to a wax plate. The septal artery was cannulated with a small polyethylene catheter and perfused with a modified Tyrode's

perfusate. For each heart, restoration of perfusion required less than 5 min. The perfusate was pumped by a peristaltic pump (Digi-Saltic, Masterflex, Barrington, IL) through a custom-made membrane gas exchanger in which partial pressures of O_2 , N_2 , and CO_2 of the perfusate were controlled. The pH of the perfusate was monitored by a glass pH electrode positioned in the perfusion line before entering the septal artery. The relative amount of CO_2 was adjusted in the membrane gas exchanger to yield a pH of 7.40. The temperature of the perfusate was maintained between 36.5 and 37.5 °C. Intraarterial pressure was maintained approximately at 45 mmHg by adjustment of the perfusion flow rate. The perfused tissue preparation was secured in a custom-designed experimental chamber.⁷

The longest muscle was chosen, attached by its tendon to a piezoresistive element (Sensonor, Horton, Norway), and stimulated at 2 Hz through a platinum wire attached at the tendinous end. The chamber was closed, and the preparation was surrounded by a humidified atmosphere. The pCO_2 of the recording chamber atmosphere was adjusted to match the pCO_2 of the perfusate. In this way, the extracellular pH of the papillary muscle could be modulated in order to test the AEIROF pH electrode. Changes in extracellular pH were also measured during no-flow ischemia, which was produced by withdrawing O_2 from the chamber and arresting flow. Forty-five seconds prior to the arrest of flow, the atmosphere in the recording chamber was changed from a mixture of CO_2 , N_2 , and O_2 to a mixture of CO_2 and N_2 . The volume fractions of O_2 and CO_2 in the recording chamber were measured using a gas analyzer. The O_2 contamination of the recording chamber atmosphere during ischemia was ≤ 6 mmHg for each experiment.

A planar pH electrode was brought into contact with the muscle surface, and a miniature Ag/AgCl reference electrode, AgCl-saturated 3 M KCl, with a flexible barrel (Cypress System, Inc., Lawrence, KS) was positioned at the septum. While the muscle was perfused, the electrode was allowed to stabilize. Ischemia was induced as described above. The muscle was allowed to recover for 30 min before another ischemic event was attempted. The magnitude of extracellular acidosis was monitored by recording the change in the emf with time after arrest of flow and after reperfusion. Perfusate solutions based on bicarbonate and HEPES buffers were used. When HEPES was used, the electrode was calibrated in situ by perfusing the muscle by the end of the experiment with two HEPES buffers of pH 6.9 and 6.4, respectively. When bicarbonate-based perfusate was used, the electrode was calibrated by changing the pH of the perfusate by adjusting the pCO_2 in both the lung and the experimental chamber.³⁰ The reference pH was measured by a Ross glass electrode placed in the perfusate stream between the gas exchanger and the chamber.

Simultaneous Measurements of Extracellular pH, K^+ , and Lactate in Ischemic Rabbit Papillary Muscle. The preparation of the isolated perfused papillary muscle was as described above. Planar AEIROF pH electrodes were used for pH measurements. Potassium electrode used was a miniature polymeric ion-selective electrode, prepared as described previously.^{26,27} The conducting salt-based amperometric lactate electrode developed in our laboratory⁶ was used for extracellular lactate measurements. The active part of this electrode was reduced by 40% (1.8×1.5 mm vs $3 \times$

(26) Kléber, A. G. *Circ. Res.* 1983, 52, 442–450.

(27) Cascio, W. E.; Yan, G.-X.; Kléber, A. G. *Circ. Res.* 1990, 66, 1461–1473.

(28) Johnson, T. A.; Engle, C. L.; Boyd, L. M.; Koch, G. G.; Gwinn, M.; Gettes, L. S. *Circulation* 1991, 83, 622–634.

(29) Fleet, W. F.; Johnson T. A.; Graebner, C. A.; Gettes, L. S. *Circulation* 1985, 72, 922–931.

(30) Cascio, W. E.; Yan, G.-X.; Kléber, A. G. *Circ. Res.* 1992;70: 409–422.

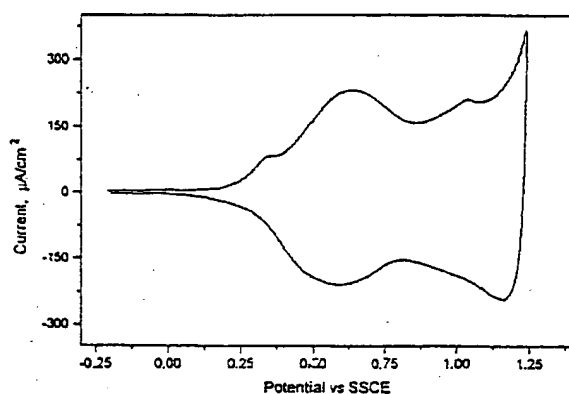


Figure 2. Cyclic voltammogram of the AEIROF on graphite; 0.5 M sulfuric acid, 50 mV/s.

1.5 mm) to fit smaller papillary muscles with typical dimensions of 1 mm (diameter) and 4 mm (length), and to improve access to the muscle for the other ion-selective electrodes. The cavity that contained the conducting salt and the enzyme was reduced by 60%. Consequently, the amount of the enzyme mixture solution used was proportionally reduced. The performance characteristics of the miniaturized electrodes are the same as those reported previously.⁶ Perfusate solution based on 10 mM HEPES buffer was used for these experiments. The electrodes were calibrated in situ, at the end of the experiment, by perfusing the muscle with two standard solutions of compositions 8 and 15 mM K⁺, 3 and 6 mM lactate, and pH 6.9 and 6.4, respectively. The standards were made using the perfusate solution. The miniature Ag/AgCl reference electrode was used as a common reference for all three electrodes. The K⁺ and pH measurements were made using a custom-made high-input impedance differential amplifier. A Princeton Applied Research model 363 potentiostat/galvanostat was used for the amperometric lactate measurements. The signal output of each electrode was measured using a separate chart recorder.

RESULTS AND DISCUSSION

Anodic Deposition of Iridium Oxide. The solution used for electrodeposition is an alkaline iridium(IV) solution containing oxalate, which prevents iridium precipitation in the alkaline medium by complex formation. Yamanaka²⁵ reported that the mechanism by which IrO₂ was formed involves anodic oxidation of the oxalato ligand to CO₂ with concomitant deposition of iridium as iridium(IV) oxide at the anode. The AEIROF showed the characteristic electrochromic behavior of IrO₂.²⁵ In the present work, the nature of the AEIROF was further proved as IrO₂ using cyclic voltammetry. Cyclic voltammograms of the AEIROF, deposited on graphite electrode (5 mA/cm² for 10 min), obtained in a 0.5 M sulfuric acid solution showed the characteristic reversible redox behavior of the activated iridium electrodes,^{31,32} as shown in Figure 2. Unlike graphite electrodes, deposits obtained on platinum electrodes tend to crack during CV experiments. CV experiments were performed during the preliminary investigations only to confirm the nature of the AEIROF, and

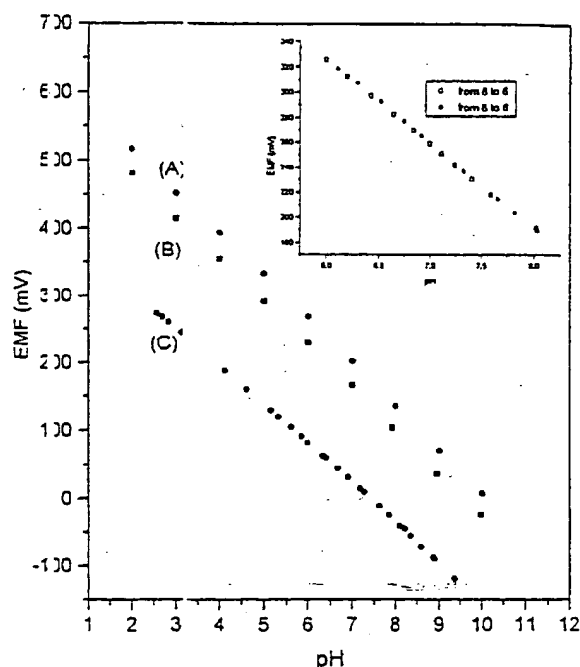


Figure 3. Typical potentiometric response of the AEIROF electrode to a series of universal buffer solutions after 2 days of conditioning. (A) Wire electrode; (B) planar electrode. (C) Potentiometric response of a planar electrode to changes in pH obtained by random additions of 1 M HCl and 1 M NaOH to tris buffer containing 140 mM NaCl as background electrolyte, after continuous soaking in tris buffer for 30 days. The inset shows the titration of 0.1 M phosphate buffer around the physiological range using a wire electrode.

because it does not have any role in the electrode fabrication, all the AEIROF electrodes on platinum were used directly without CV experiments to avoid damaging the pH-sensing layer. Although the color of the deposit may vary from blue to purple or even deep green, the performance of the electrode was found to be insensitive to small changes ($\pm 20\%$) in the deposition conditions, such as deposition time and current density, as long as the AEIROF was complete and uncracked. Typically, deposition for 6 min at a current density of 1 mA/cm² was found to be satisfactory.

Analytical Performance. No significant difference was found in the response of wire and planar electrodes. All the following results were obtained with planar electrodes unless otherwise stated. The AEIROF electrodes showed linear responses in series of universal buffer solutions (UB) in the pH range between 2 and 10, as shown in Figure 3. The linear response indicates that the different anions present in the UB do not have an adverse effect on the pH response, at least at comparable concentration levels, of the AEIROF electrodes. This presents an advantage over the polymeric-based pH electrodes, which cannot be used in the presence of the commonly used phthalate buffers due to the extraction of the lipophilic phthalate into the polymeric membranes. The AEIROF electrodes showed a near-Nernstian response of -63.5 ± 1.2 mV/pH unit after 2 days of conditioning in tris buffer, pH 7.0. This slightly super-Nernstian behavior is closer to the Nernstian response reported for IrO₂ electrodes prepared by thermal treatment^{11,19} or reactive sputtering^{18,20,21} than the super-

(31) Mozota, J.; Conway, B. E. *Electrochim. Acta* 1983, 28, 1-8.

(32) Conway, B. E.; Mozota, J. *Electrochim. Acta* 1983, 28, 9-16.

Nernstian (70–90 mV/pH unit at 25 °C) response reported for hydrous iridium oxide films prepared by potential cycling.^{14,16} The linear response implies that a two-point calibration, as typically made with a glass electrode, would be sufficient. After 1 month of continuous use, the electrodes showed a small reduction 2.5 ± 0.8 mV/pH unit in the calibration slopes. After the initial equilibration period, the observed potential drift was about 0.2 mV/h at the physiological relevant pH of 7.0.

The hysteresis of electrode response was assessed in two different ways. The electrodes ($n = 10$) were soaked for 10 min in UB of pH 2, 10, and 2, respectively. The hysteresis of the potential response was very small, i.e., 2.5 ± 0.6 mV. On another experiment, the electrodes ($n = 6$) were soaked in tris buffer, and the pH was randomly changed by addition of HCl and NaOH in the range between 2.5 and 9.5. The generated calibration curves showed correlation coefficients of 0.9987 ± 0.0005 . Finally, the reproducibility of the electrodes around the physiological range was determined by titrating 0.1 M phosphate buffer in the pH range of 6–8 using HCl and NaOH. The obtained correlation coefficients were 0.9996 ± 0.0002 . These results suggest that the AEIROF-based pH electrodes can be used for pH measurements when an accuracy of ± 0.02 pH unit is sufficient. Of course, the accuracy may be better when the electrodes are exposed to chemically similar samples in a narrower range of pH than we studied here, e.g., a 1 pH unit range usually encountered in cardiovascular research. This accuracy is much better than values reported for some other iridium oxide electrodes.¹⁷

The response time of the Nafion-coated AEIROF pH electrodes is fast and is quite sufficient for the present cardiovascular applications. Regardless of the pH, about 80% of the response was observed within 5 s after the pH step. However, complete response (± 0.5 mV) is somehow pH dependent, i.e., 0.5, 1.5, and 1 min for pH steps in the pH regions <5, 5–7, and >7, respectively. A similar behavior was observed by others for Nafion-coated sputtered IrO₂ electrodes.¹⁸

The selectivity studies showed that none of the tested cations, i.e., Na⁺, K⁺, Li⁺, NH₄⁺, Ca²⁺, and Mg²⁺, had an adverse effect on the potential response at the physiological relevant pH of 7. Because lactate ion is formed during ischemia, the effect of its presence on the potential response was tested and proved not to show interference. Redox interference is a known problem for metal oxide electrodes. However, iridium oxide is the most advantageous in this respect. Biologically relevant redox systems, such as ascorbic and uric acids and dissolved oxygen, were tested in the present work. There is no interfering effect observed for ascorbate or urate. The effect of dissolved oxygen was investigated by observing the potential change of the pH electrodes ($n = 10$) soaked in tris buffer, pH 7, before and after N₂ bubbling. The decrease in the potential readings after 15 min of N₂ bubbling was about 2–3 mV. A glass electrode immersed in the same solutions showed an increase of pH by about 0.03 pH unit, probably due to the removal of dissolved CO₂ by nitrogen bubbling. This result shows that dissolved oxygen has a minor interfering effect on the electrode response. This is a crucial point for cardiovascular applications investigating the physiology of ischemia, hypoxia, or anoxia because of the dramatic changes in oxygen tension during the experiments, e.g., normal perfusion ($pO_2 \approx 150$ mmHg) and ischemia ($pO_2 \leq 6$ mmHg). This is a

significant advantage of the present simple approach to construct metal oxide pH sensors over the recently described metal oxide–carbon ink pH electrode,²⁴ which suffers from severe redox interference.

Because the primary application of the newly developed electrodes is in vivo measurements of extracellular acidosis during ischemia in swine heart, the pH electrodes ($n = 6$) were soaked in heparinized swine blood for 6 h. This is longer than a typical experiment. Their responses were then observed in blood in the range of 6.5–7.6 by addition of HCl and NaOH. The electrodes showed very good stability after blood contact and retained their slope values and linear range.

There is one more advantage offered by metal oxide electrodes over the polymeric pH electrodes for measurements of extracellular cardiac acidosis. It is known that ischemia is accompanied by a dramatic increase in CO₂ (from 35 to 200 mmHg) tension, which can diffuse through the polymeric membrane to the inner hydrogel layer and lower its pH value. This error possibility was eliminated with metal oxide electrodes.

Measurement of Extracellular pH in Ischemic Myocardium. In normal aerobic metabolism, there is a close balance between H⁺ production and its buffering, such that intracellular and extracellular pH values remain nearly constant.^{23,24} However, under conditions of oxygen deprivation, e.g., significant reduction or arrest of coronary blood flow, this balance is significantly disturbed, and intracellular pH declines from values around 7.2²⁵ to 6.3²⁶ or even 5.7.²⁷ The net H⁺ accumulation is mainly attributed to loss of oxidative phosphorylation and the generation of protons as a consequence of anaerobic glycolysis.

In the present work, the presented data were intended to show the reliability of the developed electrodes to participate in cardiovascular physiology studies that require measurements of the extracellular pH in different preparations, such as swine heart and arterially perfused rabbit papillary muscle. Despite the relatively large number of previous reports by others for construction of iridium oxide pH electrodes, no significant applications have been presented.^{14–21} To our best knowledge, this is the first attempt of application of an iridium oxide pH electrode to physiological preparations. Figure 4 shows data obtained from three different electrodes implanted in normal (nonischemic) and in the margin and center of the ischemic zone during 10 min of regional acute ischemia during an initial occlusion. Data from these representative electrodes are shown only for clarity of representation. No significant pH change was detected in the normal zone. The extent of acidosis is much greater in the center of the ischemic zone, about 1 pH unit at the end of the 10-min period of ischemia. The marginal zone showed a smaller extracellular acidification and a slower onset of acidification, with a delay of about 3 min in comparison with the central zone. This can be explained by the diffusion of CO₂, which is generated from bicarbonate upon extracellular acidification. As shown in Figure 4D, the magnitude of acidification measured by the electrode, in the center zone, is about 0.1 pH unit less than that measured

(33) Li, S.; Pionica-Worons, D. J. *Gen. Physiol.* 1990, 96, 1247–1269.

(34) Vazghy, P. L. J. *Mol. Cell Cardiol.* 1979, 11, 933–940.

(35) Roos, A.; Baron, W. F. *Intracellular pH Rev.* 1981, 61, 296–434.

(36) Opie, L. H. *Circ. Res.* 1976, 38 (Suppl. 1), S2–74.

(37) Järobus, W. E.; Taylor, G. J.; Hollis, D. P.; Nunnally, R. L. *Nature (London)* 1977, 265, 756–758.

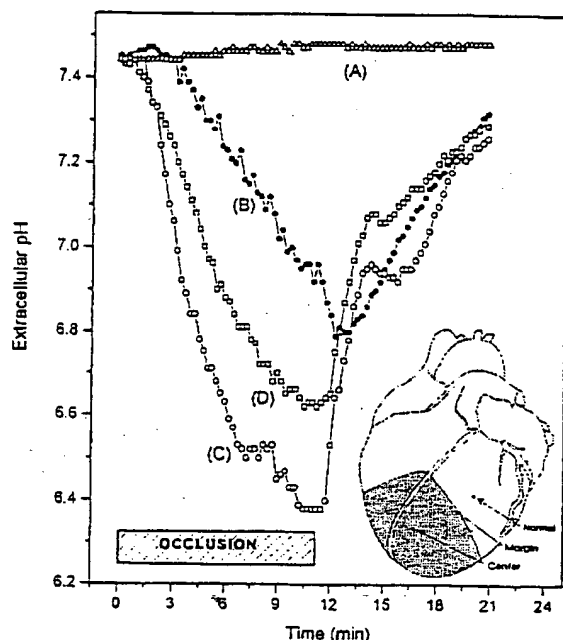


Figure 4. Extracellular pH recordings from three single planar pH electrodes implanted in the normal nonischemic zone (A) and in the margin (B) and center (C) of the ischemic zone during the first occlusion, and the same electrode in the center zone during the second occlusion (D). The corresponding implantation sites of these electrodes and the ischemic zone (dark area) are shown in the inset sketch.

during the first occlusion. This response is typical of pH changes measured from the center of the ischemic zone during sequential occlusions.²⁹

Figure 5 shows the extracellular acidosis during first and second episodes of no-flow ischemia in two different isolated rabbit papillary muscle preparations. The muscles were perfused with a solution containing 10 mM HEPES buffer at pH 7.4 before arresting the flow and after reperfusion. In this case, the initial extracellular pH value is determined by the pH value of the perfusate. The extent of acidosis measured during ischemia is greater than that observed with perfusate based on 25 mM bicarbonate buffer (data not shown) because of the lower capacity of HEPES buffer.³⁸ The shape of the curves is similar to that presented in Figure 4 for whole heart. This behavior is expected for acid accumulation during ischemia and its wash out during reperfusion.²⁹ For bicarbonate-based perfusate, the initial extracellular pH is controlled by changing the matched pCO_2 levels in the gas exchanger and the experimental chamber. Figure 6 shows the corresponding changes in the extracellular pH by changing simultaneously the pCO_2 level in the gas exchanger and the experimental chamber 10-fold during continuous perfusion. Both the on-line glass electrode and the planar AEIROF pH electrode showed the expected 1 pH unit change.

The planar pH electrode shows an initial faster response due to the immediate changes in the pCO_2 in the experimental chamber which cannot be detected by the glass electrode placed on line midway between the gas exchanger and the experimental

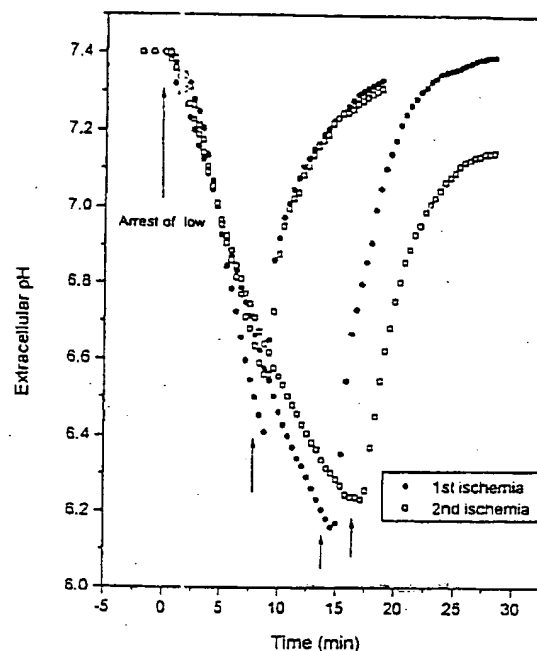


Figure 5. Extracellular pH recordings on the surface of the papillary muscle using a planar pH electrode during the first and the second episodes of no-flow ischemia. The short and long episodes correspond to two different animals. Perfusate solution (pH 7.4) contained 10 mM HEPES buffer. The upward arrows indicate restoration of flow.

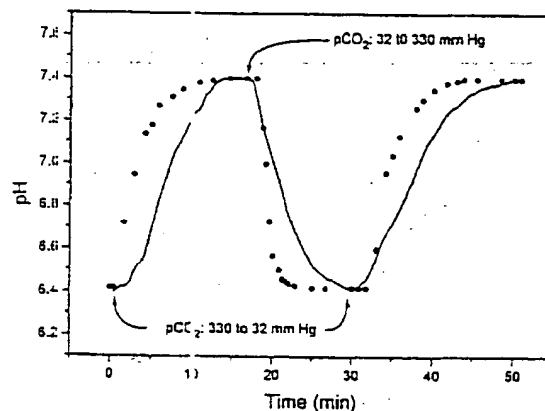


Figure 6. Extracellular pH recording on the surface of the papillary muscle using a planar pH electrode during continuous perfusion. The pCO_2 level in the gas exchanger and the experimental chamber was step changed as indicated. The dots represent the pH changes of the perfusate obtained with the on-line glass electrode.

chamber. This explains as well the faster equilibration of the glass electrode to the pH changes in the perfusate coming from the gas exchanger than the planar pH electrode placed downstream on the muscle surface. AEIROF wire pH electrodes were shown to be unsatisfactory for studies where the pCO_2 level in the chamber is not zero or at least is constant. This can be explained by the cylindrical nature of the pH-sensitive part of the wire electrode, which touches the muscle at one side and is exposed to the atmosphere inside the chamber at the other side. In such a way, the response is dictated by the CO_2 rather than the

(38) Yan, G.-X.; Kleber, A. G. *Circ. Res.* 1992, 71, 460-470.

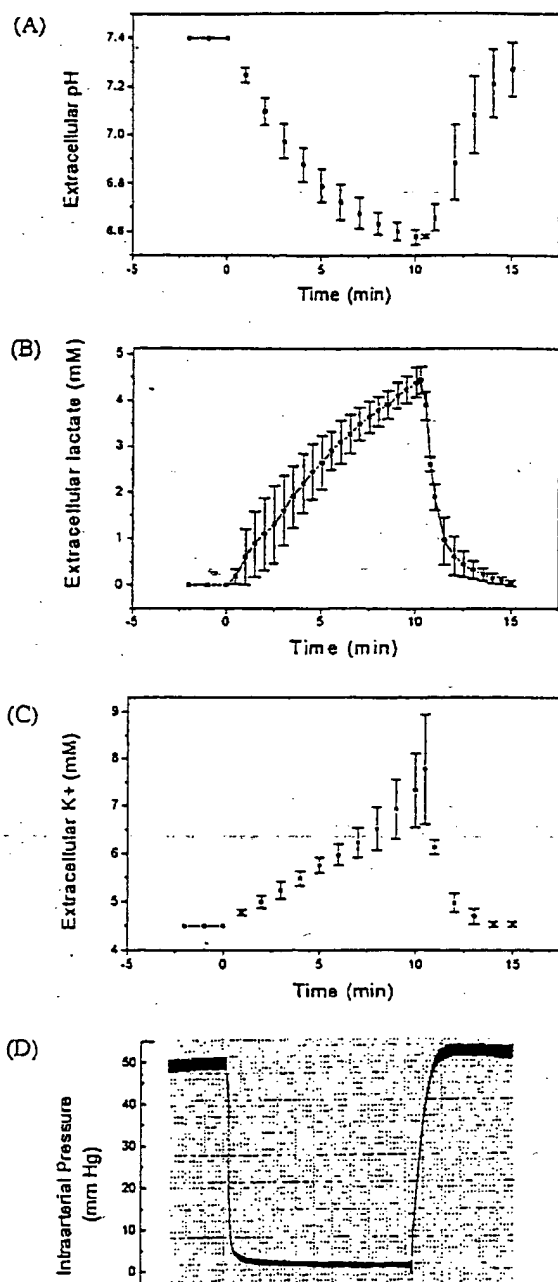


Figure 7. Simultaneous extracellular measurement of pH (A), lactate (B), and K^+ (C) during first ischemia ($n = 3$) and reperfusion of ventricular rabbit papillary muscle. (D) A real trace of the intraarterial perfusion pressure during one episode.

extracellular pH because it dissolves in the aqueous film covering the active tip and influences the pH measurements. Apparently, this will not be a limitation for use of wire electrodes if they are implanted inside the tissue, e.g., the whole heart muscle.

(39) Vandenberg, J. I.; Metcalfe, J. C.; Grace A. A. *Circ. Res.* 1993, 72, 993-1003.

Simultaneous Measurements of Extracellular pH, K^+ , and Lactate in Ischemic Rabbit Papillary Muscle. These measurements were limited, at this stage, to the papillary muscle preparation because the lactate sensor⁶ was designed specifically for this preparation and it is not suitable, in the present form, for implantation in the whole heart. Figure 7 shows the extracellular acidosis and extracellular K^+ and lactate accumulation during the first 10 min of no-flow ischemia in ventricular rabbit papillary muscle. Data were obtained from three different muscle preparations perfused with perfusate buffered with 10 mM HEPES. Arresting arterial flow reduces the intraarterial pressure to zero and initiates ischemia. Conversely, reperfusion was associated with the rapid restoration of the intraarterial pressure as shown in Figure 7D. The variation of changes in pH, K^+ , and lactate between experiments is attributed to known animal-to-animal variation. The overall changes of these values are in accordance with previously reported values for comparable ischemic periods in this preparation.^{6,39} These data represent the first simultaneous measurement of extracellular pH, lactate, and K^+ in ventricular tissue during no-flow ischemia. As shown in Figure 7, the time course of changes in pH and lactate concentration are similar during ischemia. In the absence of bicarbonate, such a relationship is expected, because sarcolemmal H^+ efflux is expected to be dependent primarily on lactate transport.³⁹ Extracellular K^+ accumulation is smaller than lactate by comparison during 4 min of ischemia. After 10 min of ischemia, the difference between K^+ and lactate accumulation narrows. This single observation suggests that a stoichiometric relationship does not exist between K^+ and lactate efflux during ischemia. This unique combination of specifically designed electrodes for concurrent use in the isolated arterially perfused papillary muscle will be used to investigate the relationships of K^+ , H^+ , and lactate efflux during ischemia.

CONCLUSIONS

The new AEIROF has excellent pH response characteristics. As such, the pH electrodes are well suited for application in cardiovascular investigations. Integration of the AEIROF pH electrodes and polymeric K^+ electrodes on much smaller planar arrays for cardiac ionic mapping is in progress. Different materials, such as stainless steel, platinized gold, and graphite, are now being tested as alternative substrates for the AEIROF to provide greater flexibility for pH electrode design. For example, tubular pH electrodes can be easily constructed from a stainless tube. In addition, application of the AEIROF to the platinum tip of a multiterminal electrode catheter is being developed for continuous measurements of intravascular pH and pCO_2 in patients.

ACKNOWLEDGMENT

This work was supported by grants P01 HL 27430 and RO1 HL 45818 from the NIH, Heart, Lung and Blood Institute.

Received for review June 3, 1998. Accepted September 15, 1998.

AC980608E

Microfabrication Technology of Flexible Membrane Based Sensors for In Vivo Applications

Richard P. Buck,** Vasile V. Cosofret,* Erno Lindner,** Stefan Ufer,* Marcel B. Adaras,* Timothy A. Johnson,***
R. Bruce Ash,**** and Michael R. Neuman*****

* Department of Chemistry, The University of North Carolina at Chapel Hill, Chapel Hill, NC 27599, USA
** Institute for General and Analytical Chemistry, Technical University of Budapest, Szent Gellert ter 4, H-1111 Budapest, Hungary
*** School of Medicine, Division of Cardiology, The University of North Carolina at Chapel Hill, Chapel Hill, NC 27599, USA
**** Department of Electrical and Computer Engineering, North Carolina State University, Raleigh, NC 27695, USA
***** Department of OB/GYN, Metro Health Medical Center, Cleveland, OH 44109, USA

Received: December 20, 1994

Final version: January 27, 1995

Abstract

Potentiometric ion-sensitive planar microelectrode arrays, and amperometric enzyme-containing biosensors were fabricated by photolithographic microelectronic technology on a flexible polyimide substrate. The steps of the microelectronics processing are summarized in more detail than previously described. The ion-selective electrodes were tested in blood serum, whole blood, and in the hamstring muscle of anesthetized rabbits. The test and performance characteristics of planar pH are emphasized, and K^+ , Na^+ , and Ca^{2+} data are included in this review. New applied results are presented from experiments where the electrodes have been implanted into an in situ porcine beating heart at the midmyocardial depth in order to monitor H^+ and K^+ changes during the course of coronary artery occlusion.

Keywords: Ion-selective electrodes, Membrane sensors, In vivo sensors, pH, Potassium ion, Calcium ion sensors

1. Introduction

Recently, we reported on the fabrication techniques and analytical performances of microelectronically fabricated ion sensors formed on flexible polyimide supports of Kapton (Du Pont) [1–5]. New sensor designs were tested using pH-sensitive PVC (polyvinyl chloride) membranes, cast from conventional and different modified PVCs, and incorporating various ionophores (tridodecylamine or phenoxazine derivatives) and plasticizers. Ionophores and ion exchanger compositions for K^+ , Na^+ , and Ca^{2+} are reported in the earlier references. In addition, these membranes have been subject to biocompatibility studies [5–7]. Membrane optimization was carried out with macroelectrodes with a massive internal solution contact. In the optimization procedure, beside the general analytical performances of the electrodes, some crucial membrane characteristics (e.g., response times, resistances) were followed with time. This article is mainly a review of our published development and characterization of flexible sensors. New results are described where our electrodes are applied in a beating porcine heart to follow changes in the proton and potassium concentrations during induced ischemia.

Results on the electrode behavior in "hostile" environments showed that modified PVCs (aminated PVC, carboxylated PVC, hydroxylated PVC) are beneficial as matrices compared with the usual high molecular weight PVC. The excellent adhesion properties of aminated and carboxylated PVC (PVC-NH₂ and PVC-COOH, respectively) to the polyimide surface are a decisive additional advantage, which is crucial in planar microelectrode fabrication [8–14]. The variation of the analytical responses and biocompatibility with the plasticizer type and quantity in the membranes has received considerable attention. In general, biocompatibility is improved if the membrane contains as little plasticizer as is possible as far as ion motion (low membrane resistance) and the maintenance of Nernstian potentiometric slopes are concerned [6, 7].

The microfabrication of reliable, reproducible, flexible, Kapton-based multi-membrane enzyme-containing ampero-

metric biosensors has also recently been achieved [15]. The technology is essentially the same as developed here for potentiometric sensors.

2. Experimental

2.1. Wafer Fabrication and Electrode Site Preparation – Potentiometric

The fabrication sequence is based on integrated circuit technology and is illustrated in Figure 1. The steps involved in the manufacture of planar electrodes on a flexible Kapton support are not simple [1]. The flexibility of the Kapton support (important in cardiology) gave rise to a number of difficulties during microelectronics processing. The Kapton wafers often became seriously bent due to differences in the dilation properties of the subsequent layers laminated on one another at different temperatures. Accordingly, the flexible sensor support was shaped on a hard silicon wafer (Fig. 1a) by spin coating a 15 μ m layer of polyimide (DuPont PI 2723 photo-definable polyimide) onto it (Fig. 1b). The silicon is only used as a substrate during fabrication to maintain wafer planarity through lithography and high-temperature processes. The polyimide layer serves as the substrate for the finished array. This polyimide layer is patterned (Fig. 1c) according to the end user's requirements (see examples in Fig. 2) to define the borders of the array. A 200 Å layer of chromium and a 2000 Å (200 nm) layer of gold are evaporated onto the patterned polyimide (Fig. 1a). The gold serves as a conductor while the chromium is used as an adhesion layer. Next the metals are patterned to define the electrode sites, bonding areas, and connecting wires. A layer of photoresist is spun onto the wafer (e) and a standard photolithography process is used to pattern it (f) to form a mask over the metal we want to retain on the wafer. The gold and chromium are chemically etched (g) and the photoresist removed (h). The metal strip left on the silicon wafer is used for layer-to-layer alignment purposes and will not be a part of the

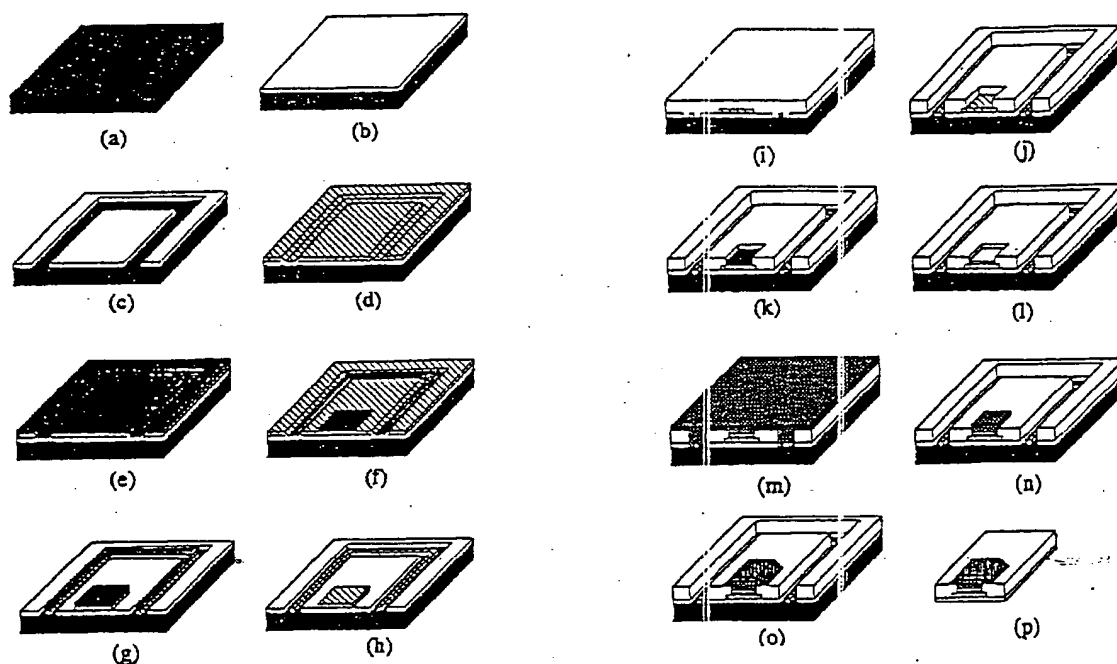


Fig. 1. The steps involved in the manufacture of planar electrodes (see details in the text).

finished array. A $30\text{ }\mu\text{m}$ layer of polyimide is spin coated onto the wafer (i) and patterned (j) to define the borders and opening for the electrode sites and bonding areas. Approximately $2\text{ }\mu\text{m}$ of silver is electroplated onto the sites (k) and a thin silver chloride layer is electrochemically deposited on top of it (l). A thin (approx. $50\text{ }\mu\text{m}$) layer of HEMA (2-hydroxyethyl methacrylate) containing 4% photo initiator (2,2-dimethoxy-2-phenyl-acetophenone) is cast onto the wafer (m) and selectively polymerized under UV (ultraviolet) light. The HEMA that is not polymerized is rinsed away with methanol, leaving hydrogel dots (poly-HEMA) on the electrode sites (n). After the hydrogel is soaked in a buffer solution (for at least 15 min in pH 7.00 Tris buffer solution containing 0.14 mol/L NaCl), an ion-selective membrane cocktail based on polyvinyl chloride is dropped onto each site (o) using a World Precision Instrument nanoliter injector (A203XVY). This is allowed to dry and the entire structure is floated off from the silicone substrate (p). At present, this final step is manual. To place the entire fabrication scheme under automation, the membrane layers are now screen printed, although this processing had not been completed at the time of writing. Some structures are shown in Figure 2.

The polyimide can be floated off from the silicon substrate by keeping the wafers in $90\text{--}95^\circ\text{C}$ aqueous electrolyte solution for several hours. Since the borders were patterned in the polyimide, the structure comes off as individual arrays ready for connection and use, rather than as a wafer of arrays. With the present design, 24 nine-site arrays (216 electrodes) are fabricated on each 3-inch (75 mm) wafer.

A number of one- and two-dimensional arrays have been fabricated as biopotential probes. Any of our flexible electrodes are biopotential probes at the exposed gold level, i.e., they can be inserted to measure the Galvani potential of a phase, as inert electrodes are generally used in the fourpoint probe experiment. However, we have found that the time constant for the establishment of any potential change is longer for inert and blocked electrodes such as gold, iridium, tungsten, and platinum

compared with Faradaic reversible electrodes. Our best example is an ion-selective probe prepared by terminating the processing at the soaked poly-HEMA stage using Ag/AgCl over gold. When these electrodes are used in media of constant chloride activity, the biopotential measurements are exceedingly rapid. The inert electrodes are commonly used in cardiology and it is not clear whether interferences from variable levels of dissolved oxygen gas cause errors, although, in principle, these inert electrodes should be sensitive to any variations in the oxygen pressure. Examples of various shaped electrodes are shown in Figure 3. The wire connections were made by using commercially available, thermally activated bonding strips (Nippon Graphite Industries, Heat Seal Connectors, Shiga Ken, Japan). Silicone rubber was applied over the entire bonding area to insulate all wire exposed to water, as well as to add mechanical stability.

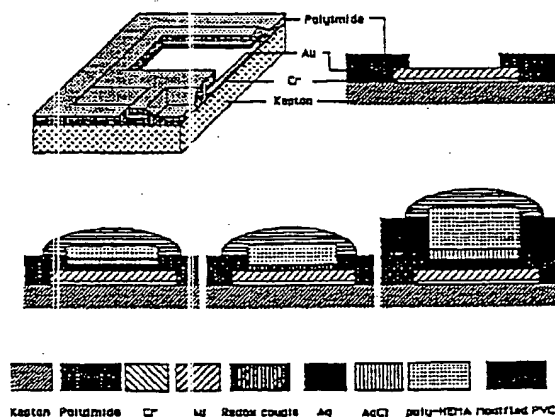


Fig. 2. Layer structures of various Kapton-based wafers and planar electrodes.

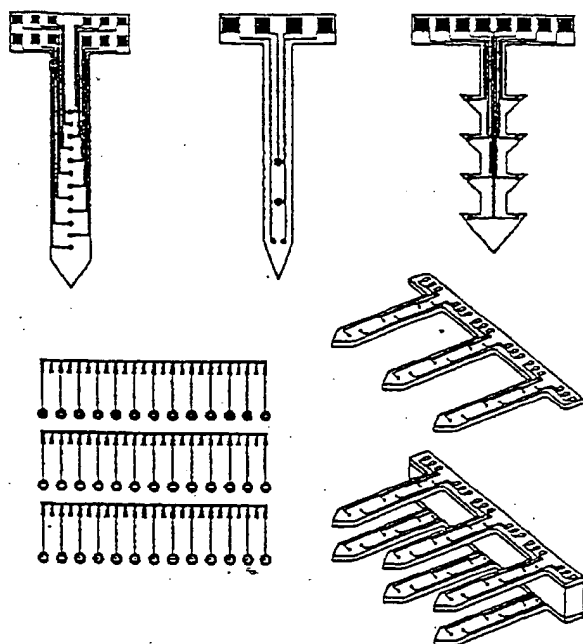


Fig. 3. Design of Kapton-based microelectrode arrays and test structures (lower left) used for biomedical applications.

2.2. Wafer Fabrication and Electrode Site Preparation – Amperometric

Fabrication of the amperometric Kapton wafers follow the same procedure up to the evaporation of gold onto the substrate. In this case, using two- or three-electrode potentiostatic control circuits, one site serves as the Ag/AgCl reference electrode. However, the two working electrodes (redundant or differential use possibilities) are platinum-plated. The remaining gold electrode is the conventional auxiliary electrode. The circular openings are generally 1 mm in diameter and exposed to the sample. Prior to plating, the Au electrodes to be platinized are cleaned by anodizing at $4\mu\text{A}$ for 20 s. Then Pt is galvanostatically deposited, using a current of $150\mu\text{A}$ for 2 min (current density 19.1 mA/cm^2). An example of an amperometric electrode substrate is shown in Figure 3.

3. Results and Discussion

3.1. General Response Characteristics

Based on the primary importance of pH-monitoring in cardiology, the new planar sensors were first tested with H^+ ion-sensitive membranes. As shown previously, the planar pH-sensors exhibited a nearly theoretical response, excellent selectivity coefficients, appropriate long-term stability, and reproducibility [1–4]. The only disadvantages we faced with the electrode construction were the long “break-in” (soaking) time before high stability readings were achieved, and some potential drift following large concentration changes (more than one decade). This problem has now been solved in a detailed study [5].

However, the construction of the new sensor arrays allows us to detect a variety of ions at the same time when the active

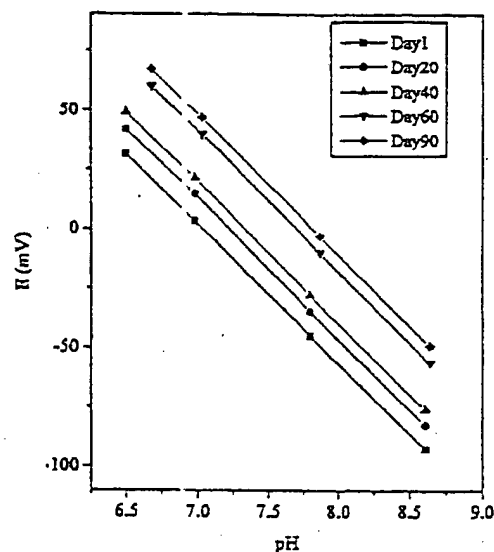


Fig. 4. Potentiometric responses of a Kapton-based pH electrode (1.0-mm diameter) in the extended physiological pH range during 90 days of continuous soaking in pH 7.0 buffer and/or in use.

sensor areas are coated with membranes sensitive to different ions, or to follow ionic inhomogeneities (across lateral zones in the heart) by applying the same membrane to several sites. Accordingly, planar electrodes with potassium- and calcium-sensitive membranes were also prepared. The only important difference in the fabrication of K^+ - and Ca^{2+} -sensors compared with planar pH sensors is that the latter was cast from aminated PVC-COOH, was used as the membrane matrix to prepare the K^+ - and Ca^{2+} -sensitive membranes. The potassium and calcium sensors incorporated valinomycin or BME 44 and ETH 1001 as ionophores, respectively. They exhibited excellent stabilities after a 24 h conditioning period (drift $< 0.1\text{ mV/h}$ for 120 h in pH 7.00 BES buffer). The slope values (tested regularly for 45 days) measured with electrodes of 0.25-mm active site diameter were found to be nearly theoretical ($58.1 \pm 0.8\text{ mV/pK}$ or $28.9 \pm 0.8\text{ mV/pCa}$, respectively) in the physiological range. In general, their analytical performances achieved or approached the features of macroelectrodes with a massive internal solution, and having the same membranes.

Figure 4 shows the recently observed response of a pH planar sensor (Ag/AgCl reference elements of 0.5-mm diameter) in the physiological pH range during a 90-day soaking period. The long-term stability of the electrode was measured by periodic calibration in buffered solutions of pH 6–9. A small drift in the offset voltage (E^0) was found within 90 days, which correlated with the small drift at any pH value. The shift in the offset voltage was much smaller than previously reported [1, 2]. This improvement in the long-term stability for the calibration plots is most likely due to the three-fold application of the membrane cocktail on each Ag/AgCl-poly-HEMA site in order to increase the amount of membrane material. An improvement in the electrode's lifetime was observed. As shown in Figure 4, the potentiometric slopes of the electrodes based on ETH 5294 (a phenoxazine derivative) did not change significantly during 90 days of continuous aqueous solution contact (slope = 59.0 mV/pH with standard deviation (SD) = 0.48 mV after 20 days of soaking; slope = 58.1 mV/pH with SD = 0.82 mV after 90 days of soaking).

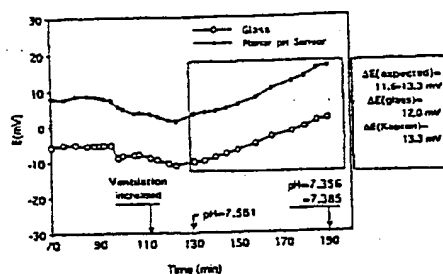


Fig. 5. Potential response of a macro glass and three planar pH sensors in a whole blood sample. The pH values indicated were determined by a blood gas analyzer. Left: Potential-time recordings before and after artificial pH changes induced by adding 1 mol/L HCl or 1 mol/L NaOH to the sample. Right: Correlation of the potential data measured in the whole blood sample (and shown on the left) with the glass and three planar electrodes. (Slopes from the top: 0.986, 0.983 and 0.979, respectively.)

Further testing included the use of blood serum of known pH and K^+ [5].

3.2. In Vivo Calibrations

Since the planar sensors have been designed for applications in living tissue, it is important that they be evaluated under these conditions. As a preliminary test of sensor performance under in vivo conditions, the planar pH sensors were intramuscularly implanted in the hamstring muscles in the legs of two anesthetized, adult, female, New Zealand white rabbits. Anesthesia was induced and maintained using intramuscularly injected ketamine and xylazine, and studies were performed for 3 h. The hamstring muscles were exposed through a small skin incision, and two 4-mm long stab wounds were made in the muscle parallel to the fibers. The polyimide-based planar pH sensors were slid into these wounds. An approximately 6-mm incision was made in a similar fashion in the muscle nearby and a laboratory combination glass electrode (5-mm diameter) was placed in this wound to serve as a standard against which the new sensors could be compared. The external reference electrode of the glass electrode serves as a reference for the planar pH-sensors as well. Cannulae were placed in the femoral artery and vein of the contra lateral leg. These were used to obtain small arterial and venous blood samples that were analyzed in a clinical blood gas analyzer, so that the tissue pH could be compared with the central circulation value.

An endotracheal cannula was also placed through a tracheostomy and connected to a ventilator. This was used to modify the animal's blood and tissue pH by changing the tidal volume and breathing rate. The induced blood pH changes were determined from time to time by the blood gas analyzer using arterial blood, and were followed continuously by the planar sensors and the macro glass electrode (see Figure 5). It is seen that the new sensors track the response from the glass electrodes, and the total potential change corresponds nicely with the calculated values based on the pH changes measured with the blood gas analyzer. The expected values were calculated on the basis of the pH values measured at the beginning and at the end of the enfram section and assuming a Nernstian slope. A range of potential change is given due to the limited reproducibility of the blood gas analyzer. However, due to the small differences in placement of the electrodes (planar vs. glass) within the muscle tissue, in addition

to the well-recognized pH difference between the capillary blood and the arterial or venous blood (arterial pH changes precede changes at the tissue level), the accuracy of the correlation is limited.

3.3. In Vivo Measurements in Porcine Hearts

Pigs weighing 28–38 kg were used in these studies. After pre-medication with ketamine (10–15 mg/kg), anesthesia was induced with thiamylal sodium (25 mg/kg) and maintained with alpha chloralose (30 mg/kg h). Ventilation via an endotracheal tube was provided by a Harvard respirator set to maintain the arterial oxygen saturation at equal to or greater than 95%, the carbon dioxide pressure between 35 and 45 mm Hg, and a pH of 7.35–7.45. Catheters were placed into the femoral artery and vein for blood pressure monitoring and venous and arterial blood sampling. After a median sternotomy, the heart was suspended in a pericardial cradle and epicardial pacing wires were sutured onto the surface of the right atria and connected to a Medtronic pacemaker. The left anterior descending coronary artery (LAD) was dissected free from the epicardial surface distal to the second diagonal branch and ligated with a thin silastic snare at a point where the zone of ischemia, identified by transient pressure on the LAD, was deemed large enough for placement of the planar pH electrodes. These electrodes were inserted to a depth > 4 mm through a small, shallow epicardial slit. Data were accepted only from electrodes demonstrating pH sensitivity within 10% of the theoretical (see Figure 6). The serum pH before and after coronary occlusion was determined using an IL Inc. whole blood gas analyzer. Extracellular hydrogen ion concentrations, expressed as pH, were calculated individually for each electrode using the calibration slope for that electrode, the pre-occlusion serum pH, and the millivolt changes produced during the TQ segment (i.e., diastole) of the electrocardiogram by each electrode throughout the course of a coronary ligation lasting 6–8 min.

3.4. Application for pH and pK^+ Change Data

It is well-known that acute myocardial ischemia often leads to impulse conduction slowing cardiac arrhythmias, ventricular fibrillation, and sudden cardiac death. Although sudden death occurs most often in individuals having recognized ischemic heart disease, unexpected cardiac arrest is the first manifestation in about 20% of all patients. While the individual events associated with acute ischemia that culminate in sudden death have been well established and extensively studied, the precise prerequisite conditions that precipitate sudden death are not understood. In spite of extensive physiological, electrochemical, and metabolic research, we remain uncertain as to why approximately 25% of acutely ischemic hearts spontaneously and unpredictably develop arrhythmias leading to ventricular fibrillation and the other 75% do not. Most researchers agree, however, that altered impulse conduction velocities (e.g., reentry circuit formation) are most likely involved. Recent studies have indicated that ionic conditions (specifically, hydrogen and potassium) have profound effects on impulse conduction [16, 17].

The cardiac impulse is actually a serial coordinated cell-to-cell membrane depolarization. This depolarization has both fast (Na^+) and slow (Ca^{2+}) channel components. The fast component of membrane depolarization can be deactivated under high extracellular potassium concentrations, while the

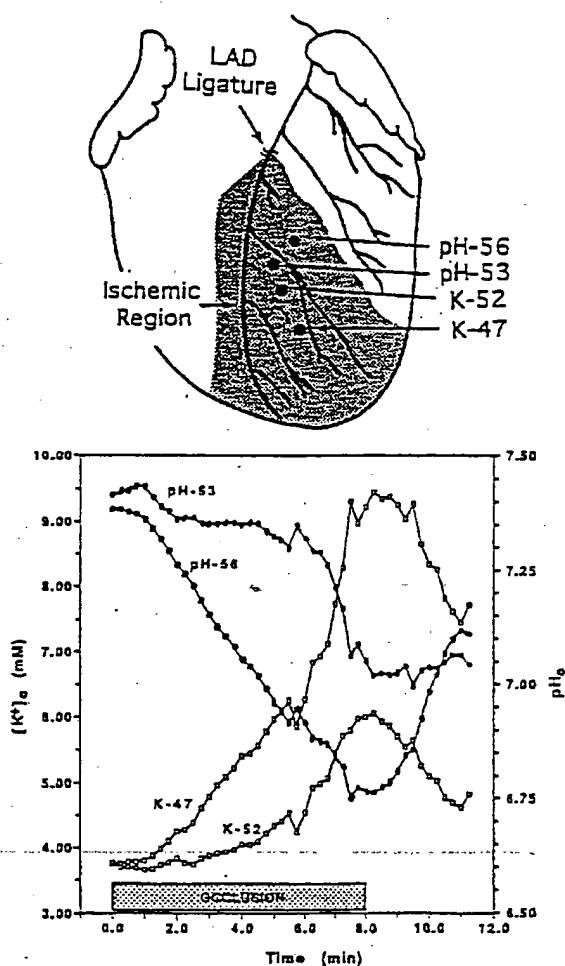


Fig. 6. Placement of two pH and two K⁺ planar sensors (active size area of 0.5-mm diameter) in the in situ porcine heart preparation at midmyocardial depth (upper panel), and the recorded fall in the pH and increase in K⁺ activity, respectively (lower panel), during 8 min of acute ischemia produced by transient occlusion of the LAD.

slow component of depolarization can be deactivated by low extracellular pH. Both ionic events are known to occur during acute ischemia in animal models, and both are known to occur heterogeneously, e.g., different variations in different places [18]. Both ionic alterations are known to occur either immediately before or simultaneously with the electrical abnormalities when hearts of animal models are subjected to the gradual withdrawal of oxygen-rich blood [19]. Given these physiological observations, it is reasonable to hypothesize that the overall slowing of conduction is precipitated by ionic changes associated with acute ischemia, and that the altered conduction pathways are a direct result of heterogeneous depolarizations caused by equally heterogeneous ionic changes in K⁺ and H⁺. Unfortunately, no direct quantitative evidence linking specific heterogeneous ionic and conduction characteristics during acute ischemia has been verified, primarily due to the sensor limitations.

Ionic changes were recorded at 15 s intervals during the course of an 8-min ischemic period produced by transient ligation [20]. In Figure 6 data are shown from two pH and two

pK⁺ sensors. Increases in both the H⁺ and K⁺ activities during ischemia are followed by the reestablishment of near-normal values in the minutes that follow.

The close correlation of potential data measured in the beating heart with both pH and K⁺ sensors and those obtained with a blood gas analyzer guarantees a reliable measurement of H⁺ and K⁺ activities. Measuring the changes in these ionic activities in the beating heart with microchemical array sensors, with several sensing spots of well-defined geometrical arrangements, will help us to determine the role that ionic changes have on the genesis of abnormal conduction disturbances with coronary disease.

4. Conclusions

Microelectronically fabricated pH, K⁺, Na⁺, and Ca²⁺ planar sensors based on polyimide substrates (Kapton) and polymeric membrane compositions demonstrate good analytical performances and extended lifetimes (up to at least three months of continuous soaking and use). The single pH and K⁺ sensors were used to monitor the increases in ionic activities during acute ischemia at several sites in a porcine beating heart. Since it is a desire by cardiovascular physiologists to use flexible multielectrodes with well-defined geometries to help describe the potential and ionic distributions in the heart as a function of time, our primary objective is to develop practical devices with good analytical and polymeric membrane properties.

5. Acknowledgements

This work was supported by the Duke-North Carolina-NCState NSF Engineering Research Center for Emerging Cardiovascular Technology Grant CDR-8622201, and NIH Grants R01 HL-49818 and P01 H127430.

6. References

- [1] E. Lindner, V.V. Cosofret, S. Ufer, R.P. Kusy, R.P. Buck, R.B. Ash, H.T. Nagle, *J. Chem. Soc., Faraday Trans.* 1993, 89, 361.
- [2] E. Lindner, V.V. Cosofret, S. Ufer, T.A. Johnson, R.B. Ash, H. Troy Nagle, M.R. Neuman, R.P. Buck, *Z. Anal. Chem.* 1993, 346, 584.
- [3] V.V. Cosofret, E. Lindner, T.A. Johnson, J.W. Kao, J.M. Anderson, R.P. Buck, *Am. Chem. Soc.* 1994, 70, 137.
- [4] V.V. Cosofret, E. Lindner, T.A. Johnson, M.R. Neuman, *Talanta* 1994, 41, 931.
- [5] V.V. Cosofret, M. Erdos, E. Lindner, T.A. Johnson, R.P. Buck, W.J. Kao, M.R. Neuman, J.M. Anderson, *Anal. Lett.* 1994, 27, 3039.
- [6] E. Lindner, V.V. Cosofret, S. Ufer, R.P. Buck, W.J. Kao, M.R. Neuman, J.M. Anderson, *J. Biomed. Mater. Res.* 1994, 28, 591.
- [7] V.V. Cosofret, M. Erdos, R.P. Buck, W.J. Kao, J.M. Anderson, E. Lindner, M.R. Neuman, *Analyst* 1994, 119, 2283.
- [8] R.P. Kusy, J.Q. Whitley, F.P. Buck, V.V. Cosofret, E. Lindner, *J. Mater. Sci. Lett.* 1994, 13, 849.
- [9] R.P. Kusy, J.Q. Whitley, F.P. McIntyre, R.P. Buck, V.V. Cosofret, E. Lindner, *Thermochim. Acta* 1994, 243, 265.
- [10] R.P. Buck, V.V. Cosofret, E. Lindner, *Anal. Chim. Acta* 1993, 282, 273.
- [11] V.V. Cosofret, E. Lindner, R.P. Buck, R.P. Kusy, J.Q. Whitley, *Electroanalysis* 1993, 5, 725.
- [12] R.P. Kusy, J.Q. Whitley, F.P. Buck, V.V. Cosofret, E. Lindner, *Polymer* 1994, 35, 2141.
- [13] V.V. Cosofret, R.P. Buck, M. Erdos, *Anal. Chem.* 1994, 66, 1592.
- [14] E. Lindner, V.V. Cosofret, T.M. Nahir, R.P. Buck, in *Diagnostic Biosensor Polymers* (Eds: A.M. Usmani, N. Akmal) ACS Symposium Series, Vol. 556, ACS Washington DC 1994, Chap. 12, pp. 149–157.
- [15] M.B. Madaras, I.C. Popescu, S. Ufer, R.P. Buck, *Anal. Chim. Acta*, submitted.

- [16] M.J. Janse, A.L. Wit, *Physiol. Rev.* 1989, 69, 1049.
 [17] L.S. Gettes, W.E. Cascio, in *Heart and Cardiovascular System - Scientific Foundations* 2nd ed. (Ed: H. Fozzard), Raven Press, New York 1992, pp. 2021-2054.
 [18] T.A. Johnson, C.L. Engle, R.P. Kusy, S.B. Knisley, C.A. Graebner, L.S. Gettes, *Am. J. Physiol.* 1990, 258, H1224.
 [19] I. Watanabe, T.A. Johnson, J.W. Buchanan, C.L. Engle, L.S. Gettes, *Circulation* 1987, 76, 127.
 [20] V.V. Cosofret, T.A. Johnson, M. Erdosy, R.P. Buck, E. Lindner, in *The Polymeric Material Encyclopedia: Synthesis, Properties and Applications* (Ed: J. Salamone), CRC Press, Boca Raton, FL, 1995.

Medical and Dental Materials

Medical and Dental Materials

edited by D.F. Williams
(University of Liverpool)

Volume 14 from the series
Materials Science and Technology edited by
R.W. Cahn, P. Haasen and
E. J. Kramer

1992. XX, 441 pages with
132 figures and 55 tables.
Hardcover. DM 450.00.
ISBN 3-527-26827-8

The application of metals, ceramics, and polymers in medical and dental engineering is

becoming ever more widespread. Technologists in these fields are provided with a unique overview of materials, performances and applications.

Contents:
Williams: Biofunctionality and Biocompatibility.
Kohn/ Ducheyne: Materials for Bone and Joint Replacement.
Baquet: Materials in the Cardiovascular System.
Aebischer/ Goddard/ Gallenti/ Lysaght: Biomaterials and Artificial Organs.
Yannas: Materials for Skin and Nerve Regeneration.
Watts: Dental Restorative Materials.

Williams: Materials for Oral and Maxillofacial Surgery.
Materials for Ophthalmology.
Causton: Medical and Dental Adhesives.

Reichert/ Saavedra: Materials Consideration in the Selection, Performance, and Adhesion of Polymeric Encapsulants for Implantable Sensors.

Campbell/ Jones: Materials for Implantable Electrodes and Electronic Devices.

Brunstedt/ Anderson: Materials for Drug Delivery.

Jones: Materials for Fixed and Removable Prosthodontics.



Materials Science

To order please contact your bookseller or:

VCH, P.O. Box 10 11 81,
D-69451 Weinheim.

Fax: 06201-60 61 84

VCH, Nordstrasse 10, P.O. Box,
D-4400 Basel

VCH, 8 Wellington Court,
Cambridge CB1 1YZ, UK

VCH, 300 R.W. 12th Avenue,
Deerfield Beach, FL 33442-1788

USA (toll-free: 1-800-367-6248)

VCH, Elbow Building, 10-9 Hongpo
1-chome, Bunkyo-ku, Tokyo 112



Please write for our comprehensive prospectus

Reprinted from *Analytical Chemistry*, 1995, 67.
Copyright © 1995 by the American Chemical Society and reprinted by permission of the copyright owner.

Anal. Chem. 1995, 67, 1647-1653

Microfabricated Sensor Arrays Sensitive to pH and K^+ for Ionic Distribution Measurements in the Beating Heart

Vasile V. Cosofret, Miklos Erdösy, Timothy A. Johnson, and Richard P. Buck*

Departments of Chemistry and Medicine, University of North Carolina, Chapel Hill, North Carolina 27599

R. Bruce Ash

Department of Electrical and Computer Engineering, North Carolina State University, Raleigh, North Carolina 27695

Michael R. Neuman

Department of OB/GYN, Metro Health Medical Center, Case Western Reserve University, Cleveland, Ohio 44109

Thick-film H^+ - and K^+ -selective sensor arrays based on solvent polymeric neutral carrier membranes are described. The sensor array design and construction allow inexpensive and mass production of disposable miniaturized probes useful in the biomedical field, especially for cardiovascular research and monitoring. They are also suitable for use as multisensor electrochemical detectors within modern flow injection analysis instrumentation. The carriers used for membrane preparation are H^+ -selective ETH 5294 chromoionophore and the well-known K^+ -selective ionophore, valinomycin. The preliminary in vivo experiments, to monitor H^+ and K^+ ionic distribution in the beating pig heart, help to determine the unique ionic conduction responsible for ventricular fibrillation in the setting of acute regional myocardial ischemia.

Microfabricated selective sensor arrays have many advantages over conventional ion-selective sensors based on polymeric membranes and containing relatively large volumes of buffered internal filling solution, i.e., small dimensions, ease of sterilization for in vivo monitoring, relatively low source impedance, and suitability for mass production.^{1,2} In recent years, there has been considerable interest in the design and development of various types of solid-state electrochemical sensors in which the polymeric

membranes are cast on solid surfaces with no internal electrolyte solution.³⁻⁷ These sensors are usually made on silicon and include integrated electronics. Microfabrication technologies, such as photolithographic reduction, thin-film metalization, chemical etching etc., have been used to produce these probes.^{8,9} These sensors have a planar two-dimensional structure. Unfortunately, reducing the size of the sensor and changing the classical membrane electrode configuration to a planar sensor arrangement brought several problems to light concerning the potential stability and reproducibility, response time, and lifetime of these sensors.¹⁰ Rigidity was one of the major disadvantages of the silicon-based sensors for in vivo cardiovascular monitoring.

Our efforts have been aimed at developing a thin-/thick-film processing scheme for fabrication of both single sensors and sensor arrays for selective monitoring of ionic constituents in biological samples. These are Faradaic process sensors based on reversible, not-blocked interfaces. They are also suited for in vivo measurements of ionic H^+ and K^+ changes during induced ischemia.¹¹⁻¹³ There has been a desire by cardiovascular

- (1) Lindner, E.; Cosofret, V. V.; Ufer, S.; Buck, R. P.; Kusy, R. P.; Ash, R. B.; Nagle, H. T. *J. Chem. Soc., Faraday Trans.* 1993, 89, 361-367.
- (2) Yin, H. S.; Kibbey, C. E.; Ma, S. C.; Kliza, D. M.; Liu, D.; Park, S. B.; Torre, C. E.; Meyerhoff, M. E. *Biosens. Bioelectron.* 1993, 8, 1-38.

- (3) Bergveld, P.; Shbbald, A. *Analytical and Biomedical Applications of Ion-Sensitive Field Effect Transistors*. In *Wilson and Wilson's Comprehensive Analytical Chemistry*; Svehla, G., Ed.; Elsevier: Amsterdam, 1988; Vol. 23.
- (4) Janata, J.; Huber, R. J. *Ion-Selective Electrodes in Analytical Chemistry*; Plenum Press: New York, 1978; Vol. 2, Chapter 3.
- (5) Janata, J.; Huber, R. J. *Ion-Sel. Electrode Rev.* 1979, 1, 31-79.
- (6) Janata, J. *Principles of Chemical Sensors*; Plenum Press: New York, 1989.
- (7) McKinley, B. A.; Houtchens, B. A.; Janata, J. *Ion-Sel. Electrode Rev.* 1984, 6, 173-208.
- (8) Wu, Q.; Lee, K. M.; Liu, C. C. *Sens. Actuators B* 1993, 13-14, 1-6.
- (9) Liu, C. C.; Zhang, Z. R. *Sel. Electrode Rev.* 1992, 14, 147-167.
- (10) Lindner, E.; Cosofret, V. V.; Kusy, R. P.; Buck, R. P.; Rosatkin, T.; Schaller, U.; Simon, W.; Jency, J.; Toth, K.; Pungor, E. *Talanta* 1993, 40, 957-967.

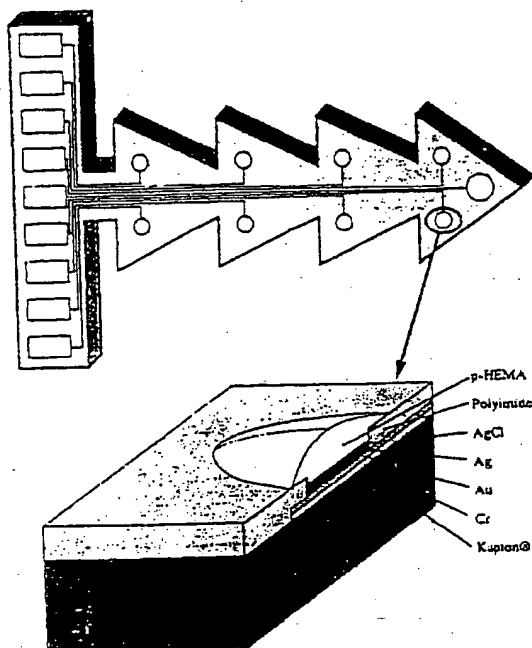


Figure 1. Nine-site Ag/AgCl electrode array used for H^+/K^+ sensors construction and cross-section of a recording site.

physiologists to obtain flexible multielectrode probes with well-defined geometries to help describe and understand the potential and ionic distribution in the heart as a function of time. Recently, we reported on the analytical performances of microelectronically fabricated ion sensors based on a flexible polyimide substrate (Kapton, Du Pont)¹¹ that can move with the muscle fibers within the wall of the beating heart. We also showed that these devices are useful for in vivo measurements.¹¹⁻¹³ Difficult, but solved problems include membrane optimization,¹⁴⁻¹⁷ reduced preconditioning time,¹⁸ greater polymeric membrane adhesion to the Kapton substrate,¹⁹ and improved membrane biocompatibility.¹⁷⁻¹⁹ These were reported in recent publications. Single H^+ and K^+ planar sensors (diameter size of internal reference element of 0.25 or 0.5 mm) were acutely implanted into a beating pig's heart and ionic changes recorded and evaluated successfully during regional, nonflow ischemia.^{12,13,20} These sensors performed well during the 4-5 h of experimentation that included several repeated occlusions of the coronary artery, and the ionic data collected were

equivalent to that obtained using other, established techniques. These encouraging results pushed us in the direction of designing and developing Kapton-based sensor arrays with nine active sites having well-defined geometrical arrangements. These sites contain selective membranes of the same type (H^+ or K^+) or different type (H^+/K^+) in order to allow spatially resolved, in vivo measurements.

In this paper, we describe the design, fabrication, and electroanalytical properties of H^+ , K^+ , and H^+/K^+ flexible sensor arrays with preliminary applications in cardiovascular monitoring and research. The potentiometric properties of these sensors are compared with those of conventional design.

EXPERIMENTAL SECTION

Chemicals and Solutions. For all experiments, deionized water (Barnstead, Nanopure II) and chemicals of analytical-reagent grade were used. Most of the products were supplied by Fluka AG (Buchs, Switzerland): H^+ carrier ETH 5294 (chromoionophore I, No. Z7086); K^+ carrier valinomycin (VAL, No. 94675); 2-nitrophenyl octyl ether (α -NPOE, No. 73741); bis(2-ethylhexyl) sebacate (DOS, No. 8483); potassium tetrakis(4-chlorophenyl)borate (KTPClPB, No. 60591). The materials used for the membrane matrix were carboxylated PVC [PVC-COOH with 1.8% (w/w) COOH groups, No. 81395] as well as aminated PVC [PVC-NH₂ with 0.7% (w/w) nitrogen], synthesized by Kusy et al.^{21,22}

Buffer solutions in the pH range 6-9 were based on a Tris buffer with 140 mM Na⁺ ionic background [10 mM NaOH + 130 mM NaCl + 10 mM tris(hydroxymethyl)aminomethane]. The pH values of the solutions were adjusted by the addition of 1.0 or 0.1 M HCl solution to the stock buffer solution and monitored with a selective glass electrode (Orion, Model 91-57). Potassium chloride standard stock solution (10^{-1} M) was prepared by dissolving dried KCl in either distilled water or pH 7.0 Tris buffer (see above). The diluted solutions were prepared by successive dilutions of the respective stock solution. Additionally, standard solutions of known pH (Tris buffer) and K^+ activities, in the physiological range, were prepared and used for the simultaneous calibration of array sensors before and after in vivo experiments. These solutions contained the same constant Na⁺ ionic background (0.14 M) and were of the following values: pH 6.0 \pm 0.1 mM K^+ , pH 7.0 \pm 4.0 mM K^+ , pH 8.0 \pm 7.0 mM K^+ , and pH 9.0 \pm 10.0 mM K^+ . The reported data are corrected for the electrode drift, which is less than 1 mV during 5-h in vivo experiment.

Microfabrication of Array Sensors. The electrode arrays are batch fabricated on a flexible polyimide (Kapton, DuPont) substrate using a combination of thin-film, thick-film, and packaging technologies. This fabrication is different from previously described processing.^{11,13} The electrode array structure can be thought of as polyimide-patterned metal-polyimide sandwich with openings in the top layer of polyimide to define the electrode sites and bonding pads. Layers of silver, silver chloride, hydrogel, and PVC-based ion-selective membrane are deposited over the site openings to form the ion-selective electrodes. This arrangement is depicted in Figure 1.

- (11) Lindner, E.; Cosofret, V. V.; Ufer, S.; Johnson, T. A.; Ash, R. B.; Nagle, H. T.; Neuman, M. R.; Buck, R. P. *Fresenius J. Anal. Chem.* 1993, 346, 584-588.
- (12) Cosofret, V. V.; Lindner, E.; Johnson, T. A.; Neuman, M. R. *Talanta* 1994, 41, 931-938.
- (13) Cosofret, V. V.; Johnson, T. A.; Erdosy, M.; Buck, R. P.; Lindner, E. Polymeric Membrane Optimization for Microchemical Sensors with Applications in Cardiology. In *The Polymeric Materials Encyclopedia: Synthesis, Properties and Applications*; Salamone, J., Ed.; CRC Press: Boca Raton, FL, in press.
- (14) Cosofret, V. V.; Nahir, T. M.; Lindner, E.; Buck, R. P. *J. Electroanal. Chem.* 1992, 327, 137-146.
- (15) Lindner, E.; Rosatzin, T.; Jeney, J.; Cosofret, V. V.; Simon, W.; Buck, R. P. *J. Electroanal. Chem.* 1993, 352, 309-312.
- (16) Cosofret, V. V.; Lindner, E.; Buck, R. P.; Kusy, R. P.; Whitley, J. Q. *J. Electroanal. Chem.* 1993, 345, 169-181.
- (17) Cosofret, V. V.; Erdosy, M.; Buck, R. P.; Kao, W. J.; Anderson, J. M.; Lindner, E.; Neuman, M. R. *Analyst* 1994, 119, 2283-2292.
- (18) Cosofret, V. V.; Erdosy, M.; Lindner, E.; Johnson, T. A.; Buck, R. P.; Kao, W. J.; Neuman, M. R.; Anderson, J. M. *Anal. Lett.* 1994, 27, 3039-3063.
- (19) Lindner, E.; Cosofret, V. V.; Ufer, S.; Buck, R. P.; Kao, W. J.; Neuman, M. R.; Anderson, J. M. *J. Biomed. Mater. Res.* 1994, 28, 591-601.
- (20) Cosofret, V. V.; Lindner, E.; Johnson, T. A.; Kao, W. J.; Anderson, J. M.; Neuman, M. R.; Buck, R. P. *Polym. Mater. Sci. Eng.* 1994, 70 (Proc. Symp. Membranes for Biomedical and Biotechnological Separations) 137-138.
- (21) Kusy, R. P.; Whitley, J. Q.; Buck, R. P.; Cosofret, V. V.; Lindner, E. *Polymer* 1994, 35, 2141-2147.
- (22) Kusy, R. P.; Whitley, J. Q.; Buck, R. P.; Cosofret, V. V.; Lindner, E. *J. Mater. Sci. Lett.* 1994, 13, 849-851.

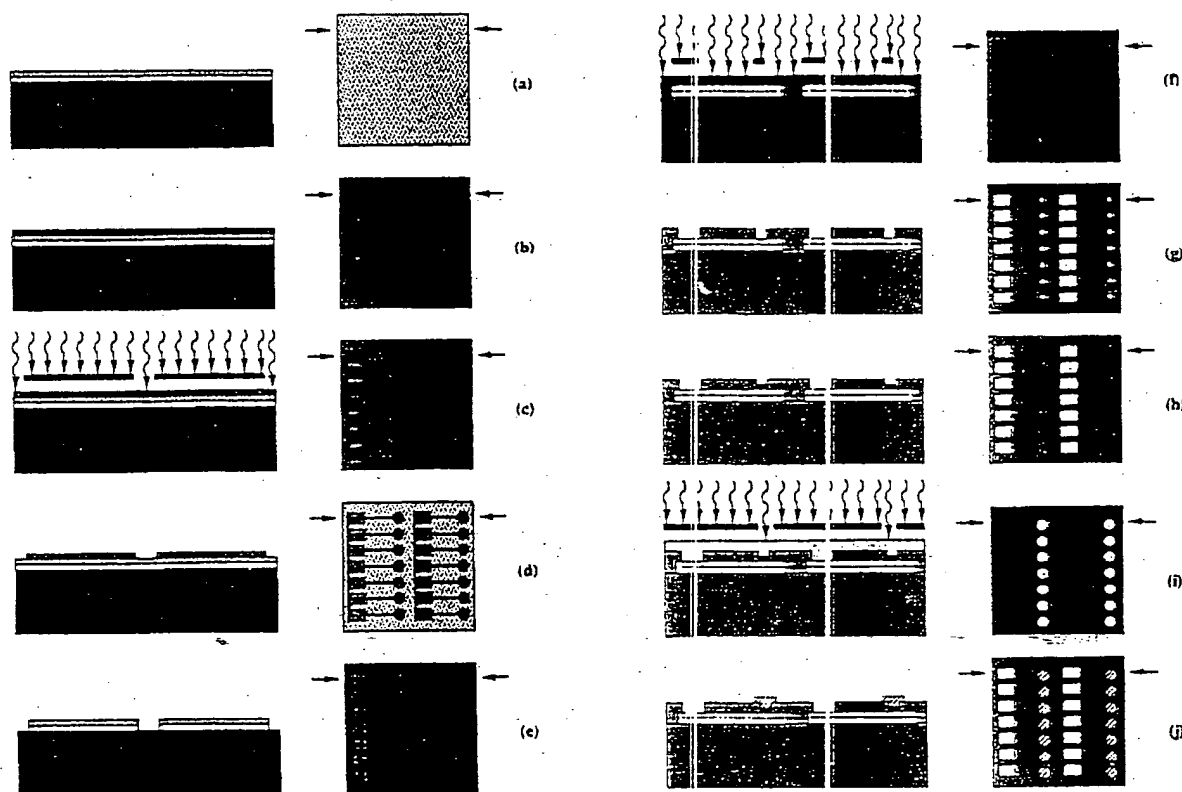


Figure 2. Fabrication sequence of planar electrode arrays (for details, see text).

The fabrication sequence is illustrated in Figure 2, where both top and cross-sectional views are shown for each step. The pattern in the figure is a simplification of a current test structure design and represents either two seven-site linear arrays or 14 discrete electrodes, depending on how they are cut out and used. A drawing of the three photomasks required for this design is shown in Figure 3. Note that the drawings in Figures 1–3 are not to scale.

Fabrication begins with a solvent cleaning of a 3 in. square by 5×10^{-3} in. thick Kapton film. The film is placed in a frame to hold it flat, and a 200-Å layer of chromium followed by a 2000-Å layer of gold is sputtered onto it (Figure 2a). The chromium acts as an adhesion layer between the polyimide and the gold. A standard photolithography process is used to pattern the metal layers and to define the electrode sites, bonding pads, and connecting traces. First, a 1.5- μm layer of positive photoresist (JSR Inc., 1 \times 700 10CP) is spin-coated onto the gold (Figure 2b). This photoresist is selectively exposed through the first photomask (or master) to 365-nm UV light (Figure 2c). This photomask is an exact pattern of the desired metal (Figure 3a) and thus blocks the light from the areas of the photoresist directly above the metal that will remain. The photoresist is developed by submerging the film in a commercial developer (JSR Inc., PD526) so that the areas exposed to the UV light are chemically removed (Figure 2d). Next, the film is submerged in a solution that selectively etches the gold over chromium or photoresist (1 part iodine:4 parts potassium iodide:40 parts deionized water) until the gold is cleared and then submerged in a commercial solution (containing perchloric acid) which selectively etches the chromium without attacking the gold or photoresist until the chromium

is cleared. The photoresist is removed from the metal by submerging it in *N*-methyl 2-pyrrolidone, leaving a patterned metal layer on the Kapton substrate (Figure 2e).

A 30- μm thick layer of photodefinable polyimide (Du Pont, PI2721) is spin-coated onto the film. It is selectively exposed to 365-nm UV light through the second photomask (master) after aligning this photomask with the patterned metal layer underneath (Figure 2f). This photomask is a pattern giving locations of the openings for the electrode sites and the bond pads in the polyimide (Figure 3b). The photodefinable polyimide is spin-developed by spraying a developer solution (6 parts 4-butyrolactone:4 parts xylenes) followed by a solvent rinse (xylenes) onto the polyimide while it is spinning until the areas not exposed to UV light are removed (Figure 2g). Two micrometers of silver is electroplated onto the gold sites from a 1% (w/v) potassium silver cyanide solution and about 25% of this silver is electrochemically converted to silver chloride in 0.1 N HCl (Figure 2h).

A layer of 2-hydroxyethyl methacrylate (HEMA) monomer containing 4% (w/w) photoinitiator (2,2-dimethoxy-2-phenylacetophenone) is cast onto the film over the Ag/AgCl sites and selectively polymerized through the third photomask using 365-nm UV light (Figure 2i). This photomask is UV transparent only in the areas where the HEMA is to be polymerized and opaque elsewhere (Figure 3c). The HEMA that is not polymerized is removed in a series of methanol rinses, leaving hydrogel domes approximately 50 μm thick only over the sites (Figure 2j). Figure 4a shows a photograph of a Kapton wafer with 30 electrode arrays, each containing nine active sites of Ag/AgCl + poly-HEMA. This is used to fabricate on-sensor arrays (Figure 4b) of biological interest. A monospecific heat seal connector, which is very

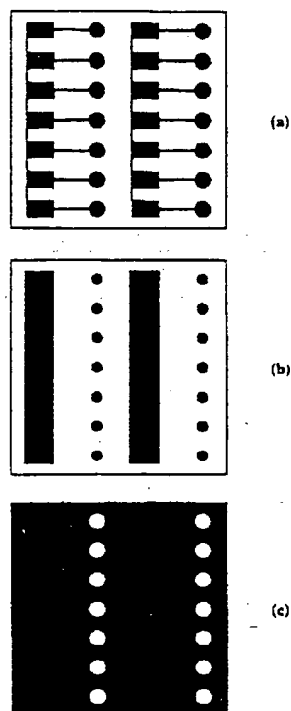


Figure 3. Schematic of photomasks required for electrode micro-fabrication.

lightweight and has excellent flex characteristics, is used for electrical connections.

Polymeric Membranes and Selective Electrodes. The sensor arrays used in this study, selective to H^+ and K^+ , respectively, were made on Kapton wafers. The procedures for fabrication of the Kapton wafers, wire connections, and electrode site preparations are described in the previous section. Each active site contains a thin-layer film of poly(hydroxyethyl methacrylate) (poly-HEMA), which was cast onto the wafer and selectively polymerized under UV light. The electrodes containing poly-HEMA were first soaked for 2 h in the proper electrolyte (10^{-2} M KCl in pH 7.0, Tris buffer). Following a brief washing with distilled water and gentle blotting of the surface, the appropriate ion-selective membrane cocktail (0.25 μ L) was applied above the active area using a 0.5- μ L Hamilton microsyringe. The membrane solutions had the same compositions as described in previous papers,^{12,13} and they consisted of ETH 5294, o-NPOE, and PVC-NH₂ (for pH sensors) and Val, DOS, and PVC-COOH (for K^+ sensors), respectively. In both cases, the membrane solutions were made in tetrahydrofuran and contained K-TpCIPB as lipophilic salt additive. After complete evaporation of tetrahydrofuran (THF), used to dissolve the membrane components, an additional membrane layer was applied (0.25 μ L). All the prepared electrodes were kept in air overnight. They were subsequently hydrated in a pH 7.0 Tris buffer solution containing 4.0 mM K^+ and 0.14 M Na^+ for at least 24 h before use. When not in use, the electrodes were stored in the same solution.

emf Measurements. Electrochemical cell voltages were measured at room temperature in an air-conditioned laboratory at 22.5 ± 0.5 °C with an Orion pH/mV meter (Model 720A) connected to a data acquisition system controlled by an IBM-compatible 486DX-33 computer. The software used for data

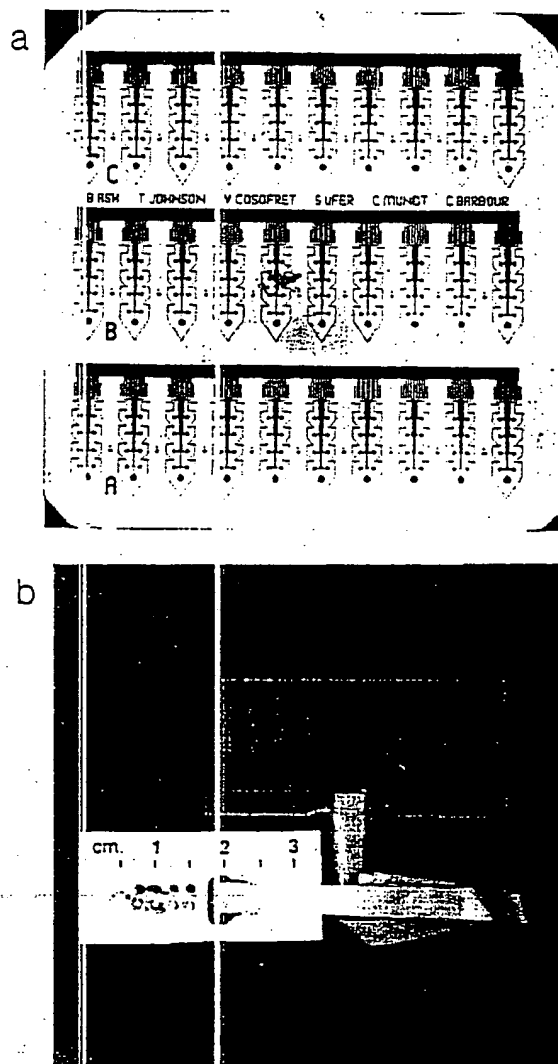


Figure 4. Kapton-based microelectrode wafer containing 30 sensor arrays, each of nine active sites (a) and a single nine-site H^+/K^+ selective sensor array with wire connections (b).

handling was written by C. Mundt of North Carolina State University, using the Lab VIEW for Windows development System (National Instruments, Inc.). As a reference electrode, a double-junction Ag/AgCl (Orion Model 90402) was used throughout in *in vitro* measurements. The solution in the outer compartment of the reference electrode consisted of 1.0 M lithium acetate. For *in vivo* measurements, the ninth site Ag/AgCl/poly-HEMA was used as a reference sensor.

Selectivity Coefficients. The selectivity coefficients for membrane sensor arrays were determined by the fixed interference method using pH buffer solutions with constant cationic background (pH electrodes; see refs 11 and 16) and by the separate solution method at 0.1 M concentration level.²³ The mean activity coefficients were calculated with the extended Debye-

(23) Iung, C. L.; Itoh, K. *Hydrogen Ion Activity*; 1979; 51, 1913-1950.

(24) Mele, P. C.; Ammann, J.; Mort, W.; Simon, W. Liquid Membrane Ion-Selective Electrodes and Their Biomedical Applications. In *Medical and Biological Applications of Electrochemical Sensors*; Horvath, L., Ed.; John Wiley and Sons: New York, 1986; pp 1-10.

Huckel equation,²⁴ and the measured emf values were corrected for changes in the liquid junction potential according to the Henderson equation.²⁴

Determination of the Internal Membrane Resistance. The internal resistance of the potentiometric cells was determined by the voltage divider method using known shunts.^{25,26} For both pH and potassium electrodes, the cell voltage was first measured in pH 7.0 Tris buffer containing 4.0 mM K⁺. Next, the cell output was loaded for 10 s by high-resistance shunts and the internal resistance of the potentiometric cell was calculated from the initial voltage, the voltage drop, and the shunt resistance.

In Vivo Measurements with Planar Sensor Arrays. The experiments were performed with pigs weighing 28–38 kg (for details, see refs 12 and 27). Serum pH and K⁺ before and after the coronary occlusion were determined using a whole-blood gas analyzer (Instrumentation Laboratories, Inc.) and an ion analyzer (AVL, Inc.), respectively. Extracellular H⁺ and K⁺ activities were calculated individually for each electrode from the array using the calibration slope for that electrode, the preocclusion serum K⁺ activity, and potential changes (in mV) produced at the time of the TQ segment in the electrocardiogram by each electrode throughout the course of a coronary ligation lasting 6–8 min. Data were collected, after 45 min of implantation, with a custom-made data amplification system²⁷ containing 128 channels in conjunction with a 128-channel, multiplexed AIMIO-16F5 A–D (National Instruments, Inc.) running under Lab Windows CVI (National Instruments, Inc.). Data were accepted only from electrodes demonstrating H⁺ and K⁺ sensitivities within 10% of a temperature-corrected theoretical Nernstian slope. Indeed, insertion of electrodes, regardless of size or construction material, leads to cellular currents of injury, evident by an offset potential at the electrode; one can be assured that all extraneous K⁺ or H⁺ artifact has been eliminated.

RESULTS AND DISCUSSION

Our main efforts were directed toward design and fabrication of H⁺ and K⁺ microsensor arrays for cardiovascular applications by using the advantages of the existing semiconductor and microelectronics technologies. We have already addressed two sources of response instability (drift) arising from thermodynamic effects, regardless of the size and shape of the sensor.¹⁷ However, by reducing the size of the sensor and by changing its configuration from a conventional one (classical membrane electrode with internal filling solution in direct contact with selective membrane) to a planar sensor arrangement, several other problems have to be overcome. Among these, the following are of great importance: (a) a shortage of chemicals in the selective membrane that may shorten the lifetime of the sensor (this follows from the decreased membrane volume); (b) the increased internal membrane resistance that follows from the reduction of membrane area and consequent instability or noise in potential measurements; and (c) by decreasing the overall dimensions of the sensor, and particularly the active area, the contact surface between the substrate (Kapton wafer) and the sensitive polymeric membrane also decreases dramatically. In other words, the adhesion between the microfabricated wafer and the selective membrane often becomes the limiting factor of the lifetime of the sensors.

In the present work, we used the accumulated knowledge and experience with single-disk ion-selective electrodes for H⁺ and K⁺, which already demonstrated good analytical properties with respect to sensitivity, selectivity, response time, and lifetime in aqueous and biological samples.^{1,11–13,17–19} These were successfully used in H⁺ and K⁺ determination in whole blood¹⁸ and in preliminary in vivo cardiovascular experiments.^{11–13} Our main objective is to fabricate small and flexible pH and K⁺ sensor arrays to determine the unique ionic conditions responsible for ventricular fibrillation in the setting of acute regional myocardial ischemia. On the basis of prior work,^{27–33} we believe that occlusion of the left anterior descending coronary artery (LAD) produces discrete regions in which extracellular potassium is elevated to approximately 10 mM, but pH is lowered by no more than 0.2 pH unit. As a result of this specific ionic combination, slow-channel-mediated responses occur and cause impulses to propagate with very slow conduction. Premature beats occurring in close proximity to these discrete regions, either as a result of spontaneous reentry^{33,34} or as a result of abnormal automaticity induced by currents of injury,³⁵ may then reenter to cause ventricular tachycardia and ventricular fibrillation. Further, we believe such areas exist in the regions between the lateral margin and the center of the ischemic zone and in subendocardial layers where the greater diffusion of CO₂ in comparison with the diffusion of potassium allows pH to remain relatively unchanged while potassium concentration rises, thereby creating the ionic combination critical to the development of slow-channel-mediated response.⁶

In order to develop and fabricate stable H⁺/K⁺ sensor arrays to address this physiological hypothesis, two main problems related to the electrode stability and analytical performances were overcome: (a) by using thermodynamically well defined conditions to establish potential differences across the membrane/solution interfaces and (b) by finding acceptable adhesion of the polymeric membrane to the polyimide-coated Kapton surface.

The first problem was solved by using poly(hydroxyethyl methacrylate) dots on the top of the silver/silver chloride reference element. These dots were obtained by selective polymerization of the HEMA monomer with 4% (w/w) photoinitiator (2,2-dimethoxy-2-phenylacetophenone) and under UV light. The poly-HEMA is a well-known swollen material³⁷ which can easily absorb a proper buffer electrolyte containing Cl[−] (see refs 1, 11, 12, 18, and 38).

The second problem was solved by using adequate polymeric matrices to incorporate the chemicals needed for H⁺ and K⁺

(25) Oesch, U.; Simon, W. *Anal. Chem.* 1980, 52, 692–700.

(26) Ammann, D.; Pretsch, E.; Simon, W.; Lindner, E.; Bezegh, A.; Pungor, E. *Anal. Chim. Acta* 1985, 171, 119–129.

(27) Johnson, T. A.; Engle, C. L.; Kusy, R. P.; Knisley, S. B.; Graebner, C. A.; Gettes, L. S. *Am. J. Physiol.* 1990, 258, H1224–H1231.

(28) Fleck, W. F.; Johnson, T. A.; Graebner, C. A.; Gettes, L. S. *Circulation* 1985, 72, 922–933.

(29) Harjter, J. R.; Johnson, T. A.; Engle, C. L.; Martin, D. G.; Gettes, L. S. *J. Cardiovasc. Electrophysiol.* 1993, 4, 661–671.

(30) Johnson, T. A.; Coronel, R.; Graebner, G. A.; Buchanan, J. V.; Janse, M. J.; Gettes, L. S. *J. Mol. Cell. Cardiol.* 1987, 19, 949–952.

(31) Johnson, T. A.; Engle, C. L.; Boyd, L. M.; Koch, G. G.; Gwinn, M.; Gettes, L. S. *Circulation* 1990, 83, 622–634.

(32) Wilinski, R. L.; Tranun-Jensen, J.; Coronel, R.; Wilde, A. A. M.; Fiolet, J. W. M.; Janse, J. M. *Circulation* 1986, 74, 1137–1146.

(33) Pngvird, S. M.; Corr, P. P. *Circ. Res.* 1990, 66, 672–695.

(34) Kapinski, E.; Ogawa, S.; Balke, W.; Dreifus, L. S. *J. Electrocardiol.* 1979, 12, 299–306.

(35) Janse, M. J.; van Capelle, F. J. L.; Morsink, H.; Kleber, A. G.; Wilms-Schopman, F. J. G.; Cardinal, R.; Nauman d'Almoncourt, C.; Durrer, D. *Circ. Res.* 1980, 47, 1069–1081.

(36) Casio, W. E.; Yan, G. X.; Kleber, A. C. *Circ. Res.* 1992, 70, 409–422.

(37) Davies, M. L.; Tighe, J. J. *Selective Electrode Rev.* 1991, 13, 159–226.

(38) Cosuñet, V. V.; Erdosy, M.; Johnson, T. A.; Buck, R. P.; Ash, R. B.; Neuman, M. H. submitted for publication in *Anal. Chim. Acta*.

Table 1. Potentiometric Response Characteristics of H⁺/K⁺ Sensor Arrays on a Flat-Form Design^a

parameter	membrane	
	H ⁺ -selective	K ⁺ -selective
linear range (pH or mol/L)	4–12	10 ⁻¹ –10 ⁻⁵
slope (mV/decade)	58.9 ± 0.2	58.3 (57.7 ^b) ± 0.2
detection limit (pH or mol/L)	<12	4.0 × 10 ⁻⁶
selectivity coeff (–log K _{M,N})		
Li ⁺	>10.9	4.4
Na ⁺	11.1	3.6
K ⁺	10.5	
Ca ²⁺	11.2	4.6
NH ₄ ⁺		1.8
reproducibility ^c (mV)	0.6	0.6

^a Based on 25 arrays; the yield of functioning sensors on an array is about 75%; the standard cell potential (E_0) changed with about 20 mV during 1 month of measurements or storage in standard solution. ^b In 0.14 M Na⁺ ionic background. ^c pH 7.0 Tris buffer with 4.0 mM K⁺ and containing 0.14 M Na⁺.

sensors, respectively. These are aminated PVC (PVC-NH₂) for pH sensors and carboxylated PVC (PVC-COOH) for K⁺ sensors. The first matrix incorporates the ETH 529⁺ H⁺ ion carrier and *o*-NPOE as polar solvent plasticizer while the second one incorporates valinomycin K⁺ carrier and DOS as a nonpolar plasticizer. Our previous studies^{1,11,19} showed that both matrices exhibit good adhesive properties to our polymeric substrate. PVC-NH₂ cannot be used as a polymeric matrix for K⁺ sensors since it has high pH sensitivity. PVC-COOH shows ion-exchange properties, and these were described and interpreted by theory and experiments for H⁺- and M⁺-sensitive membrane sensors.³⁹ In both cases, in order to make highly selective sensors, the carrier concentration in the membrane should exceed total available sites due to the matrix dissociation and from added lipophilic salt additives, i.e., tetraphenyl borate derivatives. Our earlier data³⁹ suggested a way of determining fixed-site concentration by observing membrane compositions where selectivities change dramatically, corresponding to the approximately equal concentration of carrier and sites.

Linear Concentration Ranges, Sensitivities, and Selectivities. Fortunately, both H⁺ and K⁺ membranes did not change their linear activity ranges and slopes of the calibration curves after changing from the classical electrode design, with a large volume of internal bathing solution, to the planar array structure.

Table 1 summarizes the potentiometric response characteristics of H⁺/K⁺ planar sensor arrays containing four H⁺- and four K⁺-selective membranes. The ninth site of the array remained uncovered by any selective polymeric membrane since it has been designed to be used as a common external reference electrode for the other eight ion sensors. It contains Ag/AgCl and a poly-HEMA layer. Experimental verification of this reference sensor design is under way, and the results will be reported later.

The linearity of the calibration curves, as well as the sensitivities, remained constant up to at least 1 month of continuous hydration and/or use.

Short-Term Stability of Potential Measurements. The potential vs time transients following one decade H⁺ or K⁺ activity change (response time curves) are slightly different for the conventional macrosensors and the planar microsensors. The fast transient signal is generally followed by a small driftlike potential

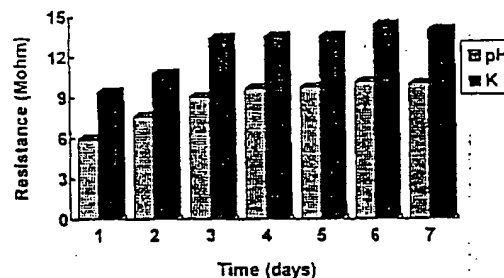


Figure 5. Membrane resistances of pH and K⁺ sensors placed on the same planar Kapton array structure during 7 days of continuous use and/or aqueous solution contact.

change by the planar sensors. The average drift potential for pH sensors was found to be 0.25 mV/h ($n = 16$; SD = 0.09) during a 5-h measurement period in pH 7.0 Tris buffer solution containing 4.0 mM K⁺. In the same solution and for the same time frame, the drift of K⁺ sensors was only 0.09 mV/h ($n = 12$; SD = 0.07). We attribute this difference in the short-term stability of potential measurements to small differences in the adhesion of H⁺-selective membrane (based on a polar solvent such as *o*-NPOE; $\epsilon_0 = 23.9$) vs K⁺-selective membrane (based on nonpolar solvent DOS, $\epsilon_0 = 3.9$).^{18,19}

It is well-known that a constant composition of the ion-selective membrane in the sensor fabrication is a key factor when reliable sensors are being developed for acute and chronic biomedical applications.⁴⁰ The continuous, but fortunately small, potential drift in the offset voltage of the electrochemical cells containing the H⁺/K⁺ sensor array is a sign that, slowly, the membrane composition is changed over time. The lifetime of these devices is now under investigation. Based on our experience with single sensors of the same type, structure, and size, we expect to have these devices last for about 90 days of continuous use.

Internal Membrane Resistance. Internal membrane resistances of H⁺ and K⁺ sensors on a multiple sensing array are different because the plasticizer polarities of the membranes used to detect H⁺ and K⁺, respectively, are different. Both membranes show resistances of less than 10 MΩ in the first day after potential equilibration (Figure 5), which are acceptable for direct potentiometric measurements. The small changes in the membrane resistances, observed with elapsed time, are attributed to the dissolution of membrane components into the contacting bathing solution.⁴⁰

pH and K⁺ Monitoring in Beating Pig Heart. As it was described above, different ionic combinations may occur within various regions of the ischemic zone (between the lateral margin and the center of the ischemic zone). In the center of the ischemic zone, potentially lethal ionic changes (i.e., elevated extracellular K⁺ without substantial extracellular acidification) should occur only transiently because of the rapidity with which potassium rises and pH falls in this region during occlusion.

Unfortunately, until now, no direct quantitative evidence linking specific heterogeneous ionic and conduction characteristics during acute ischemia has been verified, primarily due to the sensor limitations. The data we are presenting in this work are

(39) Cosofret, V. V.; Buck, R. P.; Erdosy, M. *Anal. Chem.* 1994, 66, 3592–3599.

(40) Lindner, E.; Cosofret, V. V.; Nahir, T. M.; Buck, R. P. Characterization of Stability of Modified Poly(vinyl chloride) Membranes for Biomedical Applications. In *Diagnostic Biosensor Polymers*; Usmani, A. M., Akmal, N., Eds.; American Chemical Society: Washington, DC, 1994; pp 149–157.

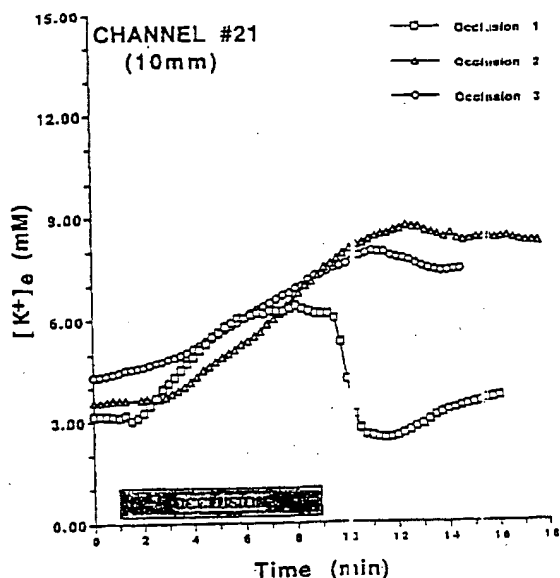


Figure 6. Extracellular potassium rise seen during regional ischemia in a Lagendorff perfused swine heart. Ischemia was induced by ligation of the LAD proximal to the second diagonal branch on three serial occasions for 8 min followed by 52 min of normal perfusion. (Recordings from channel No. 21 of the data acquisition system were 10 mm from the epicardial surface.)

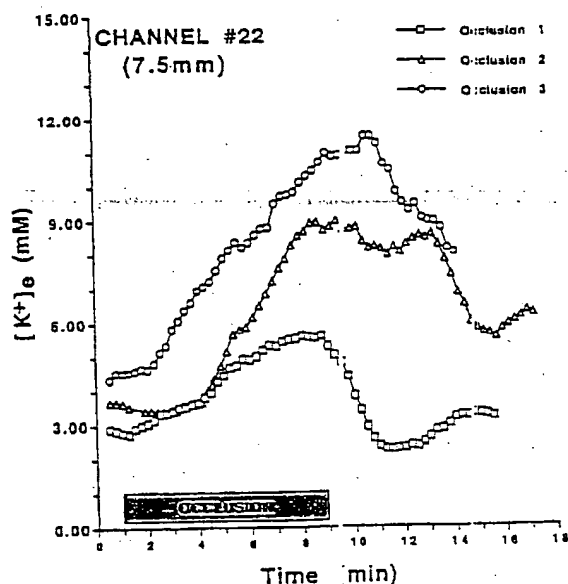


Figure 7. Recordings from channel No. 22 (7.5 mm from the epicardial surface). See Figure 6 legend.

encouraging. The potentiometric responses of H^+/K^+ sensor arrays, implanted in an in situ porcine heart preparation at a midmyocardial depth are shown in Figures 6–8. The extracellular potassium data ($[K^+]_e$, mM) from the two electrodes shown in Figures 6 and 7 are typical for transitional, subendocardial, and central, midmyocardial ischemic recordings with regard to the rate and magnitude of ionic change observed during 8 min of acute ischemia.²⁸ The rapid recovery to normal $[K^+]_e$ observed at these two sites during the minutes following flow restoration in occlusion 1 was not seen in either occlusion 2 or 3 since vasospasm of the

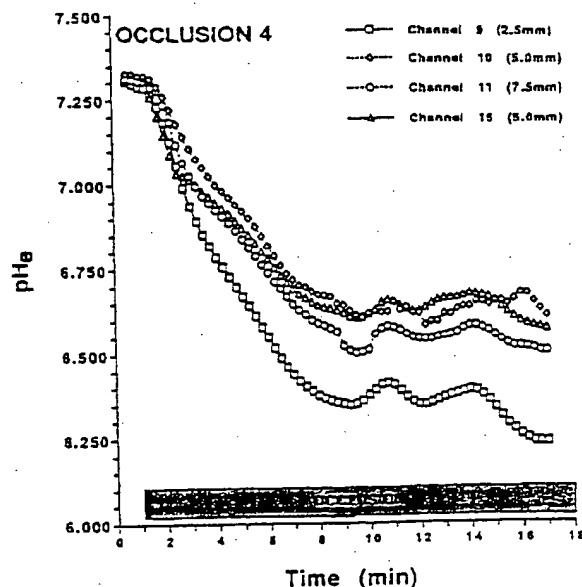


Figure 8. Four extracellular pH recordings from a single electrode site of the array pH electrode during a final 18-min ligation of the LAD. Recordings are from the same experimental preparation of Figure 6. Electrode distances from the epicardial surface are shown in the legend.

left anterior descending coronary artery occurred. Further, the pH_e changes observed for one pH electrode at several transmural sites (Figure 8) is consistent with current hypotheses that suggest the possibility of transmural pH and K^+ gradients, similar to those of the lateral margin described above, although the exact characterization of those gradients in the Lagendorff preparation is still under investigation.

CONCLUSIONS

Microelectronically fabricated H^+/K^+ sensor arrays based on a polyimide substrate (Kapton) and containing four proton- and four potassium-sensitive sites show good analytical properties (linear ranges, slopes of the calibration curves, selectivities, reproducibility, and potential drift). The electrode processes have been optimized. The sensor arrays were used to monitor the H^+ and K^+ ionic changes during acute ischemia at several sites in a porcine heart. Measuring both H^+ and K^+ activities in the beating heart will help us to understand better the contribution of the slow and fast depolarizing channels responsible for normal conduction and allow us to determine the role that ionic change has on the genesis of abnormal conduction disturbances with coronary disease.

ACKNOWLEDGMENT

This work was supported by NSF Engineering Research Center (Grant CDR-3622201) and NIH Grants R01 HL49818 and P01-HL27430. We thank Mr. Stefan Ufer for the microelectronics fabrication.

Received for review December 5, 1994. Accepted March 1, 1995.*

AC941179X

* Abstract published in *Advance ACS Abstracts*, April 1, 1995.

23. N. E. Bagshaw, R. L. Clarke, and K. Kendall, Abstract 2, p. 2, The Electrochemical Society Extended Abstracts, Vol. 90-2, Seattle, WA, Oct. 14-19, 1990.
24. D. Pavlov and N. Kapkov, *This Journal*, **137**, 17 (1990).
25. D. Pavlov and N. Kapkov, *ibid.*, **137**, 21 (1990).
26. D. Pavlov and N. Kapkov, Bulgarian Pat. 43,335 and 43,336 (May 1988).
27. G. N. Reich, U.S. Pat. 4,415,410 (1983).
28. G. A. Parker, U.S. Pat. 4,388,210 (1983).
29. A. R. Reid, U.S. Pat. 2,159,226 (1939).
30. Belgian Patent 723,018 (1968).
31. Y. Matsumura, S. Saito, A. Miura, Y. Ishikawa, A. Komaki, and T. Hayakawa, Japanese Pat. Pub. No. 62/145664 (1985).
32. Spanish Patent 8,801,559 (1988).
33. J. A. Orsino, U.S. Pat. 2,658,097 (1953).

Limiting Current Enhancement by Self-Induced Redox Cycling on a Micro-Macro Twin Electrode

Tsutomu Horiuchi, Osamu Niwa, Masao Morita, and Hisao Tabei

NTT Basic Research Laboratories, Nippon Telegraph and Telephone Corporation, Tokai, Ibaraki 319-11, Japan

ABSTRACT

The current arising from a reversible redox reaction involving soluble species occurring at a microelectrode may be increased by moving a large electrode at open circuit close to the microelectrode. This phenomena is readily explained. The product of the electrochemical reaction at the microelectrode diffuses the short distance to the nearest part of the macroelectrode and alters the concentration of the redox species at this location on the macroelectrode, compared to other locations at the electrode surface. In this situation, the macroelectrode behaves as a shorted concentration cell and attempts to reduce the concentration aberration caused by the reaction occurring at the microelectrode. This is accomplished by producing more of the original reactant for the microelectrode. This, in turn, increases the flux of reactant to the microelectrode and, therefore, also the current at the microelectrode.

Microelectrodes have been well studied because of their utilization for detecting materials in a very small area or a very small amount of solution (1-10). Microelectrodes have the advantages of high mass transport density, small double layer capacitance, and small ohmic losses. Nevertheless, the current flowing through a microelectrode is very small, due to its small area. Ensembling microelectrodes is one effective way of increasing the magnitude of current in order to keep the advantages of the single microelectrode with respect to high current density and small ohmic drop (11-17).

Using two potentiostated, closely spaced microelectrodes shows another interesting characteristic for measuring reversible redox species. Since each electrode of the pair can be potentiostated separately, an electroactive species generated at one electrode can diffuse to the second electrode, where it is observed. The diffusion of the redox species between the twin microelectrodes takes place in a confined space, resulting in a steady-state current. Theoretical and experimental approaches have been reported for closely spaced microband electrodes (18) and interdigitated array electrodes (19, 20).

The interdigitated array electrode is one form of twin electrodes which exhibits a high sensitivity, 10^{-8} mol/dm³, and fast response time, a few tenths of a ms. This is principally due to the fact that large limiting currents can be obtained with a high S/N ratio, due to the large amount of redox cycling between two electrodes (21). Since the limiting current of the interdigitated array electrode is increased by decreasing its bandgap, a new vertically separated interdigitated array electrode with a very narrow gap has been proposed to enhance the limiting currents (22).

However, if one electrode of the interdigitated array electrode is not potentiostated, that is, is at its open-circuit potential, a peak shaped voltammogram is obtained. The peak is small because no redox cycling exists. Since the products from the potentiostated electrode diffuse to the unpotentiostated electrode from both sides, and the diffusion layer is superimposed, its electrochemical characteristics are similar to a single macroelectrode. In this situation, the unpotentiostated electrode behaves like an insulator. However, if the unpotentiostated electrode is very large compared to the potentiostated electrode, it seems to take a lot of time to superimpose the diffusion

layers. Before the diffusion layers are superimposed, the microelectrode positioned close to the macroelectrode or to the macro conducting plate will show different electrochemical characteristics from that positioned near a macro nonconducting plate.

Recently, we proposed a new type of twin electrode (Fig. 1), where a microdisk array electrode is vertically separated from a macroelectrode by a thin insulating film (23). The characteristic of our new electrode is that the macroelectrode area is much larger than the total area of the microelectrodes. The current enhancement at this new electrode is caused by redox cycling by the same mechanism as that for the interdigitated array electrode and microband array.

Surprisingly, there was no reduction of limiting current when the macroelectrode was disconnected from the potentiostat. Similar phenomena have also been reported for a tip of a scanning electrochemical microscope (SECM)

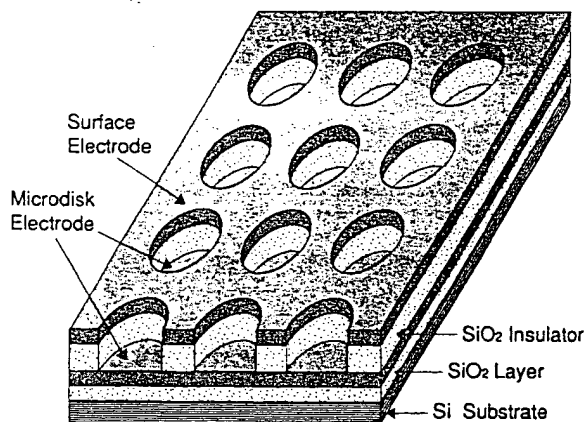


Fig. 1. Schematic diagram of a microdisk array electrode embedded in the surface (MDAS) electrode. The disks were arranged in a square lattice; the lattice distance, disk radius, and number of disks were 800 μ m, 5.0 μ m and 100 respectively. The SiO₂ insulator thickness was of the order of 0.25-0.3 μ m.

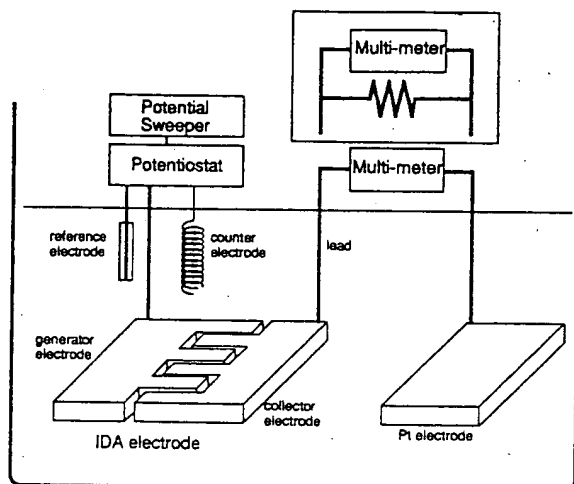


Fig. 2. Schematic diagram for the measurement of the voltammogram and potential difference between the cathode of an interdigitated array electrode (IDA) and a macro platinum electrode.

when it is scanned near a macro conductive surface (24). In this paper we explain this phenomena.

Experimental

Electrodes.—We prepared three types of electrodes; the ordinary microdisk array electrode (MDA), the bi-layered microdisk array electrode (MDAS: microdisk array electrode embedded in surface electrode, see Fig. 1), and interdigitated array electrode (IDA). The MDAS and the IDA were used as an example of a micro-macroelectrode pair. The IDA is a twin microelectrode, in which the two electrodes are the same size. We connected an extra platinum electrode to the one electrode of the interdigitated array in order to complete a micro-macroelectrode pair. This micro-macro combination electrode (IDA-Pt) is useful for monitoring the charge migration between regions of the macroelectrode by inserting a multimeter, low impedance current mode, between one electrode of the interdigitated array and the Pt electrode, see Fig. 2. All electrodes were fabricated on thermally oxidized silicon wafers by photolithography. The detailed fabrication methods have been described elsewhere (19, 21). The electrode matrix was cut to a 1×2 cm rectangle. The disks of both types were arranged in a square lattice; the lattice distance, disk radius, and number of disks were $800 \mu\text{m}$, $5.0 \mu\text{m}$, and 100, respectively. The surface electrode's area was about 12,700 times as large as the total area of the disk electrodes. The interdigitated array electrode was composed of two series of interdigitated electrodes. The widths of the two finger electrodes were both $3 \mu\text{m}$; their lengths were 2 mm . The gap and the number of pairs of electrodes were $2 \mu\text{m}$ and 50, re-

spectively. The total area of each electrode was $3 \times 10^{-3} \text{ cm}^2$.

Chemicals and apparatus.—(Ferrocenylmethyl)trimethylammoniumbromide [$\text{C}_5\text{H}_5\text{FeC}_5\text{H}_4\text{CH}_2\text{N}(\text{CH}_3)_3\text{Br}$, (aq-ferrocene)] was used as purchased, Tokyo Kasei. A pH 7.0, 0.1 mol/dm^3 phosphate buffer solution was used for the electrolyte, NACALAI TESQUE. Electrochemical measurements were performed using a twin potentiostat HECS 990, HUSO, or DPGS-1, Nikko Keisoku, a potential sweep unit HECS 980, HUSO, or PAR 175, Princeton Applied Research, a digital multi-meter 177, Keithley, and an X-Y recorder 3025 YOKOGAWA.

Procedure.—Electrochemical measurements were carried out in 1 mmol/dm^3 aq-ferrocene in a phosphate buffer solution. Each electrode was mounted on a custom-made connector to attach it to the electrochemical apparatus. The auxiliary electrode was a platinum wire. The reference electrode was an Ag/AgCl electrode. In the twin potentiostat experiment, the potential of the macroelectrode, surface electrode of the MDAS, was held at 0 V , whereas that at the microelectrode, disk array electrode of MDAS, was swept between 0 and 0.7 V at a sweep rate of 100 mV/S . The cyclic voltammetry of the ordinary microdisk array electrode and that of the bi-layered microdisk array electrode with the surface electrode on open circuit was performed under the same scan conditions.

A digital multimeter or a $10 \text{ M}\Omega$ resistance could be inserted between the cathode of the interdigitated array and Pt electrode to measure either the current or the potential difference between them while performing the cyclic voltammetry, Fig. 2.

Results and Discussion

The voltammogram of the microdisk array electrodes at a scan rate of 100 mV/S is shown in Fig. 3. The limiting current of the bi-layered microdisk array electrode, two electrodes potentiostated, was larger than that of the ordinary microdisk array electrode, because of the redox cycling between the microdisk electrode and the macro surface electrode (21). Although the macro surface electrode in the bi-layered microdisk array electrode is not connected to a potentiostat, macroelectrode on open circuit, the oxidized limiting current is much larger than that of the ordinary microdisk array electrode and is equal to that of the two electrode potentiostated bi-layered microdisk array electrode experiment. This result indicates that the microelectrode embedded in the conducting surface shows a larger limiting current than that embedded in the nonconducting surface and also suggests that the current enhancement reaction, reductive reaction in this case, could take place on the unpotentiostated surface electrode.

The fact that limiting current of the bi-layered microdisk array electrode is larger than that of an ordinary microdisk electrode with an equivalent electrode area suggests that a large amount of redox cycling still exists between the microdisk and macro surface electrode even when the macro surface electrode is not connected to an external circuit.

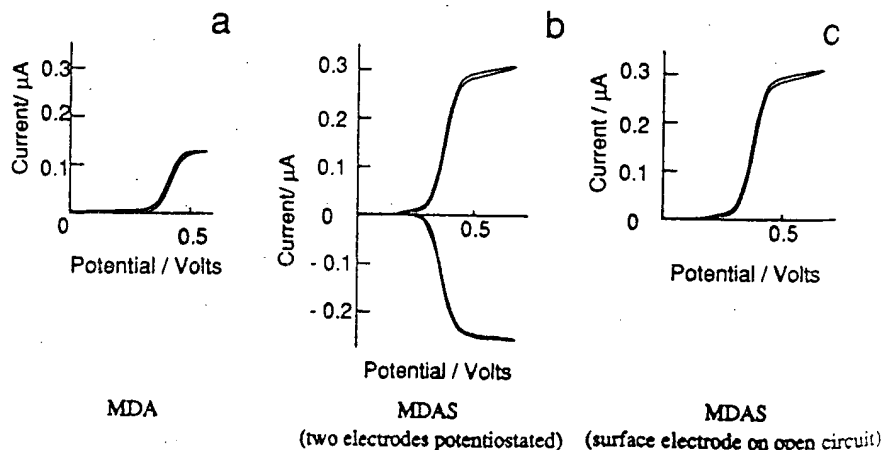


Fig. 3. Cyclic voltammograms of the microdisk array (MDA) electrode and the microdisk array electrodes embedded in the surface (MDAS) electrode. a, The oxidized current of the MDA electrode. b, The oxidized and reduced current of the MDAS electrode obtained on the two electrodes potentiostated. c, The oxidized current of the MDAS electrode obtained in surface macroelectrode on open circuit. The scan rate is 100 mV/S .

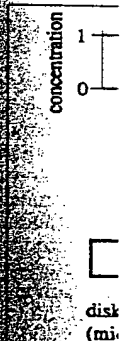


Fig. 4. Mechanism of the concentration gradient microelectrode.

The species electrode forms electrode. The current enhancement of the bi-layered microdisk array electrode is higher than that of the ordinary microdisk array electrode.



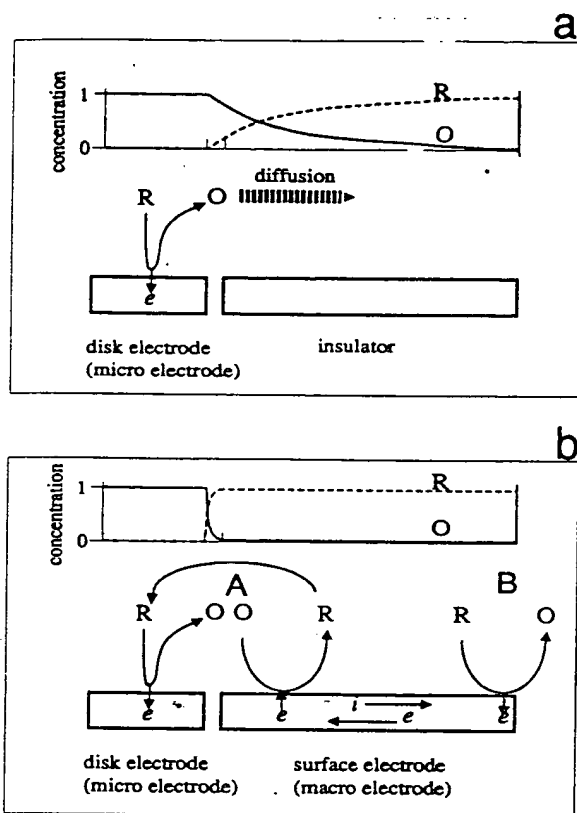


Fig. 4. Mechanism of the current enhancement by the local concentration gradient. a, Microelectrode placed in non-conducting plate. b, Microelectrode placed close to a macro conducting plate, macroelectrode.

The species generated electrochemically at the microelectrode forms a local concentration gradient near the macroelectrode. This concentration gradient is related to the current enhancement at the microelectrode.

A hypothesis for the current enhancement mechanism of the bi-layered microdisk electrode is illustrated in Fig. 4b. The oxidized species produced on the microdisk electrodes diffuse to the neighborhood of the macro surface electrode, Fig. 4b, point A, and forms a local concentration distribution near the macro surface electrode. The concentration of the oxidized ferrocene at point A, is much higher than that at point B. In order to maintain the equi-

librium on the surface electrode, the reductive reaction, $O \rightarrow R$, is induced in the vicinity of point A and the oxidation reaction, $R \rightarrow O$, is induced in the vicinity of point B. The reduced species generated on the surface electrode in the vicinity of point A diffuse back to the disk electrodes and are oxidized again, i.e., self-induced redox cycling is established.

Charge must be conserved for the entire surface electrode. As a result, current flows in the surface electrode in the direction of point B from point A. This situation is same as the shorted concentration cell. Because of this simultaneity of the reduction and the oxidation on the same electrode, the concentration of the oxidized species is uniform at the surface electrode and the concentration profile on open-circuit experiment using the bi-layered microdisk array electrode is the same as that on the two electrodes potentiostated experiment.

To support the hypothesis of current enhancement mechanism in the bi-layered microdisk array electrode, we used a IDA-Pt combination electrode as a model of a micro-macroelectrode pair. The one electrode of the interdigitated array that is potentiostated and another electrode that is connected to the macro Pt electrode correspond to the microdisk electrode and surface macro electrode of the bi-layered microdisk array electrode, respectively. By using the model system, the current flowing between the one electrode of the interdigitated array and Pt electrodes can be directly monitored by a digital multi-meter in the manner described in Fig. 2. Figure 5d shows the anodic current in the combination electrode when the potential is swept from 0 to 0.7 V. The area of the Pt electrode is about 300 times larger than that of the small electrode. The anodic current of the combination electrode on open circuit, Fig. 5d, is much higher than that of the ordinary interdigitated array electrode on open circuit, Fig. 5c, and is equal to that when the two electrodes are potentiostated, Fig. 5a. This result is similar to that for the bi-layered microdisk array electrode, suggesting that the combination electrode can be used as a good model of the bi-layered microdisk array electrode. Figure 5e shows the current flowing between the cathode of the interdigitated array and the Pt electrode in the combination electrode. The magnitude and profile of this current is similar to that of the cathodic current of the two electrodes potentiostated ordinary interdigitated array electrode experiment, Fig. 5b, except for some hysteresis.

A 10 M Ω standard resistance was inserted between the interdigitated array cathode and Pt electrodes in the combination electrode to measure the potential difference between them when little current can flow. Figure 5f shows the anodic current of the combination electrode after inserting the 10 M Ω resistance. This anodic current becomes almost equal to that of the ordinary interdigitated array electrode on an open circuit, Fig. 5c, indicating that the

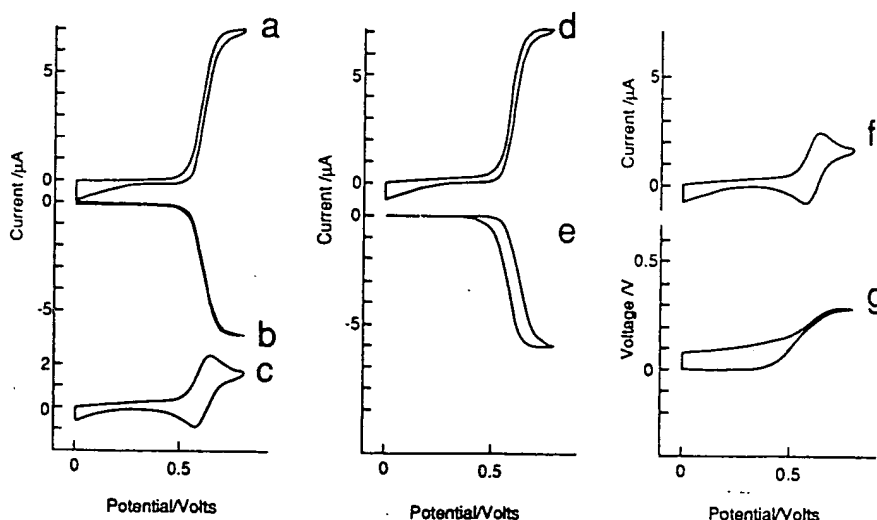


Fig. 5. Cyclic voltammograms of the interdigitated array electrode (IDA) and that of a combination of the IDA and the macro platinum (IDA-Pt) electrode. The scan rate is 100 mV/S. Curve a, Oxidized current of two IDA electrodes potentiostated. Curve b, Reduced current of two IDA electrodes potentiostated. Curve c, Oxidized current of one IDA electrode on open circuit. Curve d, Oxidized current of IDA-Pt electrode. Curve e, Current from IDA cathode to the Pt electrode. Curve f, oxidized current of the IDA-Pt electrode, with 10 M Ω resistance inserted between the IDA cathode and Pt electrodes. Curve g, Potential difference of the IDA cathode and the Pt electrode using 10 M Ω resistance.

current enhancement reaction is much reduced by suppressing the electrons flowing from the Pt to the interdigitated array cathode with the $10\text{ M}\Omega$ resistance. The variation in the potential difference between the Pt and the interdigitated array cathode is also shown in Fig. 5g. The potential difference starts to increase as it is induced by the concentration changes of the oxidized and reduced ferrocene. The maximum potential difference increased to 0.27 V , which is a sufficient potential difference to bring about the oxidation and reduction reactions at the Pt and interdigitated array cathode, respectively.

From the combination electrode experiment, the potential difference induced concentration cell effect and the shorted concentration cell current were observed directly and hypothesis of current enhancement mechanism caused by self-redox cycling is confirmed.

The current enhancement at the micro-macroelectrode strongly depends on the area of the macroelectrode. Figure 6 shows the limiting currents of the oxidized species on the interdigitated array anode, open circles, and the current from the interdigitated array cathode to the Pt electrode, filled circles, as a function of the Pt electrode area normalized by the interdigitated array cathode area. Here the cathode area is not the geometrical value, but that obtained from the peak current of the cyclic voltammogram, another electrode on open circuit, $9.53 \times 10^{-3}\text{ cm}^2$. The area of the Pt electrode is also obtained from the peak current of the cyclic voltammogram. The anodic limiting current and the current in the combination electrode increases with an increase in the Pt electrode area, and achieves the steady values which are equal to the oxidized limiting current A , and the reduced limiting current, C , of the two electrodes potentiostated interdigitated array electrode experiment.

On the other hand, the anodic limiting current approaches that of the open-circuit interdigitated array experiment, O , when Pt area is small. These results indicate that the reoxidation reaction of the ferrocene at the Pt electrode which compensates for the charge consumed by the reductive reaction of the ferrocene at the cathode is the rate-determining step when the Pt area is not sufficiently large.

Since the currents between the interdigitated array cathode and Pt electrodes are driven by the potential difference between them, the potential difference was evaluated by changing the Pt area. Figure 7 shows the potential difference between the interdigitated array cathode and Pt electrodes as a function of normalized Pt area. Theoretically, the open-circuit potential between the electrodes does not depend on the Pt area because the concentration ratio of reduced and oxidized ferrocene, C_O/C_R , at both the interdigitated array cathode and Pt electrode is kept at a constant value, if no current flows between the electrodes, when the Pt electrode is very far from the interdigitated array electrode.

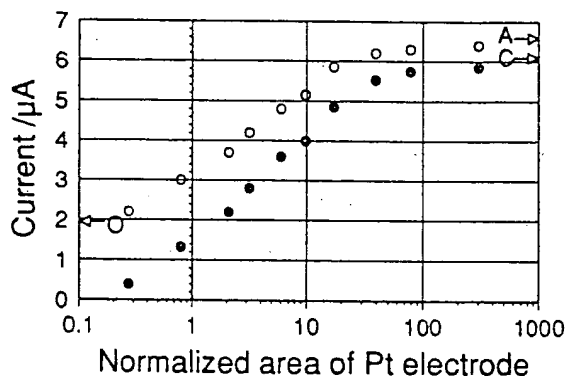


Fig. 6. Oxidized limiting currents of the IDA-Pt electrode, open circles, and the currents from the IDA cathode to the Pt electrode, filled circles, as a function of the Pt electrode area. The area of the Pt electrode is normalized by the IDA cathode, $9.53 \times 10^{-3}\text{ cm}^2$. The scan rate is 100 mV/s .

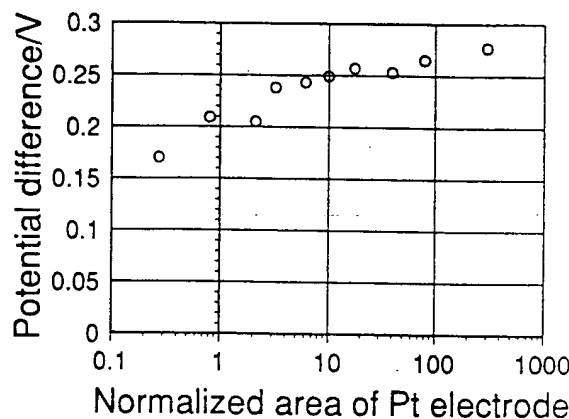


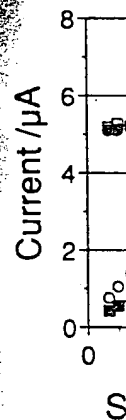
Fig. 7. Potential difference between the IDA cathode and the Pt electrode as a function of the normalized area of the Pt electrode.

However, the measured potential difference is increased by enlarging the Pt electrode area. This Pt area dependence of the potential difference between the interdigitated array cathode and Pt electrode is caused by the fact that the $10\text{ M}\Omega$ resistance allows a very small current to follow. This small current increases the C_O/C_R at the Pt electrode, and reduces the C_O/C_R at the interdigitated array cathode, therefore, the potential difference between the electrodes is decreased. This concentration change is restricted to balance the amount of ferrocene reduced on the cathode and oxidized on the Pt electrode. When the area of the Pt electrode is large, a small concentration change is adequate for balancing the amount of reduced ferrocene on the interdigitated array cathode and that of oxidized ferrocene on the Pt. On the other hand when the Pt area is small, a large concentration change is required on the Pt electrode. As a result, the potential difference between the electrodes is increased by enlarging the Pt area.

Figure 8a shows the anodic limiting current of the ferrocene at the interdigitated array electrode and at the combination electrodes as a function of the scan rate. The oxidized limiting current of the two electrodes potentiostated interdigitated array electrode experiment, open squares, is steady state, due to the redox cycles between anode and cathode, when the scan rate is below 0.1 V/s , equivalent to $0.316\text{ (V/s)}^{1/2}$. However, it starts to increase when the scan rate is higher than 0.1 V/s , suggesting that the steady-state concentration profile near the interdigitated array anode becomes a diffusion-controlled reaction. On the other hand, the limiting current of the interdigitated array electrode on an open circuit, filled squares, is proportional to the square root of the scan rate, reflecting the diffusion controlled property.

When the Pt electrode is large, the anodic limiting currents, filled circles, are very similar to those of the two electrodes potentiostated interdigitated array electrode experiment. This suggests that the Pt electrode in the combination electrode has an electrode area which is large enough to oxidize the ferrocene with a higher rate than that of the interdigitated array anode. On the other hand, in the lower scan region, the limiting currents of the IDA-small Pt electrode, open circles, show a similar magnitude to those of the one interdigitated array electrode on open circuit. However, the magnitude of the currents of the IDA-small Pt electrode at higher scan rates becomes much higher than those of the one interdigitated array electrode on an open circuit.

The difference between the limiting current in the IDA-small Pt and that in the interdigitated array electrode in the open circuit is also due to the redox reaction on the Pt as shown in Fig. 8b, because the current flowing from the interdigitated array cathode to the Pt, open circles, corresponds to the difference between the anodic current of the interdigitated array electrode and that of IDA-small Pt electrode. Since the reoxidation rate of the ferrocene at the Pt electrode is increased by decreasing the electrolysis



time, in other words, the limiting scan rate.

Figure 8b shows the current of the large Pt electrode combined with the scan rate. The anodic current of the large Pt electrode is higher than the IDA-Pt current, and the scan rate is slow response.

An enhanced species was observed at the electrode pair, stated. By the micro-macro electrode, that the current between the electrodes is induced by the limiting current when the Pt magnitude current on difference is inserted between the electrode, the interdigitated array electrode, the difference and reduce dependence property of was small.

Manuscript received

Nippon in meeting

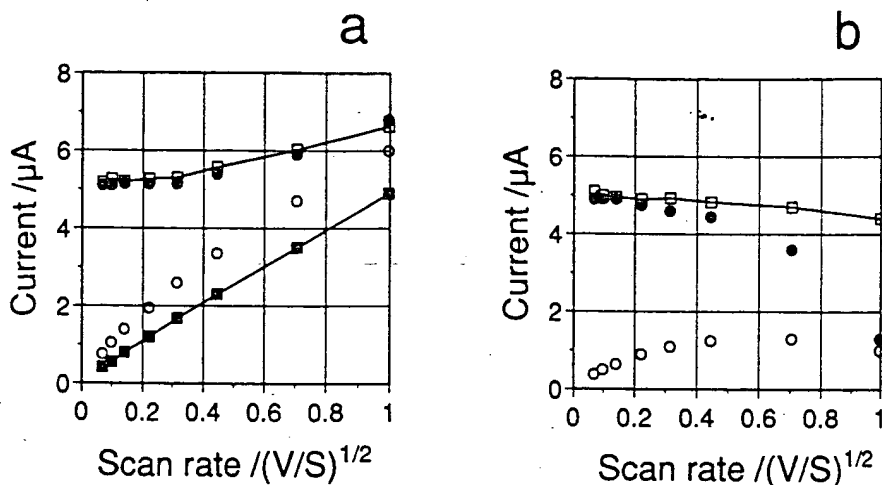


Fig. 8. Variation in the oxidized and reduced limiting currents of the IDA and the oxidized current and the current from the IDA cathode to the Pt of the IDA-Pt electrodes as a function of the square root of the scan rate. —a, Oxidized current of the IDA-Pt, when the Pt electrode area is 10 times larger than that of the IDA cathode, filled circles, and is equal to that of the IDA cathode, open circles. Oxidized limiting current of the IDA measured in two IDA electrodes potentiostated, open squares, and one electrode on open circuit, filled squares. b, Current from the IDA cathode to the Pt in the IDA-Pt, when the Pt electrode area is 10 times larger than that of the IDA cathode, filled circles, and equal to that of the IDA cathode, open circles. Reduced limiting current of the IDA measured in two IDA electrodes potentiostated, open squares.

time, in other words; by increasing the scan rate, because of the propagation of the diffusion layer, the difference in the limiting current could be increased by increasing the scan rate.

Figure 8b also shows the variation in the cathodic current of the interdigitated array electrode and the current in the large Pt combined electrode. The current in the large Pt combined electrode shows good agreement with the cathodic current in the interdigitated array electrode, when the scan rate is low. However, it is much lower than the cathodic current of the interdigitated array electrode at the higher scan rate. Since the two electrodes potentiostated interdigitated array electrode shows a quicker response than the conventional macroelectrode, the decrease of the IDA-Pt current in high scan rate region may reflect the slow response of the large Pt electrode.

Conclusions

An enhancement of the limiting current for the redox species was found in a closely spaced micro-macroelectrode pair, when the macroelectrode was not potentiostated. By the voltammetric measurement of the IDA-Pt, micro-macro, combination electrode pair, it became clear that the current was enhanced by the redox cycling between the interdigitated array cathode and Pt electrodes induced by the localized concentration gradient. The limiting current at the combination electrode rapidly increased when the Pt electrode area was increased, and reached the magnitude of the interdigitated array electrode limiting current on two electrodes potentiostated. The potential difference between the two ends of a 10 M Ω resistance inserted between electrodes depended on the area of the Pt electrode, because the small current flowing from the interdigitated array cathode to the Pt electrode decreased the difference in the concentration ratio of the oxidized and reduced species of both electrodes. The scan rate dependence of the IDA-Pt limiting currents reflected the property of the Pt electrode when the Pt electrode area was small or the scan rate was high.

Manuscript submitted October 26, 1990; revised manuscript received July 26, 1991.

Nippon Telegraph and Telephone Corporation assisted in meeting the publication costs of this article.

REFERENCES

1. M. Fleischmann, S. Pons, D. R. Rolison, and P. P. Schmidt, "Ultramicroelectrodes," Datatech Systems, Inc., Morganton (1987).
2. R. M. Wightman and D. O. Wipf in "Electroanalytical Chemistry," Vol. 15, A. J. Bard, Editor, Marcel Dekker, New York (1989).
3. R. M. Wightman, *Science*, **240**, 415 (1988).
4. S. Pons and M. Fleischmann, *Anal. Chem.*, **59**, 1391A (1987).
5. R. M. Wightman, *ibid.*, **53**, 1125A (1981).
6. K. Aoki, K. Tokuda, and H. Matsuda, *J. Electroanal. Chem.*, **235**, 87 (1987).
7. J. O. Howell and R. M. Wightman, *Anal. Chem.*, **56**, 524 (1984).
8. L. Geng, A. G. Ewing, J. C. Jernigan, and R. W. Murray, *ibid.*, **54**, 852 (1986).
9. J. Janata and A. Bezech, *ibid.*, **60**, 62R (1988).
10. D. C. Johnson, M. D. Ryan, and G. S. Wilson, *ibid.*, **60**, 147R (1988).
11. H. Reller, E. Kirowa-Eisner, and E. Gileadi, *J. Electroanal. Chem.*, **161**, 247, (1984).
12. J. Cassidy, J. Ghoroghchian, F. Sarfarazi, and S. Pons, *Can. J. Chem.*, **63**, 3577 (1985).
13. J. Cassidy, J. Ghoroghchian, F. Sarfarazi, J. J. Smith, and S. Pons, *Electrochim. Acta*, **31**(6), 629 (1986).
14. T. Hepe and J. Osteryoung, *This Journal*, **133**, 752 (1986).
15. R. M. Penner and C. R. Martin, *Anal. Chem.*, **59**, 2625 (1987).
16. I. F. Cheng and C. R. Martin, *ibid.*, **60**, 2163 (1988).
17. B. R. Scharifker, *J. Electroanal. Chem.*, **240**, 61 (1988).
18. A. J. Bard, J. A. Crayston, G. P. Kittlesen, T. V. Shea, and M. S. Wrighton, *Anal. Chem.*, **58**, 2321 (1986).
19. D. G. Sunderson and L. B. Anderson, *ibid.*, **57**, 2388 (1985).
20. K. Aoki, M. Morita, O. Niwa, and H. Tabei, *J. Electroanal. Chem.*, **256**, 269 (1988).
21. O. Niwa, M. Morita, and H. Tabei, *Anal. Chem.*, **62**, 447 (1990).
22. O. Niwa, M. Morita, and H. Tabei, *J. Electroanal. Chem.*, **267**, 291 (1989).
23. T. Horiuchi, O. Niwa, M. Morita, and H. Tabei, *ibid.*, **295**, 25 (1990).
24. A. J. Bard, F.-R. F. Fan, J. Kwak, and O. Lev, *Anal. Chem.*, **61**, 132 (1989).

Preliminary note

Fabrication and characteristics of vertically separated interdigitated array electrodes

Osamu Niwa *, Masao Morita and Hisao Tabei

NTT Basic Research Laboratories, Nippon Telegraph and Telephone Corporation, Tokai, Ibaraki 319-11 (Japan)

(Received 7 June 1989)

INTRODUCTION

The interdigitated array (IDA) electrode has been attracting much attention [1], because of its microelectrode-like behavior, despite its large electrode area. With dual potentiostated usage [2] it can be used to make highly sensitive and fast response electrochemical sensor probes [3], as well as flow cell or chromatographic detectors [4]. We found [5,6] that the limiting current resulting from redox cycling [7] increases as the microband width and the gap between the microbands in an IDA electrode are decreased, and this leads to a sensitivity of $1 \mu M$ when an IDA electrode with a μm -order gap is used. However, the fabrication of IDA electrodes with microband and gap widths of less than $1 \mu m$ is very difficult due to the resolution limit of photolithography. Even a weak contact between a pair of microbands causes an electrical connection, and makes electrochemical measurement impossible.

Several efforts were made to miniaturize the electrode. Wrighton et al. fabricated an array electrode composed of 8 microbands with a gap of about 50 nm by using conventional photolithography and the shadow deposition technique [8]. However, the shadow deposition process is not so reliable for IDA fabrication, because IDA electrodes consist of many microbands and microgaps. A narrow microband electrode consisting of a cross section of thin metal film sandwiched between two insulating films and its significant electrochemical behavior have been reported [9,10]. Narrow microband array electrodes could be fabricated by layering metal and insulating films alternately, but band electrodes in this structure cannot be easily addressed individually.

* To whom correspondence should be addressed.

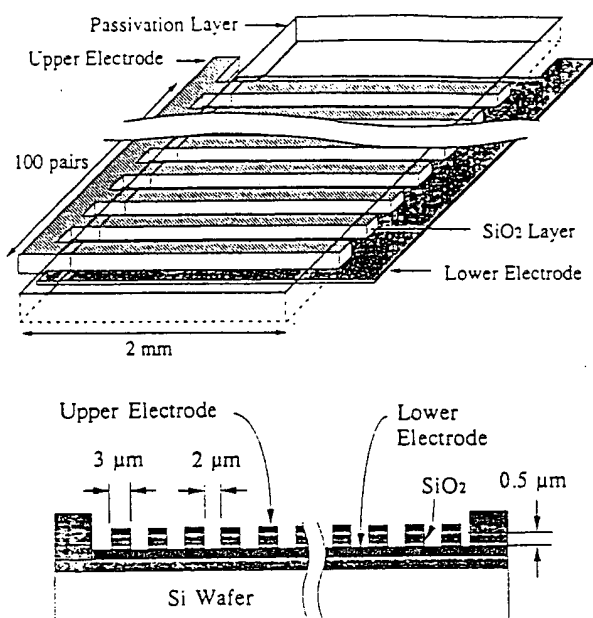


Fig. 1. The new type of vertically separated IDA electrode. The upper and the lower electrodes are separated by a $0.5\ \mu\text{m}$ thick SiO_2 layer.

We have created a new electrode similar to an IDA with a narrow gap by using conventional photolithography and a dry-etching technique. Figure 1 shows the structure of the new electrode. The lower electrode is covered with an array of microband-structured SiO_2 ; therefore, the shape of the electrochemically active electrode area is also a microband structure array. The upper electrode lies on the SiO_2 layer, so the whole electrode has a hollow and protruding structure. The adjacent microband electrodes are separated from each other vertically by an SiO_2 step.

This structure has two advantages compared with ordinary planar IDA electrodes. First, the gap between microband electrodes is defined by the thickness of the insulation layer which can easily be thinner than a lithographically defined pattern. Secondly, the total electrode area is smaller because the gap between the upper and lower electrodes acts as a vertical wall and thus reduces the total area.

This note presents a new type of IDA-like electrode which exhibits excellent electrochemical performance.

EXPERIMENTAL

Fabrication of the new IDA-like electrodes

Figure 2 shows the fabrication procedure of the new IDA-like electrodes. A positive photoresist MP1400-27 (Shiplay) was coated on an oxidized silicon wafer

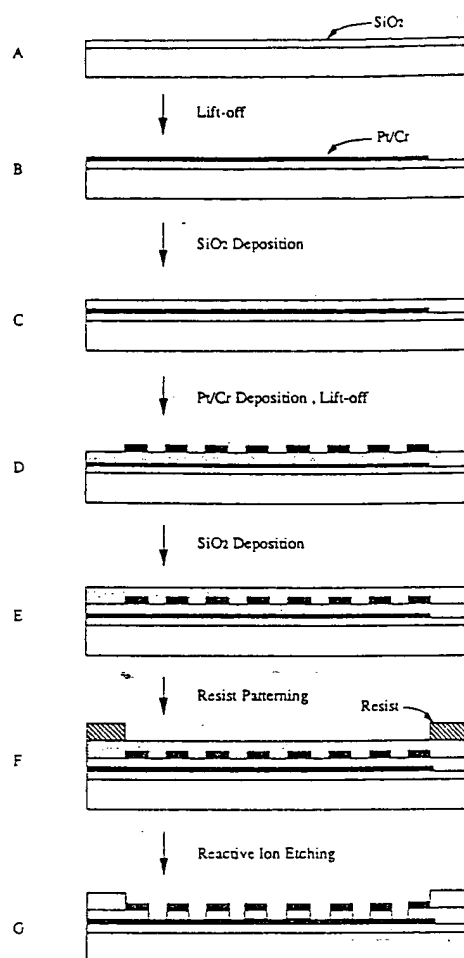


Fig. 2. Fabrication procedure of the new IDA-like electrodes. An oxidized silicon wafer (A) is coated with photoresist, exposed, developed, then Cr and Pt are deposited, and lifted off (B). The wafer is covered with SiO₂ (C), then the upper Pt/Cr electrode is fabricated (D). The wafer is again covered with SiO₂ (E), and a photoresist pattern is delineated (F). The SiO₂ is etched until the lower electrode is exposed (G).

(Fig. 2A). The resist film was exposed to UV light through a photomask by using a PLF-521 contact mask aligner (Canon, Tokyo) and was developed in an MF-319 resist developer (Shiplay), and rinsed in deionized water. Platinum was sputter-deposited on the wafer to a thickness of about 100 nm, followed by the deposition of a thin chromium film (5 nm) with vacuum conditions maintained throughout. The wafer was immersed in methylethylketone and the metalized resist pattern was lifted off. The platinum pattern formed on the wafer after the lift-off is the lower electrode of the new IDA-like electrode (Fig. 2B). SiO₂ was sputter-deposited on the

wafer to a thickness of $0.5\ \mu\text{m}$ (Fig. 2C). Then the platinum upper electrodes were formed by photolithography, platinum sputter-deposition and lift-off techniques in the manner described above (Fig. 2D). The wafer was again covered with $0.3\ \mu\text{m}$ thick SiO_2 by sputter deposition (Fig. 2E). A photoresist film was spin-coated, exposed and developed, and was used as an etching mask (Fig. 2F). The SiO_2 film was etched by DEM-451 (ANELVA, Tokyo) reactive ion etching equipment with tetrafluoromethane using the photoresist and upper electrode patterns as masks until the lower electrode and the pad were exposed (Fig. 2G).

Chemicals and apparatus

Ferrocene, acetonitrile and tetraethylammonium tetrafluoroborate were used as purchased. The electrochemical behavior at the new IDA-like electrodes was studied using a dual potentiostat DPGS-3 (Nikko Keisoku, Atsugi, Japan) and a Ag/AgCl reference electrode.

In measuring the cyclic voltammogram, the potential of the cathode was held at 0 V, and that of the anode was swept between 0 and 0.7 V. The anodic and cathodic currents were recorded against the anode potential. In measuring the chronoamperometry, the potential of the anode was stepped up from 0 to 0.5 V, whereas that of the cathode was held at 0 V.

The current-time transient curves of both electrodes were stored in a digital memory oscilloscope Model 4094B (Nicolet Japan, Tokyo), then recorded with a two-pen X-Y recorder.

RESULTS AND DISCUSSION

Figure 3 shows a voltammogram for $1\ \text{mmol/dm}^3$ ferrocene at a new IDA-like electrode with an upper and lower electrode band width of $5\ \mu\text{m}$ and a step height of $0.5\ \mu\text{m}$ compared with one for a planar IDA with a band width and gap of $5\ \mu\text{m}$. The new IDA-like electrode has 100 pairs of microband electrodes, and the planar electrode has 50 pairs. Each electrode has the same total area consisting of both microband electrodes and gaps. The gap of the electrode is regarded as the thickness of the insulated SiO_2 layer, and was evaluated with a JSM-840 scanning electron microscope (JEOL, Tokyo).

Figures 3a and c show the voltammograms in the generation-collection mode, in which both microband array electrodes were potentiostated, whereas Figs. 3b and d show the voltammograms in the open-circuit mode, in which only one of the arrays was potentiostated. Steady-state currents were observed at the electrodes when the potential of the upper electrode (cathode) was held at 0 V and that of the lower electrode (anode) was cycled between 0 V and 0.7 V at a scan rate of $10\ \text{mV/s}$. As shown in Figs. 3a and c, the limiting current at the new IDA-like electrode is about 5 times higher than that at the planar electrode. There are two causes for this high current. First, the number of microbands arranged in the new IDA-like electrode is twice that of the planar IDA electrode with the same total electrode area. Secondly, the small gap of the new IDA-like electrode leads to an increase in the magnitude of

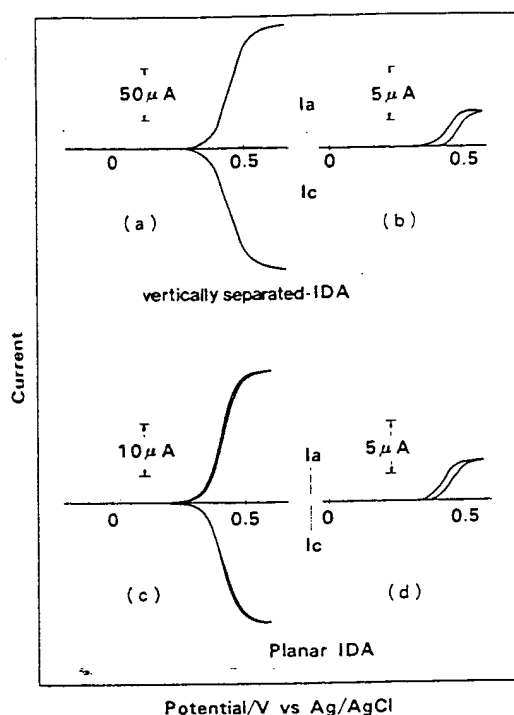


Fig. 3. Cyclic voltammograms of 1 mmol/dm³ ferrocene in an acetonitrile solution containing 0.1 mol/dm³ tetrabutylammonium tetrafluoroborate at the new IDA-like and an ordinary planar IDA electrode with or without potentiostating the cathode. The microband width for both the planar and the new IDA-like electrodes is 5 μ m, whereas the gap is 0.5 μ m for the new IDA-electrode, and 5 μ m for the planar IDA electrode. (a) New IDA-like electrode (cathode: 0 V; sweep rate: 10 mV/s); (b) new IDA-like electrode (cathode: open; sweep rate: 5 mV/s); (c) planar IDA electrode (cathode: 0 V; sweep rate: 10 mV/s); (d) planar IDA electrode (cathode: open; sweep rate: 5 mV/s).

the limiting currents due to the increase in redox cycling between the anode and the cathode [5]. The magnitude of the limiting current in the open circuit mode at the new IDA-like electrode, on the other hand, decreases compared to that in the generation collection mode, and it has almost the same value as that at the planar IDA electrode because of the shielding effect [7].

The number of redox cycles can be assumed from the ratio of the anodic limiting current in the generation-collection mode to that in the open-circuit mode. This number at the new IDA-like electrode is about 35, whereas that at the planar IDA is only 7, indicating the narrowing effect of the gap. The narrow gap also leads to an increase in the collection efficiency. The collection efficiency at the new IDA-like electrode is almost 100% indicating that very little oxidized ferrocene diffuses into the solution, whereas it is 90.6% at the planar one.

The anodic and cathodic limiting currents and collection efficiencies of ferrocene at the new IDA-like electrodes with different geometric parameters are summarized

TABLE 1

Limiting currents and collection efficiencies of ferrocene at the new IDA-like electrodes with different geometric parameters

$W_a^a/\mu\text{m}$	$W_c^b/\mu\text{m}$	$W_g^c/\mu\text{m}$	m^d	$I_a/\mu\text{A}$	$I_c/\mu\text{A}$	$I_{\text{calc}}/\mu\text{A}$	C.E. $^e/\%$
10	5	0.5	50	54.5	53.2	53.5	97.6
5	5	0.5	100	110.5	110.0	95.2	99.5
3	5	0.5	100	100.5	100.0	88.6	99.5
3	2	0.5	100	87.5	87.5	74.8	100.0

^a Microband width of anode (lower electrode).

^b Microband width of cathode (upper electrode).

^c Gap width (thickness of insulator).

^d Number of pairs of microbands.

^e Collection efficiency.

in Table 1. In each case, the lower electrode was the anode and the upper electrode was the cathode. The limiting current at the new IDA-like electrode varied with the microband width. In a previous paper, the diffusion-controlled limiting current at a

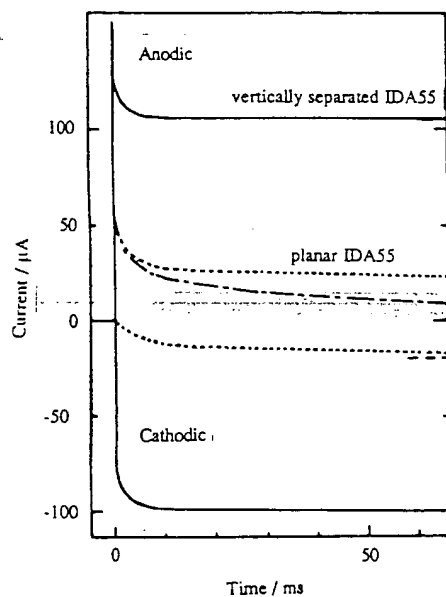


Fig. 4. Chronoamperometric current-time curves for potential step oxidation of 1 mmol/dm³ ferrocene in a solution of 0.1 mol/dm³ tetrabutylammonium tetrafluoroborate in acetonitrile at the new IDA-like electrode compared to that at the ordinary planar one. The width of the microband at the new IDA-like electrode and at the planar IDA electrode is 5 μm . The gaps at the new IDA-like electrode and at the planar IDA55 electrode are 0.5 μm and 5 μm , respectively. (—) Response of the new IDA-like electrode, (·····) IDA55; (-·-·-) the new IDA-like electrode in the open circuit mode.

planar IDA was expressed by [4]

$$|I_{lim}| = mbnFDc \left\{ 0.637 \ln \left[2.55 \left(1 + w/w_g \right) \right] - 0.19 \left[w_g / (w + w_g) \right]^2 \right\} \quad (1)$$

where m and b are the number and the length of the microband, respectively. W is the band width of the IDA, W_g is the gap width, and the other variables have their usual meaning. The calculated limiting currents when regarding the thickness as the gap almost fit the experimental values, indicating that eqn. (1) can be used as a primary approximation. The limiting currents at the new IDA-like electrode are, in fact, a little higher than the calculated values. Since the side wall of the upper electrode, whose thickness is about $0.05 \mu\text{m}$, works as an electrode, the extra current due to the side edges increases the total limiting current. Evaluation of the upper electrode thickness may be necessary to measure the limiting current quantitatively.

Dual potentiostated chronoamperometric curves resulting from potential steps at the new IDA-like electrode with $5 \mu\text{m}$ microband width and $0.5 \mu\text{m}$ gap compared with those at the ordinary planar electrode with $5 \mu\text{m}$ microband width and gap are shown in Fig. 4. The current reached the steady state within a few tens of milliseconds, whereas it took more than 100 ms at the planar electrode. This fast establishment of the steady state at the electrode is due to the high number of redox cycles in the narrow gap. The anodic current-time curve in the open circuit mode is also shown in Fig. 4. When the cathode is not potentiostated, the anodic limiting current does not reach the steady state due to the absence of redox cycles between the electrodes.

CONCLUSIONS

A new type of IDA-like electrode is demonstrated. The two arrays of microband electrodes are separated by a thin insulating step, fabricated by conventional photolithography and dry-etching techniques. A step height of $0.5 \mu\text{m}$ can be realized easily. The electrodes show high limiting currents because of the large number of redox cycles and their high collection efficiency. Fast establishment of the steady state, within a few tens of milliseconds, is also observed at this electrode due to the fast formation of a concentration gradient across the narrow gap.

REFERENCES

- 1 C.E. Chidsey, B.J. Feldman, C. Lundgren and R.W. Murray, *Anal. Chem.*, **58** (1986) 601.
- 2 D.G. Sanderson and L.B. Anderson, *Anal. Chem.*, **57** (1985) 2388.
- 3 F. Mansfield, *J. Electrochem. Soc.*, **135** (1988) 1354.
- 4 L.E. Fosdick, J.L. Anderson, T.A. Baginski and R.C. Jaeger, *Anal. Chem.*, **58** (1986) 2750.
- 5 K. Aoki, M. Morita, O. Niwa and H. Tabei, *J. Electroanal. Chem.*, **256** (1988) 269.
- 6 O. Niwa, M. Morita and H. Tabei, *Anal. Chem.*, submitted.
- 7 A.J. Bard, J.A. Crayston, G.P. Kittlesen, T.V. Shea and M.S. Wrighton, *Anal. Chem.*, **58** (1986) 2321.
- 8 E.T.T. Jones, O.M. Chyas and M.S. Wrighton, *J. Am. Chem. Soc.*, **109** (1987) 5526.
- 9 H.S. White, *J. Phys. Chem.*, **91** (1987) 3559.
- 10 K.R. Wehmeyer, M.R. Deakin and R.M. Wightman, *Anal. Chem.*, **57** (1985) 1913.

is with different

C.E. %
97.6
99.5
99.5
100.0

per electrode
ried with the
current at a

dm³ ferrocene
new IDA-like
new IDA-like
ode and at the
new IDA-like

Theory of the steady-state current of a redox couple at interdigitated array electrodes of which pairs are insulated electrically by steps

Koichi Aoki *

Department of Electronic Chemistry, Graduate School at Nagatsuta, Tokyo Institute of Technology, Nagatsuta, Midori-ku, Yokohama 227 (Japan)

(Received 30 March 1989)

ABSTRACT

The possibility of constructing an interdigitated array electrode (IDA) with a submicrometre gap is proposed in which adjacent microband electrodes are separated from each other by an insulated step. Then the IDA is an assembly of protrusive and hollow microband electrodes. The unit model of the IDA consisted of half of the lower (hollow) microband electrode, an insulated step and half of the upper (protrusive) microband electrode with a finite thickness on the step. The boundary value problem involving the two-dimensional Laplace equation is presented for redox cycling at the IDA under diffusion control and is solved numerically by a boundary element method. The steady-state current was computed as a function of the height of the step and the thickness of the upper electrode. It was larger than the current at the ordinary IDA, partly because the true electrode area was larger than the area of the ordinary IDA. The current varied linearly with the logarithm of the step height. It was expressed by a simple approximate equation in order to facilitate prediction of its numerical value.

INTRODUCTION

A significant characteristic of an interdigitated array electrode (IDA) is acquisition of the steady-state current by dual potentiostatic control [1-5]. The steady state is established by diffusional recycling of a redox couple between the microband anodes and microband cathodes without controlled convection of the solution. Similar recycling is observed at a twin electrode in a thin-layer cell. Since the IDA has an uncompensated resistance much smaller than that of a twin electrode in a thin-layer cell, it is suitable for accurately controlled potentiostatic measurements under the steady state.

* Present address: Department of Applied Physics, Faculty of Engineering, Fukui University, 3-9-1 Bunkyo, Fukui-shi 910, Japan.

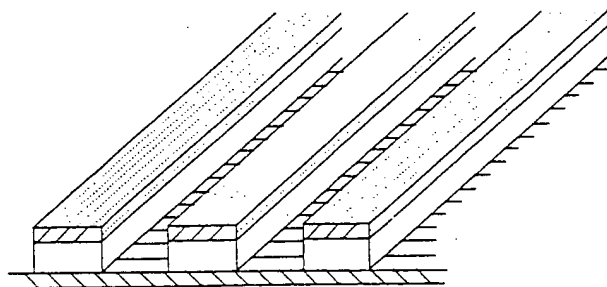


Fig. 1. Illustration of the IDA with a submicrometre gap. The adjacent microband electrodes are separated by insulated steps.

In a previous paper [4], expressions for the steady-state current by recycling at an IDA were derived by application of the theory of complex variables, and a simple approximate equation was presented for an IDA with the same width as the microband electrodes. According to that equation, the steady-state current varies linearly with $\ln(w/w_g)$, where w_g is the width of the gap and w is the width of the unit cell, i.e. the sum of w_g and the width of the microband electrode. This variation indicates that diminishing w_g under a given w leads to enhancement of the current. A study [6] on chronoamperometry at the IDA has demonstrated that the relaxation time toward the steady-state current has a dependence of $\exp(w_g/w)$. Consequently, diminishing w_g makes the current response rapid. Fortunately, it is not as unfavourable to diminish only w_g as it is to diminish both w_g and w .

One way to construct an IDA with a submicrometre gap is to separate adjacent microband electrodes three-dimensionally by a thin insulated layer with microband incisions so that there is a step between one pair of microband electrodes and the other, as shown in Fig. 1. Then the IDA consists of a set of protrusive electrodes and a set of hollow ones. The method of construction will be described in detail in another paper [7]. This report is devoted to evaluating numerically the steady-state current at the IDA by use of the boundary element method [8].

MODEL AND BOUNDARY ELEMENT METHOD

The electrochemical system treated here is a simple redox couple that is soluble in supporting electrolytes. All the symbols used below are defined at the end of this paper. The following five assumptions are made: (1) a large value of m ($> \text{ca. } 20$); (2) a common width of each microband electrode; (3) sufficiently long microband electrodes, i.e. $b \gg w_g$; (4) diffusion coefficient common to the redox couple; and (5) diffusion-controlled mass transport. Assumptions (1) and (3) serve to reduce the IDA to a two-dimensional unit model, as shown in Fig. 2. The model unit involves half of the microband anode, half of the microband cathode and an insulated step. Then the behaviour at the whole IDA is an assembly of the behaviour at $2 \times m$ unit cells. The upper layer of the actual electrode is at least 50 nm thick in order to keep the metallic property. Since the thickness cannot be neglected compared with w_g , a

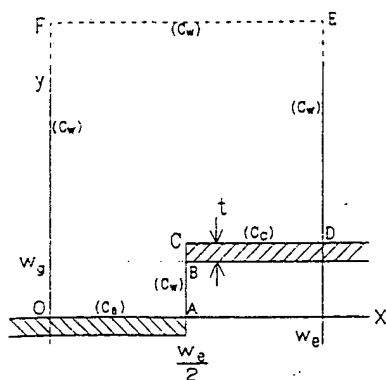


Fig. 2. A model of the unit cell, where $C_a = OA$, $C_c = BCD$ and $C_w = AB$ and $DEFO$.

finite thickness has been introduced into the model. Because of the common value of the diffusion coefficient, the sum of the concentrations of the redox couple is equal to c^* at any point in the diffusion space.

When the potentials at the anode and cathode are set to sufficiently positive and negative values, respectively, the boundary value problem for the reduced species under the steady state in the unit cell is expressed by

$$D(\partial^2 c / \partial x^2 + \partial^2 c / \partial y^2) = 0 \quad (1)$$

$$0 \leq x \leq w_e/2 \quad y = 0 \quad (\text{on } C_a): c = 0 \quad (2)$$

$$\left. \begin{aligned} x = w_e/2 \quad w_g \leq y \leq w_g + t \\ w_e/2 \leq x \leq w_e \quad y = w_g + t \end{aligned} \right\} (\text{on } C_c): c = c^* \quad (3)$$

$$\left. \begin{aligned} x = 0 \quad y > 0 \\ x = w_e/2 \quad 0 < y < w_g \\ x = w_e \quad y > w_g + t \end{aligned} \right\} (\text{on } C_w): \partial c / \partial x = 0 \quad (4)$$

The boundary value problem was solved numerically by the boundary element method [8]. Since nodal values in this method are defined only on given boundaries rather than in an enclosed domain, computer memory can be saved in comparison with the finite element method. Thus discretization on the boundary can be made fine without prolongation of the computation time.

Multiplying eqn. (1) by $\ln(r)$, integrating it over the solution phase and applying Green's theorem [9] to the resulting equation yields

$$\int_{C_a} K ds + \int_{C_c} K ds + \int_{C_w} K ds = \pi c \quad \text{on } C_w, C_a, C_c \quad (5)$$

where

$$K = c \{ \partial \ln(r) / \partial \nu \} - (\partial c / \partial \nu) \ln(r) \quad (6)$$

Inserting eqns. (2), (3) and (4) into eqn. (5) and transferring the terms with known values to the right-hand side leads to

$$\int_{C_w} c \{ \partial \ln(r) / \partial \nu \} ds - \int_{C_a + C_c} (\partial c / \partial \nu) \ln(r) ds - \pi c = -c^* \int_{C_c} \{ \partial \ln(r) / \partial \nu \} ds \quad (7)$$

on C_w, C_a, C_c

The boundary was discretized into N elements, which were numbered 1 to L on C_a , $L+1$ to L' on C_c and $L'+1$ to N on C_w . It was assumed that c and $\partial c / \partial \nu$ were invariant on each discretized element and that the value of c or $\partial c / \partial \nu$ at the mid-point of two adjacent nodes was represented by the arithmetic average of the two nodal values. When r is located at the mid-point of the i -th element, eqn. (7) becomes

$$\sum_{k=L'+1}^N c_k U_{i,k} - \sum_{K=1}^{L'} (\partial c / \partial \nu)_K V_{i,k} = -c^* \sum_{K=L+1}^{L'} U_{i,k} \quad (i = 1, 2, \dots, N) \quad (8)$$

where

$$U_{i,k} = \int_K \{ \partial \ln(r_{i,k}) / \partial \nu \} ds - \pi \delta_{i,k} \quad (9)$$

$$V_{i,k} = \int_K \ln(r_{i,k}) ds \quad (10)$$

The terms c_k for $k = L'+1$ to N and $(\partial c / \partial \nu)_k$ for $k = 1$ to L' in eqn. (8) are unknown while the terms on the right-hand side are known. Thus eqn. (8) is a simultaneous equation for c_k and $(\partial c / \partial \nu)_k$.

The integrals in eqns. (9) and (10) were evaluated by a conventional method as described in a textbook of the boundary element method [8]. The simultaneous equation was solved by the Gauss-Jordan elimination method. The computer was a Vax-11/780 (DEC). The computer program was written in FORTRAN-77. When the height (OF in Fig. 2) of the diffusion space was taken to be over $5w_e$, the current value did not vary with the height within 0.5% error. All computations were made at $5w_e$ for the height. Each of the two sides (OA, CD) and the top side (EF) on the boundary were divided into 30 elements of the same length. The sides AB and BC were divided into 20 and 10 elements, respectively. The other vertical boundaries were divided into 30 elements whose lengths were proportional to y^2 on OF and to $(y - w_g - t)^2$ on DE. Under this discretization, the total current at the IDA is expressed by

$$I = 2mbnF \int_{C_a} D(\partial c / \partial y)_{y=0} dx = -mbnFD(w_e/L) \sum_{j=1}^L (\partial c / \partial \nu)_k \quad (11)$$

The factor 2 in the middle term comes from the involvement of half of the anode in the unit cell. The number of total elements was 180 and hence the matrix size was 180×180 . The matrix was featureless, i.e. not symmetric or having no band form.

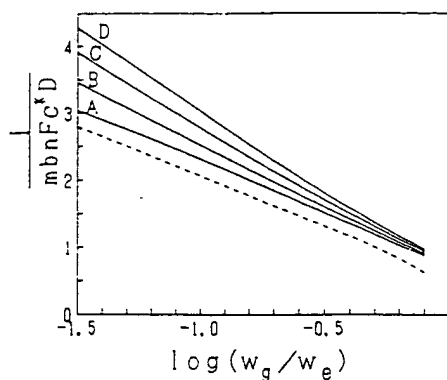


Fig. 3. Dependence of the dimensionless current on $\log(w_g/w_e)$ for $t/w_e =$ (A) 0.0, (B) 0.01, (C) 0.05 and (D) 0.1. The dashed curve denotes the current at the ordinary IDA, expressed by eqn. (12).

The computation time was ca. 20 s per geometry. In order to confirm the validity of the program, the values of the currents for the ordinary IDA were computed; they agreed with analytical values [4] within 0.8% error.

RESULTS AND DISCUSSION

Figure 3 shows variations of $I'/mbnFc*D$ against $\log(w_g/w_e)$ for various values of t/w_e . All the currents are larger than the current at the ordinary IDA (dashed line in Fig. 3), which has been expressed approximately by

$$I' = mbnFc*D \left[0.636 \ln \left\{ 2.55 \left(1 + w_e/w_g \right) \right\} - 0.19 \left(1 + w_e/w_g \right)^{-2} \right] \quad (12)$$

The gain of the current is ascribed partly to the increase in the electrode area of the IDA with steps, $((w_e + t)b)$, which is larger than the area of the ordinary IDA $((w_e - w_g)b)$. The former area is larger than the projected area $(w_e b)$ by tb because of the three-dimensional structure. The gain of the current is remarkable with an increase in t/w_e .

Of interest is the significant variation of the current with t/w_e when t/w_e and w_g/w_e are small. This variation is due to the contribution of the electrolysis on the BC side which provides a much larger current density than that on the side CD. For example, the ratios of the average current density on the side BC to that on the side CD are 13.0, 4.5 and 1.3, respectively, for $t/w_e = 0.001, 0.01$ and 0.1 at $w_g/w_e = 0.1$. Since the BC side contributes appreciably to the total current, it is necessary to measure accurately the thickness of the electrode for the purpose of quantitative analysis.

For $w_g/w_e < 0.5$, the current varies linearly with $\log(w_g/w_e)$. The linearity is slightly better than that at the ordinary IDA. The differences between the slopes at non-zero values of t/w_e and the slope (-1.55) at $t/w_e = 0$ were plotted against t/w_e in a logarithm-logarithmic scale. The plot fell on a straight line with a slope of

0.45. Then the slopes in Fig. 3 can be expressed by $-1.55 - 2.27(t/w_e)^{0.45}$. All the straight lines in Fig. 3 go through a common point $(-0.24, 1.15)$. From these arithmetic features of the curves, the current is expressed approximately by

$$I = mbnFc^*D \left[1.13 - \left\{ 1.55 + 2.27(t/w_e)^{0.45} \right\} \left\{ 0.24 + \log(w_g/w_e) \right\} \right] \quad (13)$$

This equation is valid for $w_g/w_e \leq 0.5$ and $t/w_e \leq 0.1$ within 3% error. Since practically constructed IDAs have dimensions $0.05 \leq t \leq 0.07 \mu\text{m}$, $0.5 \leq w_g \leq 1.0 \mu\text{m}$ and $1 \leq w_e \leq 10 \mu\text{m}$, most of them can be covered by eqn. (13).

The functional form of eqn. (13) looks rather different from that of eqn. (12). By considering that $w_e + w_g$ at the ordinary IDA is equivalent to w_e (or w) at the IDA with steps, eqn. (12) is reduced to

$$I' = mbnFc^*D \{ 0.595 - 1.46 \log(w_g/w_e) \} \quad (14)$$

where the term involving 0.19 in eqn. (12) has been neglected because of the minor contribution. On the other hand, the limiting form for $t \rightarrow 0$ in eqn. (13) is given by

$$I = mbnFc^*D \{ 0.758 - 1.55 \log(w_g/w_e) \} \quad (15)$$

Therefore both functional forms are the same. From a comparison of eqns. (14) and (15), the current at the IDA with very thin electrode thickness is approximately 25% larger than that of the ordinary IDA.

In conclusion, the characteristics of an IDA with steps are as follows:

- ✓ (A) presentation of a current larger than that at an ordinary IDA;
- ✓ (B) a current that is sensitive to the thickness of the upper electrode;
- ✓ (C) it possesses an electrode area larger than the projected area; and
- ✓ (D) it shows a linear variation of the current with $\log(w_g/w_e)$, as expressed by eqn. (13).

LIST OF SYMBOLS

b	length of microband electrodes of the IDA
c	concentration of the reduced species
c^*	sum of the concentrations of the reduced and the oxidized species
C_a	boundary between the anode and solution in the unit cell
C_c	boundary between the cathode and solution in the unit cell
C_w	boundary between the walls and solution in the unit cell
D	diffusion coefficient common to the reduced and the oxidized species
F	Faraday constant
I	total current at the IDA under the steady state
I'	total current at the ordinary IDA under the steady state
L	number of divisions on the anode
$L' - L$	number of divisions on the cathode
m	number of microband anodes or microband cathodes in the IDA
n	number of electrons transferred

N	number of elements on the boundary
r	distance between a given point and any point on the boundary
$r_{i,k}$	distance between the centre of the i -th element and that of the k -th one
s	length on the boundary
t	thickness of the upper electrode
w	width of the unit cell, equal to w_e at the IDA with steps and equal to $w_e + w_g$ at the ordinary IDA
w_e	width of the anode or cathode
w_g	width of the gap
x	axis on the unit cell
y	axis on the unit cell
δ_{ik}	unity at $i = k$, zero at $i \neq k$
ν	length of the vector directing out from the diffusion space
\int_k	integration over the k -th element

ACKNOWLEDGEMENTS

The author wishes to thank M. Morita, O. Niwa and H. Tabei at NTT Basic Research Laboratories, Nippon Telegraph and Telephone Corporation for guiding this research.

REFERENCES

- 1 D.G. Sanderson and L.B. Anderson, *Anal. Chem.*, 57 (1985) 2388.
- 2 C.E. Chidsey, B.J. Feldman, C. Lundgren and R.W. Murray, *Anal. Chem.*, 58 (1986) 601.
- 3 B.J. Feldman and R.W. Murray, *Anal. Chem.*, 58 (1986) 2844.
- 4 K. Aoki, M. Morita, O. Niwa and H. Tabei, *J. Electroanal. Chem.*, 256 (1988) 269.
- 5 M. Morita, O. Niwa and H. Tabei, *Anal. Chem.*, submitted.
- 6 K. Aoki and M. Tanaka, *J. Electroanal. Chem.*, 266 (1989) 11.
- 7 O. Niwa, M. Morita and H. Tabei, *J. Electroanal. Chem.*, 267 (1989) 291.
- 8 C.A. Brebbia, *Progress in Boundary Element Methods*, Vol. 1, Pentech Press, London, 1981, pp. 45-83.
- 9 C.A. Brebbia in ref. 8, p. 46.

support from NATO (International Grants Division) is also acknowledged. We thank Professor K.B. Oldham for providing a preprint of his work.

REFERENCES

- 1 R.M. Wightman, *Science*, **240** (1988) 415.
- 2 J.O. Howell and R.M. Wightman, *Anal. Chem.*, **56** (1984) 524.
- 3 A.M. Bond, M. Fleischman and J. Robinson, *J. Electroanal. Chem.*, **168** (1984) 299.
- 4 A.M. Bond, M. Fleischman and J. Robinson, *J. Electroanal. Chem.*, **172** (1984) 11.
- 5 C. Amatore, M.R. Deakin and R.M. Wightman, *J. Electroanal. Chem.*, **225** (1987) 49.
- 6 W. Thormann, P. van der Bosch and A.M. Bond, *Anal. Chem.*, **57** (1985) 2764.
- 7 A.M. Bond, T.L.E. Henderson and W. Thormann, *J. Phys. Chem.*, **90** (1986) 2911.
- 8 A.J. Bard and L.R. Faulkner, *Electrochemical Methods*, Wiley, New York, 1980.
- 9 J. Newman, *Electrochemical Systems*, Prentice-Hall, Englewood Cliffs, NJ, 1973, pp. 231-234.
- 10 G. Charlot, J. Badoz-Lamblin and B. Tremillon, *Les Reactions Electrochimiques*, Masson, Paris, 1959, pp. 13-24.
- 11 S. Bruckenstein, *Anal. Chem.*, **59** (1987) 2098.
- 12 E. Brunner, *Z. Phys. Chem.*, **58** (1907) 71.
- 13 A. Eucken, *Z. Phys. Chem.*, **59** (1907) 72.
- 14 J. Newman, *Ind. Eng. Chem. Fundam.*, **5** (1966) 525.
- 15 J. Newman, *Electrochemical Systems*, Prentice-Hall, Englewood Cliffs, NJ, 1973, pp. 353-381, 414-425.
- 16 K.B. Oldham, *J. Electroanal. Chem.*, **250** (1988) 1.
- 17 K.B. Oldham, *J. Electroanal. Chem.*, **122** (1981) 1.
- 18 C.A. Amatore, M.R. Deakin and R.M. Wightman, *J. Electroanal. Chem.*, **206** (1986) 23.
- 19 M.R. Deakin, R.M. Wightman and C. Amatore, *J. Electroanal. Chem.*, **215** (1986) 49.
- 20 C.A. Amatore, B. Fossel, M.R. Deakin and R.M. Wightman, *J. Electroanal. Chem.*, **225** (1987) 33.
- 21 A.J. Fry and W.E. Britton in P.T. Kissinger and W.R. Heineman (Eds.), *Laboratory Techniques in Electroanalytical Chemistry*, Marcel Dekker, New York, 1984, p. 378.
- 22 J. van de Poel and H.M. Neumann, *Inorg. Synth.*, **11** (1968) 53.

J. Electroanal. Chem., **256** (1988) 269-282
Elsevier Sequoia S.A., Lausanne - Printed in The Netherlands

Quantitative analysis of reversible diffusion-controlled currents of redox soluble species at interdigitated array electrodes under steady-state conditions

Koichi Aoki

Department of Electronic Chemistry, Graduate School at Nagatsuda, Tokyo Institute of Technology, Nagatsuda, Midori-ku, Yokohama 227 (Japan)

Masao Morita*, Osamu Niwa and Hisao Tabei

NTT Basic Research Laboratories, Nippon Telegraph and Telephone Corporation, Tokai, Ibaraki 319-11 (Japan)

(Received 18 July 1988)

ABSTRACT

Equations for diffusion-controlled currents at interdigitated array electrodes (IDA) were derived analytically for the reversible redox reactions of soluble species under steady-state conditions. The two-dimensional diffusion equation was solved by the Schwarz-Christoffel transformation. Current and concentration distributions were obtained. The total current was expressed by the ratios of the two complete elliptic functions and the geometric widths of the anode, the cathode and the gap. The current at each microband electrode of the IDA depended on the ratios of the three widths rather than the absolute values of the widths. Platinum IDAs were fabricated by photolithography on silicon wafers. The widths of the microband electrodes were 3-10 μm while those of the gap were 2-5 μm . Voltammograms of ferrocene were measured with a dual potentiostat under steady-state conditions. The collection efficiency was ca. 95%. The limiting current agreed with the theoretical prediction.

INTRODUCTION

Arrays of microelectrodes have extensive applications such as charge flow control devices based on molecular materials [1,2], enhancement of current response retaining desirable characteristics of single microelectrodes [3-6], the monitoring of zone distribution in electrophoresis [7,8], use as a microarray channel electrode in a flow cell or for a liquid chromatographic detector [3,9-15] and as a model of heterogeneity on solid electrodes [16-22]. Another application involves steady-state measurements at a coplanar interdigitated array electrode (IDA) [23-25]. Since each

* To whom correspondence should be addressed.

microband electrode in the IDA can be potentiostated alternately, an electroactive species generated at one microband electrode diffuses across a thin gap to the adjacent electrode, at which the species is detected. The concept of this electrochemical technique is similar to that at a rotating ring-disk electrode and a twin electrode in a thin layer [26,27]. Mass transport at the IDA is similar to that at the twin electrode in that diffusion takes place within a finite space, resulting in the exhibition of a steady-state current. Advantages of the IDA in comparison with the rotating ring-disk electrode are:

- (a) steady-state currents without involvement of noise due to the rotation,
 - (b) high collection efficiency reaching unity,
 - (c) simple handling and feasibility of installing the IDA in another instrument for in-situ measurements.
- The IDA overcomes the disadvantages of the twin electrode in a thin layer on the following points:
- (d) specific control and determination of the interelectrode distance,
 - (e) accurate potential control without paying a penalty for serious resistance problems in the thin layer.

In addition most characteristics of a single microband electrode [28-31] may be retained.

In a pioneer study on the IDA the steady-state current was observed and a semi-empirical equation for the current presented [23]. Application of the IDA has been directed to measurement of the redox electron conduction through polymer-coated films [24,25]. An attempt to quantify the mass transport has been made by digital simulation at two- and three-electrode pairs in the different context of the IDA [2]. These studies, however, have not dealt quantitatively with even the simplest diffusion-controlled behavior at the IDA. For instance, Sanderson and Anderson's work [23] poses the following two questions:

- (a) Why was the effective interelectrode separation ($0.665 \mu\text{m}$) estimated from the current quite different from the coplanar geometric separation ($50 \mu\text{m}$)?
- (b) Why was the time (a few minutes) of approaching the steady-state current so long in comparison with the time (a few seconds) of developing the diffusion layer between the interelectrode distance?

In this paper, we address the first question by presenting a theory of the diffusion-controlled current in the steady state. We have fabricated IDAs with various kinds of geometry by means of photolithography as illustrated in Fig. 1, and have measured the steady-state current in order to demonstrate the validity of the theoretical expression.

THEORY

Derivation of expressions for the current

The electrochemical system treated here is a soluble redox couple of which the charge transfer step obeys the Nernst equation. The following assumptions are made:

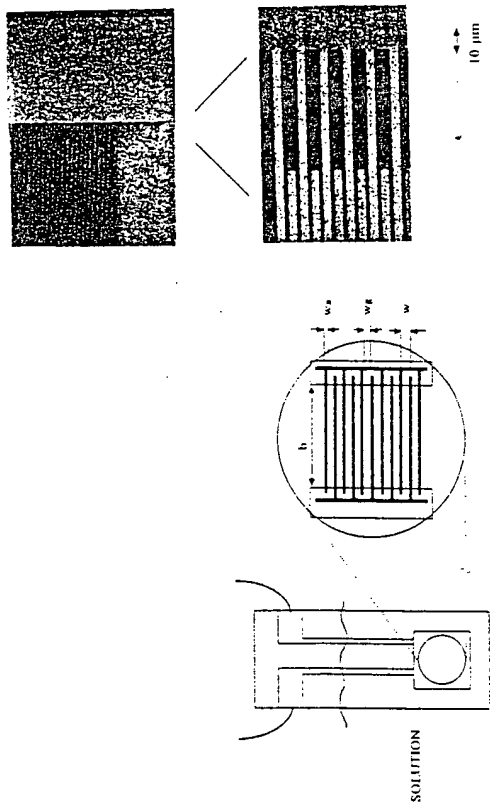


Fig. 1. Illustration of the IDA (A), a magnified view (B) and scanning electron microscope photographs of the IDA ($w_a = w_c = 3 \mu\text{m}$, $w_b = 2 \mu\text{m}$) fabricated by photolithography (C). Surfaces enclosed by dotted lines in Fig. 1B are sealed with silicon dioxide. The SEM photographs were taken before silicon dioxide deposition.

- (i) The IDA is composed of so many microband electrodes that edge effects at either side of the IDA have a negligible influence on the total current.
- (ii) The length of the element microband electrode is much longer than its width.
- (iii) The diffusion coefficients of the reduced and the oxidized species have a common value, D .
- (iv) The system is fully in the steady state.

From (i) and (ii), the electrode behavior at the IDA can be regarded as a simple assembly of the two-dimensional unit cell, in which halves of the anode and cathode are involved, as shown in Fig. 2A. The unit cell is placed on the complex variable z -plane with x - and y -axes. The anode, the cathode and the gap are on the real axis (x).

Concentration of the reduced and the oxidized species, denoted by c_R and c_O respectively, are subject to the two-dimensional diffusion equation under steady-state conditions:

$$\partial^2 c / \partial x^2 + \partial^2 c / \partial y^2 = 0 \quad (1)$$

[A] [B] [C]

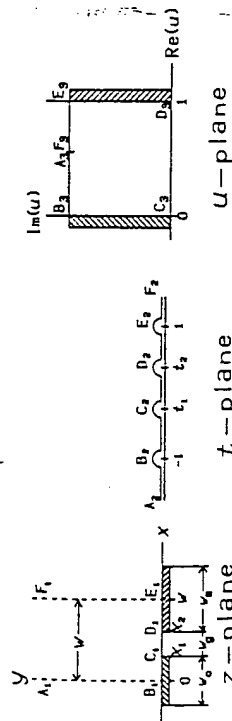


Fig. 2. Model of the unit cell on the z -plane (A) where the real and imaginary parts of z are x and y , respectively. A_1, B_1, C_1, D_1, E_1 and F_1 in (A) are mapped onto the real axis of the t -plane at corresponding positions with subscript 2 (B). They are further mapped onto the rectangle of the u -plane at positions with subscript 3 (C).

where c represents c_R or c_O . When the anode and the cathode are potentiostated at E_a and E_c , respectively, boundary conditions are given by

$$c_O/c_R = \exp[(nF/RT)(E_c - E^{\circ'})] \quad \text{at the cathode } (0 \leq x \leq x_1, y = 0) \quad (2)$$

$$c_O/c_R = \exp[(nF/RT)(E_a - E^{\circ'})] \quad \text{at the anode } (x_2 \leq x \leq w, y = 0) \quad (3)$$

$$D(\partial c_R/\partial y + \partial c_O/\partial y) = 0 \quad \text{both at the anode and the cathode} \quad (4)$$

$$\partial c/\partial y = 0 \quad \text{at the gap } (x_1 \leq x \leq x_2 \text{ and } y = 0) \quad (5)$$

$$\partial c/\partial x = 0 \quad \text{on the walls in the unit cell}$$

$$(x = 0, x = w)$$

where w is the width of the unit cell, $2x_1, 2(w - x_2)$ and $x_2 - x_1$ are lengths of the cathode, the anode and the gap, respectively, n is the number of electrons, and $E^{\circ'}$ is the formal potential. From eqns. (1), (4) and (5), the sum of c_R and c_O is a constant, c^* , i.e.,

$$c_R + c_O = c^* \quad (6)$$

Since the boundary value problem includes the two-dimensional Laplace equation, a solution is composed basically of analytic functions satisfying the boundary conditions [32]. The problem is attributed to transformation of the boundary so that a concentration profile can be expressed by a simple analytic function. A transformation expedient to polygonal boundaries is the Schwarz-Christoffel transformation [33]. The first step of the transformation is to map the semi-infinite rectangle into a line (Fig. 2B). Here, we have assigned the origin (B_1) on the z -plane to -1 (B_2) on the t -plane, x_1 to t_1 , x_2 to t_2 and w to 1 . Now t_1' and t_2 are unknown. The relation between z and t for this mapping is given by [33]

$$\frac{dz}{dt} = \frac{C_1}{\sqrt{(t+1)(t-1)}} \quad (7)$$

where C_1 is a constant to be determined. Integrating eqn. (7) with the condition $t = -1$ at $z = 0$ yields

$$z = C_1 i [\arccos(t) + \pi] \quad (8)$$

where $i = \sqrt{-1}$. Imposing the condition $t = 1$ at $z = w$ on eqn. (8) yields $C_1 i = w/\pi$. Then we have

$$t = -\cos\{(z/w)\pi\} \quad (9)$$

Unknowns t_1 and t_2 can be determined by inserting x_1 and x_2 into eqn. (9):

$$t_1 = -\cos\{(x_1/w)\pi\} \quad (10)$$

$$t_2 = -\cos\{(x_2/w)\pi\}$$

The next step is to map this line in the t -plane onto the u -plane involving a rectangular enclosure, as shown in Fig. 2C, where t_1 and t_2 have been assigned to the origin and 1 on the u -plane, respectively. The other points, A_2, B_2, E_2 and F_2 , are unknown at this stage. The differential equation for the mapping is given by

$$\frac{du}{dt} = \frac{C_2}{\sqrt{(t+1)(t-1)}(t-t_1)(t-t_2)} \quad (11)$$

where C_2 is a constant. Integrating eqn. (11) from t_1 (at $u = 0$) to any t yields the incomplete elliptic integral, F [34]:

$$u = \frac{2C_2}{\sqrt{(1-t_1)(1+t_2)}} F(g(t) | p) \quad (12)$$

where

$$F(\phi | k) = \int_0^\phi \frac{dt}{\sqrt{1-k^2 \sin^2(t)}} \quad (13)$$

$$g(t) = \arcsin \sqrt{\frac{(t_2+1)(t-t_1)}{(t_2-t_1)(t+1)}} \quad (14)$$

$$p = 2(t_2 - t_1)/(1 - t_1^2)(t_2 + 1) \quad (15)$$

Note that this definition of the elliptic integral is due to that in ref. 35, which is different from that in ref. 34. By inserting eqn. (10) into eqn. (15) and using relations between circular functions, the parameter p can be rewritten as

$$p = 4S/(1 + S)^2 \quad (16)$$

with

$$S = \frac{\sin[\pi w_a/2w]}{\cos[\pi(w_a - w_c)/4w]} \quad (17)$$

where w_a , w_c and w_g are the widths of the anode, the cathode and the gap,

respectively, corresponding to $2x_1$, $2(w - x_2)$ and $x_2 - x_1$, and w is given by

$$w = \frac{1}{2}(w_a + w_c) + w_g \quad (18)$$

Value of p are less than unity for any combinations of w_a , w_c and w_g . Inserting the condition $u = 1$ at $t = t_2$ yields

$$C_2 = \frac{\sqrt{(1-t_1)(1+t_2)}}{2K(p)}$$

where $K(p)$ is the complete elliptic integral [35]. Then eqn. (12) is reduced to

$$u = F(g(t) | p) / K(p) \quad (19)$$

Combination of eqns. (9) and (19) provides the transformation from z to u through the parameter p , or combinations of w_a , w_c , and w_g .

On the u -plane, the anode faces the cathode in the rectangle. Thus the concentration profile varies linearly with the real part of u (denoted by $\text{Re}(u)$). Substituting eqn. (19) for $\text{Re}(u)$ and considering that $K(p)$ is a real value, we obtain

$$\frac{C_0}{C^*} = \frac{1}{1 + \exp(-\xi_c)} + \frac{H \text{Re}[F(g(t) | p)]}{K(p)} \quad (20)$$

with

$$H = \frac{1}{1 + \exp(-\xi_a)} + \frac{1}{1 + \exp(-\xi_c)} \quad (21)$$

$$\xi_a = (nF/RT)(E_a - E^{\circ'}) \quad \xi_c = (nF/RT)(E_c - E^{\circ'}) \quad (22)$$

where we have employed eqns. (2), (3) and (6). Since the variable t is a complex number, $g(t)$ is also complex. Let the real and imaginary part of $g(t)$ be g_x and g_y , respectively, so that $g(t) = g_x + ig_y$. Explicit forms of g_x and g_y are given by

$$g_x = \arcsin \left[\frac{\sqrt{(1+X)^2 + Y^2}}{2} - \frac{\sqrt{(1-X)^2 + Y^2}}{2} \right] \quad (23)$$

$$g_y = \text{arccosh} \left[\frac{\sqrt{(1+X)^2 + Y^2}}{2} + \frac{\sqrt{(1-X)^2 + Y^2}}{2} \right]$$

where X and Y are the real and imaginary parts of $\sqrt{(t_2 + 1)(t - t_1)/(t_2 - t_1)(t + 1)}$. By applying eqn. (17.4.11) of ref. 35 to eqn. (20), the concentration profile can be expressed by

$$\frac{C_0}{C^*} = \frac{1}{1 + \exp(-\xi_c)} + \frac{HF(\arctan(r^{-1/2}) | p)}{K(p)} \quad (24)$$

where r is a positive root of the quadratic equation:

$$r^2 - \{\cot^2 g_a + p \sinh^2 g_y / \sin^2 g_x + p - 1\} r + (p - 1) \cot^2 g_a = 0 \quad (25)$$

By use of eqn. (20), the current density, j , at the cathode ($0 \leq x \leq x_1$, $y = 0$ or

$-1 \leq t \leq t_1$) or at the anode ($x_2 \leq x \leq w$, $y = 0$ or $t_2 \leq t \leq 1$) is given by

$$j = nFD \frac{\partial C_0}{\partial y} = \frac{nFc^* HD}{K(p)} \frac{\partial}{\partial y} [F(g(t) | p)] \quad (26)$$

According to Cauchy's definition of an analytic function [36], $\partial[\text{Re}(u)]/\partial y$ equals $-\text{Im}(du/dz)$; thus carrying out the differentiation in eqn. (26) and substituting x for t by use of eqns. (9) and (10) yields

$$\frac{jw}{nFc^* HD} = \frac{\pm \pi(1+S) \cos[\pi(w_a - w_c)/4w]}{2K(p) \{[\cos(\pi x_1/w) - \cos(\pi x/w)] \{ \cos(\pi x_2/w) - \cos(\pi x/w) \} \}} \quad (27)$$

where the plus and the minus signs are for the anodic and the cathodic current, respectively. On assumption (i), the total current at the anode, I , is given by the integral of eqn. (27):

$$I = 2bm \int_{x_2}^w j dx = \frac{mbnFc^* HD}{K(p)} \int_{t_2}^1 \frac{(1+S) \cos[\pi(w_a - w_c)/4w]}{\sqrt{(1-t^2)}(t-t_1)(t-t_2)} dt$$

$$= 2mbnFc^* HDK(1-p)/K(p) \quad (28)$$

where b is the length of the microband electrode of the IDA and m is the number of microband anodes or cathodes. The dimensionless current, $I/(mbnFc^* HD)$, is a function of the geometric parameter p only. Since p is a function of the ratios w_a/w , w_c/w and w_g/w , the current at each microband electrode is independent of the absolute values of w_a , w_c and w_g . The total current at the cathode can be obtained by integrating j from 0 to x_1 . The expression has been demonstrated to be identical with eqn. (28) except for the sign, indicating the mass balance of the electroactive species.

The function $K(1-p)/K(p)$ in eqn. (28) can be rewritten using the Nome $q(p)$ expansion through the relation: $K(1-p)/K(p) = -(1/\pi) \ln(q(p))$:

$$q(p) = p/16 + 8(p/16)^2 + 84(p/16)^3 + 992(p/16)^4 + \dots \quad (29)$$

Thus eqn. (28) becomes

$$I = -(2/\pi)mbnFc^* HD \ln \left[p/16 + 8(p/16)^2 + 84(p/16)^3 + 992(p/16)^4 + \dots \right] \quad (30)$$

Numerical computation

The concentration profile was calculated numerically from eqns. (24) and (25) by the use of FORTRAN on a 16-bit personal computer PC9801 (NEC, Tokyo). The FORTRAN supported arithmetic operations of complex variables. Values of the complete elliptic integral were computed from the following polynomial approximate equation [35]:

$$K(1-x) = 1.38629 + 0.111972x + 0.0725296x^2$$

$$-(0.5 + 0.121348x + 0.0288729x^2) \ln(x) \quad (31)$$

A complex number of the incomplete elliptic integral was separated into its real and the imaginary parts by using eqn. (17.4.11) of ref. 35, each of which was evaluated by application of Landen's transformation. The real part represents the concentration distribution whereas the imaginary part represents the distribution of the current flow. In Fig. 3, concentration profiles (solid lines) of c_0 and lines of the current flow (dotted lines) are shown for $w_a = w_g = w_c/2$. They show that the equi-concentration contour intersects normally with the insulator walls, that the current line flows out normally to the electrodes and that the current line crosses normally with the equi-concentration contours. These facts demonstrate that the above calculation is reasonable. The reasonability is further supported not only by the symmetry of the concentration profiles with respect to $x = w/2$, but also by the fact that $c(x, y) + c(w-x, y) = c^*$ when $w_c = w_a$.

Figure 4 shows the distribution of the current densities at the cathode and the anode for various combinations of w_c and w_a at $w_g = w/2$, calculated from eqn. (27). As readily predicted, the current density is infinite at both edges. A drastic change in the current density occurs in the range within $0.05w$ from both edges. Thus the electrode with $w_c < 0.1w$ exhibits non-uniform current distribution over the cathode. Since the total current at the cathode is identical with that at the anode, the current density increases with a decrease in the electrode width.

Figure 5 shows the variation of the dimensionless total current with p , calculated from eqns. (28) and (31). As the values of p become small, corresponding to a decrease in the gap, the current increases proportionally to $-\ln(p)$ (see eqn. 30). Conversely, as the gap increases or values of p approach unity, the current tends

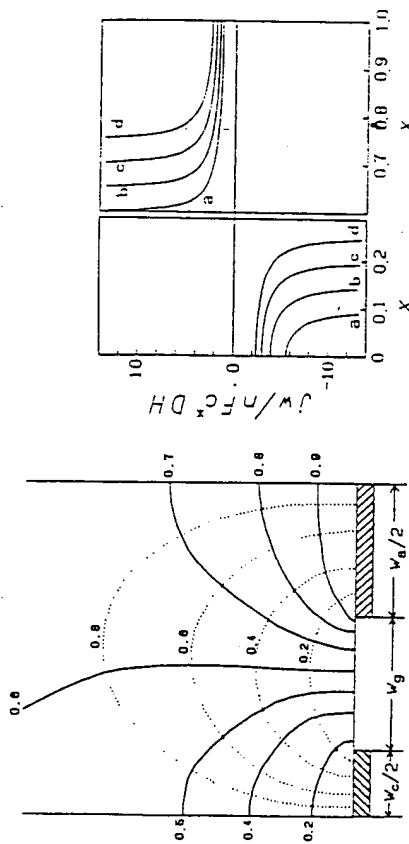


Fig. 3. Equi-concentration contours (—) and current lines (·····) when $E_c \ll E^*$ and $E_a \gg E^*$ at $w_a = w_g = w_c/2$. Digits on the equi-concentration contours denote values of c_0/c^* whereas those on the current lines denote $\ln[F(g(r)|p)]/K(p)$.

Fig. 4. Distribution of current densities at the cathode (negative values of j) and at the anode (positive values of j) at $w_g = w/2$ for $(w_c/w, w_a/w) =$ (a) (0.2, 0.8), (b) (0.3, 0.7), (c) (0.4, 0.6) and (d) (0.5, 0.5).

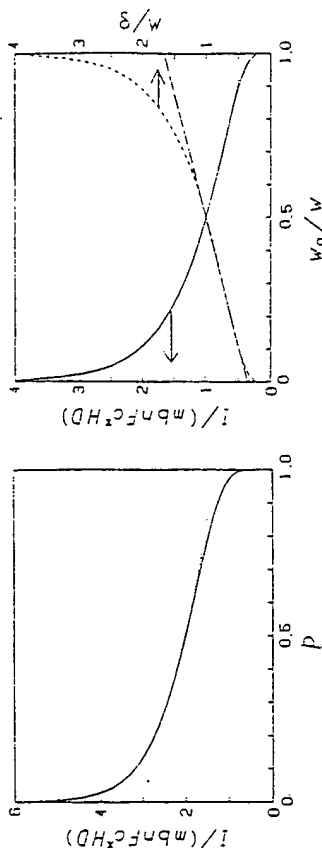


Fig. 5. Variation of the dimensionless total current with the reduced geometric parameter p . The solid curve was calculated from eqns. (28) and (31) whereas the dotted one was from eqns. (29) and (30).

Fig. 6. Variation of the dimensionless total current (at the left ordinate) with w_g/w when $w_a = w_c$. The dotted curve was calculated from eqn. (33). The dashed line (at the right ordinate) shows the variation of δ/w with w_g/w at $w_a = w_c$, along which the tangent line (---) was drawn.

rapidly to zero because the electrode area decreases. The dotted curve in Fig. 5 is the variation of the current evaluated from eqn. (30). Equation (30) is valid within 1, 2, 4 and 10% errors at $p \leq 0.58, 0.66, 0.72$ and 0.87 , respectively.

In the special case of $w_a = w_c = w$, p can be written as

$$p = \frac{4 \sin(\pi w_g/2w)}{(1 + \sin(\pi w_g/2w))^2}$$

indicating that the current is a function of w_g/w only. In Fig. 6, the variation with w_g/w is shown. When $w_g < 0.1w$, the current increases rapidly with a decrease in w_g/w . The enhancement of the current is obviously ascribed to the decrease in the length of the current line or the increase in the concentration gradient. For $p < 0.31$ or $w_g < 0.059w$, $\ln(g(p))$ can be approximated as $\ln(p/16)$ within 4% error, according to eqn. (29). Then p equals $2\pi w_g/w$, and eqn. (30) becomes

$$I = (2/\pi)mbnFc^*HD \ln[8w/(\pi w_g)] \quad (32)$$

for $w_g < 0.059w$ at $w_a = w_c = w$. By modification of eqn. (32), we obtained an empirical application of the following form:

$$I = mbnFc^*HD \{0.637 \ln(2.55w/w_g) - 0.19(w_g/w)^2\} \quad (33)$$

for $w_g < 0.85w$ at $w_a = w_c$. This equation has less than a 2% error for $w_g/w < 0.85$. This is helpful for a simple evaluation of the total current.

A specific geometry of the IDA is the case of $w_a = w_c = w$. Sanderson and Anderson have employed an electrode with these dimensions because of its balance between analytical requirements and several restrictions imposed by the fabrication

process [23]. In this case, eqn. (28) is reduced greatly to

$$I = mbnF_c \cdot HD \quad (34)$$

This is quite different from the empirical equation found by Sanderson and Anderson:

$$I = (50/0.665)mbnF_c \cdot HD \quad (35)$$

It is of interest to approximate the current by the expression for a twin electrode in a rectangular thin layer [23], as shown in Fig. 2C, where the width of the twin electrode is w . The interelectrode distance, δ , was determined to fit the equation for the twin electrode,

$$I = mbnF_c \cdot HDw/\delta \quad (36)$$

to eqn. (33). Then we have $\delta/w = (0.637 \ln(2.55w/w_g) - 0.19(w_g/w)^2)^{-1}$. As shown in Fig. 6, δ/w depends on w_g/w . Consequently, the approximation is not good. A modification of the approximation is to find a simple relation of δ with w and w_g . If a tangent line (dash-dotted) is drawn along the curve of δ/w in Fig. 6, drawn, the current at the IDA can be represented roughly by the twin electrode through the following relation:

$$\delta = 1.29w_g + 0.36w \quad \text{for } 0.05 < w_g/w < 0.6 \quad \text{at } w_s = w_c \quad (37)$$

EXPERIMENTAL

Fabrication of the interdigitated array electrode

Oxidized dummy silicon wafers with (100) orientation, 7.62 cm in diameter and 0.3 mm in thickness including the 1 μ m oxidation layer, which were purchased from Osaka Titanium Co. Ltd. (Osaka), were used as the substrate of the IDA.

In order to make the surface of the wafer hydrophobic, a mixture of hexamethyldisilazane (33% by volume) and xylene was spin-coated on the oxidized Si wafer at 6000 rpm for 40 s. An MP1400-27 (Shiplay) positive photoresist was also spin-coated on the hydrophobic wafer at 6000 rpm for 40 s, followed by prebaking at 90 °C for 30 min. The thickness of the resist was 0.9 μ m.

A pattern of a negative photographic mask designed is depicted in Fig. 1B. The pattern was composed of spaces for the microband electrodes and their leads. One substrate had 16 IDA units. The mask was ordered from NTT Electronics Technology (Tokyo). A mask aligner PLF-501F (Canon Ltd. Tokyo) was used to expose the photoresist. An ultra high pressure mercury lamp was used as a light source through a filter so that the effective wavelength of the source was i-line (365 nm) and g-line (436 nm). The photoresist was exposed to the light for 20 s. The image was developed for 1 min in the 1:1 mixture of Shiplay MP concentrated developer and deionized water, rinsed in deionized water for 5 min and then dried by blowing nitrogen gas.

Chromium was sputter-deposited on the wafer up to a thickness of about 5 nm with SPF-332H sputter deposition equipment (ANELVA, Tokyo). Then platinum was deposited up to a thickness of about 100 \pm 2 nm without breaking the vacuum.

TABLE 1

Dimensions of platinum interdigitated array electrodes

Electrode	$w_g/\mu\text{m}$	$w_s/\mu\text{m}$	$w_c/\mu\text{m}$	h/nm	m
A	5.0	10.0	10.0	2.00	25
B	5.0	5.0	5.0	2.00	50
C	5.0	3.0	3.0	2.00	50
D	2.0	10.0	10.0	2.00	25
E	2.0	5.0	5.0	2.00	50
F	2.0	3.0	3.0	2.00	50

The wafer was immersed in methylethylketone and the metalized resist pattern was lifted off by a sonication bath during 15 min. The wafer was cleaned in methylethylketone for 15 min and then dried by blowing nitrogen gas.

The wafer was sputter-deposited with silicon dioxide up to 300 nm thickness. A photoresist film of 1 μ m was spin-coated on the silicon dioxide coated wafer. The photoresist film was exposed and developed in the same manner as described above. The silicon dioxide film was etched by a DEM-451 reactive ion etching equipment (ANELVA, Tokyo) with hexafluoroethane until the surface of the IDA electrode and the pad were exposed, whereas the leads of the electrode were masked by photoresist pattern.

Electrical leads were connected on the pads by solder. The dimensions of the electrode thus constructed are listed in Table 1. SEM pictures of the IDA are shown in Fig. 1C.

Chemicals and apparatus

Ferrocene, acetonitrile and tetrabutylammonium perchlorate were used as purchased. The reference electrode was a saturated calomel electrode, which was connected to the acetonitrile solution through a salt bridge filled with 0.1 mol/dm³ tetrabutylammonium perchlorate in acetonitrile. The counter electrode was a platinum wire. Electrochemical measurements were made by a dual potentiostat, DPGS-3 (Nikko Keisoku, Atsugi, Japan), at 25 \pm 1 °C. Voltammograms were recorded with a two-pen x-y recorder.

RESULTS AND DISCUSSION

An example of the voltammograms for ferrocene is shown in Fig. 7, in which the potential at one electrode was set at -0.15 V vs. SCE and the other was cycled. The anodic and cathodic waves at a sweep rate < 100 mV/s were sigmoidal with slight hysteresis, indicating that the voltammogram was in the steady state. As the sweep rate increased, the hysteresis was appreciable and the cathodic limiting current was smaller than the anodic one. These trends were noticeable as the gap width increased. They are obviously ascribed to the transient behavior.

The ratio of the cathodic limiting current to the anodic one, namely collection efficiency, ranged from 0.87 to 0.95 at 20–100 mV/s. The collection efficiency at electrodes D–F ($w_g = 2 \mu\text{m}$) was higher than that at electrode A–C ($w_g = 5 \mu\text{m}$). When the cathode and the anode were interchanged, the same ratio was observed. Thus several percent of the anodic current runs off into the counter electrode. The loss of collection efficiency may be a sacrifice of controlling potentials at both electrodes. Use of a two-electrode system might yield 100% efficiency. However, potentiostatic conditions could not be established at the two-electrode system.

According to eqn. (33), the limiting current per microband electrode, I_{lim}/m , should be proportional to values of $0.632 \ln(2.55w/w_g) - 0.19(w/w_g)^2$. Figure 8 shows this dependence for the six electrodes of Table 1. Figure 8 also shows the theoretical line with the slope of $\ln Fc^*D$, where D was taken to be $2.4 \times 10^{-5} \text{ cm}^2/\text{s}$ [37]. The experimental values of I_{lim}/m fall on the theoretical line, demonstrating agreement of the experiment with the theory. Equation (33) predicts that I_{lim}/m does not vary with absolute values of w and w_g so long as the ratio, w/w_g , is retained. Although electrode A has roughly twice the dimensions of electrode E, the values of I_{lim}/m are similar at both electrodes. This fact verifies the prediction. The independence of the absolute value may not require miniaturizing to the size of the IDA. If an IDA with conventional dimensions is employed for cyclic voltammetry, one should use a very slow potential sweep rate in order to maintain the steady state. Then the electrochemical system might suffer from fluctuations such as those due to natural convection during the long electrolysis, and hence the voltam-

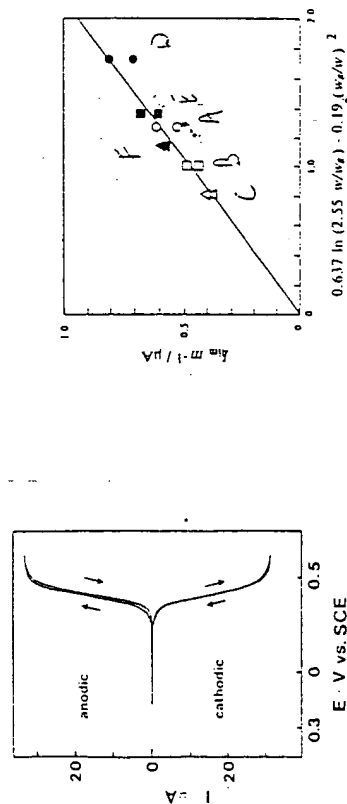


Fig. 7. Cyclic voltammograms of 1.0 mmol/dm^3 ferrocene in the acetonitrile solution involving 0.1 mol/dm^3 tetrabutylammonium perchlorate at IDA (D) in Table 1 at 25°C . The cathode was potentiostated at -0.15 V vs. SCE whereas the potential at the anode was swept at $v = 100 \text{ mV/s}$.

Fig. 8. Plot of I_{lim}/m against $0.637 \ln(2.55w/w_g) - 0.19(w/w_g)^2$ at the IDAs in Table 1: (○) A, (□) B, (Δ) C, (●) D, (■) E, (▲) F. The limiting currents were measured under the same conditions as in Fig. 7. The upper symbols denote anodic current.

grams might lose reproducibility. So miniaturization of the IDA is required for real voltammetric measurements.

In conclusion, the diffusion-controlled limiting currents at both anode and cathode are expressed by

$$|I_{\text{lim}}| = m b n F c^* D \left[0.637 \ln \left\{ 2.55 \left(1 + w_g/w \right) \right\} - 0.19 \left(1 + w_g/w \right)^2 \right] \quad (38)$$

when $0.18w_g < w_g = w_c$. This is valid only under steady-state conditions.

REFERENCES

- 1 D. Belanger and M.S. Wrighton, *Anal. Chem.*, **59** (1987) 1426 and references therein.
- 2 A.J. Bard, J.A. Crayston, G.P. Kittlesen, T.V. Shea and M.S. Wrighton, *Anal. Chem.*, **58** (1986) 2321.
- 3 W.L. Caudill, J.O. Howell and R.M. Wightman, *Anal. Chem.*, **54** (1982) 2532.
- 4 N. Sleszynski, J. Osteryoung and M. Carier, *Anal. Chem.*, **56** (1984) 130.
- 5 K. Aoki and J. Osteryoung, *J. Electroanal. Chem.*, **125** (1981) 315.
- 6 W. Thormann, P.V. Bosch and A.M. Bond, *Anal. Chem.*, **57** (1985) 2764.
- 7 E. Schumacher, W. Thormann and D. Arn in F.M. Livernais (Ed.), *Analytical Isotachophoresis*, Elsevier, Amsterdam, 1981, pp. 33–39.
- 8 W. Thormann, D. Arn and E. Schumacher, *Electrophoresis*, **5** (1984) 323.
- 9 D.E. Weisshaar, D.E. Tallman and J.L. Anderson, *Anal. Chem.*, **53** (1981) 1809.
- 10 V.Yu. Filinovsky, *Electrochim. Acta*, **25** (1980) 309.
- 11 D.E. Tallman and D.E. Weisshaar, *J. Liq. Chromatogr.*, **6** (1983) 2157.
- 12 J.L. Anderson, K.K. Whiten, J.D. Brewster, T.-Y. Ou and W.K. Nonidez, *Anal. Chem.*, **57** (1985) 1366.
- 13 L.E. Fosdick and J.L. Anderson, *Anal. Chem.*, **58** (1986) 2481.
- 14 L.E. Fosdick, J.L. Anderson, T.A. Baginski and R.C. Jaeger, *Anal. Chem.*, **58** (1986) 2750.
- 15 J.L. Anderson, T.Y. Sou and S. Moldoveanu, *J. Electroanal. Chem.*, **196** (1985) 213.
- 16 T. Gueshi, K. Tokuda and H. Matsuda, *J. Electroanal. Chem.*, **89** (1978) 247.
- 17 T. Gueshi, K. Tokuda and H. Matsuda, *J. Electroanal. Chem.*, **101** (1979) 29.
- 18 T. Tokuda, T. Gueshi and H. Matsuda, *J. Electroanal. Chem.*, **102** (1979) 41.
- 19 S. Moldoveanu and J.L. Anderson, *J. Electroanal. Chem.*, **185** (1985) 239.
- 20 O. Contamin and E. Levart, *J. Electroanal. Chem.*, **136** (1982) 256.
- 21 H. Reller, E. Kirova-Eisner and E. Gileadi, *J. Electroanal. Chem.*, **138** (1982) 65.
- 22 D.G. Sanderson and L.B. Anderson, *Anal. Chem.*, **57** (1985) 2388.
- 23 C.E. Chidsey, B.J. Feldman, C. Lundgren and R.W. Murray, *Anal. Chem.*, **58** (1986) 601.
- 24 B.J. Feldman and R.W. Murray, *Anal. Chem.*, **58** (1986) 2844.
- 25 L.B. Anderson and C.N. Reiley, *J. Electroanal. Chem.*, **10** (1965) 295.
- 26 B. McDuffie, L.B. Anderson and C.N. Reiley, *Anal. Chem.*, **38** (1966) 883.
- 27 K. Aoki, T. Tokuda and H. Matsuda, *Denki Kagaku (J. Electrochem. Soc. Jpn.)*, **54** (1986) 1010.
- 28 K. Aoki, K. Tokuda and H. Matsuda, *J. Electroanal. Chem.*, **225** (1987) 19.
- 29 K. Aoki, K. Tokuda and H. Matsuda, *J. Electroanal. Chem.*, **230** (1987) 61.
- 30 K. Aoki and K. Tokuda, *J. Electroanal. Chem.*, **237** (1987) 163.
- 31 R.V. Churchill, J.W. Brown and R.F. Verhey, *Complex Variables and Applications*, McGraw-Hill Kogakusha, Tokyo, 1974, pp. 209–218.
- 32 R.V. Churchill, J.W. Brown and R.F. Verhey, *Complex Variables and Applications*, McGraw-Hill Kogakusha, Tokyo, 1974, pp. 239–261.
- 33 I.S. Gradshteyn and I.M.R. Ryzhik, *Table of Integrals, Series and Products*, Academic Press, New York, 1980, p. 242.

- 35 M. Abramowitz and I.A. Stegun (Eds.), *Handbook of Mathematical Functions*, Dover Publications, New York, 1970, pp. 589-598.
 36 E.T. Whittaker and G.N. Watson, *A Course of Modern Analysis*, Cambridge University Press, London, 1973, pp. 83, 84.
 37 T. Kuwana, D.E. Duhlitz and G. Hoh, *J. Am. Chem. Soc.*, **82** (1960) 5811.

J. Electroanal. Chem., **256** (1988) 283-289
 Elsevier Sequoia S.A., Lausanne - Printed in The Netherlands

Reverse pulse voltammetry at microelectrodes

Theory of the reversible case

Zbigniew Stojek

Warsaw University, Department of Chemistry, ul. Pasteura 1, 02-093 Warsaw (Poland)

(Received 12 May 1988; in revised form 14 July 1988)

ABSTRACT

A theoretical equation describing the reversible wave in reverse pulse voltammetry at a disc microelectrode is derived. Due to the steady state current which develops during the rest potential period, the initial conditions at the microelectrode surface are easily regained, as in reverse pulse polarography, and there is no need to stir the solution between consecutive pulses. For $p = 4Dt/\tau^2 > 40$ (τ is the sum of the rest time and the pulse time, and r is the microelectrode radius), the ratio i_{RP}/i_{AC} is practically independent of p and the number of potential steps. On the other hand, this ratio is strongly dependent on the parameter $n_p = 4Dt_p/r^2$ (t_p is the reverse pulse time). The theory was verified experimentally.

INTRODUCTION

At very small disc electrodes $\sqrt{Dt}/r \gg 1$, where r denotes the electrode radius and D is the diffusion coefficient. The chronoamperometric current is independent of time due to spherical diffusion taking place at such electrodes [1,2]. Under these conditions, transport of substrates and products is much faster than with regular sized electrodes, for which diffusion is mainly planar. The faster diffusion of products means, among other things, that under certain conditions, e.g. for $p = (nFv/RTD)^{1/2} \ll 1$, there is no reverse peak in cyclic voltammetry [3,4]; v is the potential scan rate and RT/nF is the Nernstian factor. Reverse pulse voltammetry, RPV, is the technique which, applied together with microelectrodes, gives a combination of the steady state for substrates and the time dependent current for products (product monitoring is possible). The usefulness of this technique in electroanalytical chemistry has been demonstrated in refs. 5-7.

In RPV and RPP (reverse pulse polarography) the potential waveform is formed in the same way as in normal pulse polarography (voltammetry). However, the rest potential is chosen to sit well on the plateau of the regular polarographic wave, and

0022-0728/88/\$03.50 © 1988 Elsevier Sequoia S.A.

**This Page is Inserted by IFW Indexing and Scanning
Operations and is not part of the Official Record**

BEST AVAILABLE IMAGES

Defective images within this document are accurate representations of the original documents submitted by the applicant.

Defects in the images include but are not limited to the items checked:

- ☐ **BLACK BORDERS**
- ☐ **IMAGE CUT OFF AT TOP, BOTTOM OR SIDES**
- ☐ **FADED TEXT OR DRAWING**
- ☐ **BLURRED OR ILLEGIBLE TEXT OR DRAWING**
- ☐ **SKEWED/SLANTED IMAGES**
- ☐ **COLOR OR BLACK AND WHITE PHOTOGRAPHS**
- ☐ **GRAY SCALE DOCUMENTS**
- ☐ **LINES OR MARKS ON ORIGINAL DOCUMENT**
- ☒ **REFERENCE(S) OR EXHIBIT(S) SUBMITTED ARE POOR QUALITY**
- ☐ **OTHER:** _____

IMAGES ARE BEST AVAILABLE COPY.

As rescanning these documents will not correct the image problems checked, please do not report these problems to the IFW Image Problem Mailbox.

